論文 / 著書情報
Article / Book Information

題目(和文)	
Title(English)	The study on β-glucan masking mechanism to evade the host immunity in the emerging pathogen Candida auris
著者(和文)	SELISANASHIELA MARIE GINES
Author(English)	Shiela Marie Gines Selisana
出典(和文)	学位:博士(学術), 学位授与機関:東京工業大学, 報告番号:甲第12935号, 授与年月日:2024年9月20日, 学位の種別:課程博士, 審査員:梶原 将,折原 芳波,一瀬 宏,小倉 俊一郎,柘植 丈治,小畠 英理
Citation(English)	Degree:Doctor (Academic), Conferring organization: Tokyo Institute of Technology, Report number:甲第12935号, Conferred date:2024/9/20, Degree Type:Course doctor, Examiner:,,,,,
学位種別(和文)	博士論文
Type(English)	Doctoral Thesis

Doctoral Thesis

The study on β-glucan masking mechanism to evade the host immunity in the emerging pathogen *Candida auris*

Shiela Marie Gines Selisana

DEPARTMENT OF LIFE SCIENCE AND TECHNOLOGY

SCHOOL OF LIFE SCIENCE AND TECHNOLOGY

TOKYO INSTITUTE OF TECHNOLOGY

2024

ACKNOWLEDGEMENT

First and foremost, I would like to express my utmost gratitude to Professor Kajiwara for accepting my application to join his esteemed laboratory and for his valuable guidance and much-needed financial support to conduct this research. It was truly an honor to be a member of the Kajiwara and Orihara Laboratory.

I am immensely grateful to Associate Professor Orihara for her helpful comments and advice both in my research and personal life. I truly appreciate her effort in carefully reading my lengthy reports, writing invaluable feedback, and showing empathy towards her students. I can never forget how she consoled me when I cried my heart out when I was on the brink of losing all the files on my laptop.

I would also like to give my sincere thanks to all members of the Kajiwara and Orihara Laboratory, especially to Assistant Professor Chen for all the help in conducting experiments and for patiently answering all the questions I have regarding the protocol, reagents, and anything related to research. To the rest of my labmates, I can confidently say that you all are the best labmates that I can ever ask for. Thank you for sharing the laughter and the tears (plus stress), for the emotional support when laboratory work gets tough, and for all the trips, *izakaya* nights, and karaoke sessions that I enjoy.

To my Filipino support group – Niña, Dave, Razelle, Jeff, Clyde, and friends from the Association of Filipino Students in Japan (AFSJ) for all the travels, lunches, and dinners that we shared. I am blessed to have known each one of you and I sincerely treasure the friendship we have built.

To my loving partner, Chaivarakun, for supporting me in all my endeavors even if it means that we have to be miles apart. I appreciate that you always ensure my safety whenever I have long or overnight experiments. Thank you for always having my back and helping me cope with stress and anxiety throughout my PhD journey.

To my ever-supportive family, Papa Romeo, Mama Ursula, and sisters Ann and Mae, I can never thank you enough for your unconditional love and support. Thank you very much for constantly praying for my success, for always wishing me the best in everything, and for always encouraging me to finish this PhD.

Last but not least, I am indebted to the Japanese government for providing financial support through the Monbukagakusho (MEXT) scholarship.

ABSTRACT

Candida auris is an emerging pathogenic yeast that has been designated as a global public health threat. Despite this, the immune response against *C. auris* infection is still not well understood. Humans fight *Candida* infections through the immune system that recognizes β-glucan, mannan, and chitin on the cell wall. In this study, *C. auris* was subjected to different physiologically relevant stimuli. Flow cytometric analyses of stained cells revealed that lactate and hypoxia trigger a reduction, while low pH triggers an increase in β-glucan. There is no inverse relationship between exposure levels of β-glucan and mannan. A reduction in β-glucan leads to reduced uptake of *C. auris* by PMA-differentiated THP-1 and RAW 264.7 macrophages. Lactate-induced β-glucan masking leads to reduced production of CCL3/MIP-1α upon co-incubation with macrophages, but TNF-α and IL-10 levels and ROS production within the macrophage remain unchanged. Looking into the mechanisms behind the masking of β-glucan, cAMP-PKA and calcium-calcineurin signaling pathways may not be involved in β-glucan masking in lactate- and hypoxia-grown *C. auris.* RNA sequencing revealed that 213 genes were differentially expressed in lactate-grown cells versus glucose only-grown cells. Two of the most upregulated genes code for a putative glucose transporter and GPI-anchored protein. For the *in vivo* infection analysis using silkworm larvae, the decrease in β-glucan on the fungal cell wall was found to increase the lethality of *C. auris*. This study demonstrates that β-glucan masking occurs in *C. auris* and serves as an escape mechanism from immune cells. This study sheds light on the dynamics of yeast cell wall remodeling and immune cell interaction.

TABLE OF CONTENTS

CHAPTER 4: EFFECT OF BETA-GLUCAN MASKING IN *CANDIDA AURIS* ON THE HOST IMMUNE RESPONSE

CHAPTER 5. EFFECT OF BETA-GLUCAN MASKING IN *CANDIDA AURIS* ON ITS VIRULENCE ON DOMESTIC SILKWORM (*Bombyx mori* Linnaeus, 1758)

CHAPTER 6: ELUCIDATION OF THE MOLECULAR MECHANISM BEHIND BETA-GLUCAN MASKING IN *CANDIDA AURIS*

LIST OF FIGURES

CHAPTER 1: RESEARCH BACKGROUND

CHAPTER 2: EFFECT OF ENVIRONMENTAL STIMULI ON BETA-GLUCAN SURFACE EXPRESSION OF *CANDIDA AURIS*

CHAPTER 3: CORRELATION BETWEEN BETA-GLUCAN AND MANNAN SURFACE EXPOSURE IN *CANDIDA AURIS*

CHAPTER 4: EFFECT OF BETA-GLUCAN MASKING IN *CANDIDA AURIS* ON THE HOST IMMUNE RESPONSE

CHAPTER 5. EFFECT OF BETA-GLUCAN MASKING IN *CANDIDA AURIS* ON ITS VIRULENCE ON DOMESTIC SILKWORM (*Bombyx mori* Linnaeus, 1758)

CHAPTER 6: ELUCIDATION OF THE MOLECULAR MECHANISM BEHIND BETA-GLUCAN MASKING IN *CANDIDA AURIS*

LIST OF TABLES

LIST OF ABBREVIATIONS

AO	Acridine orange
ATCC	American Type Culture Collection
βGRP	Beta-1,3-glucan recognition protein
BLAST	Basic Local Alignment Search Tool
BSA	Bovine serum albumin
CDC	Centers for Disease Control and Prevention
CGD	*Candida* Genome Database
CM-H_2DCFDA	Chloromethyl 2′,7′-dichlorodihydrofluorescein diacetate
Dectin-1	Dendritic cell-associated C-type lectin-1
DEG	Differentially expressed gene
DMEM	Dulbecco's Modified Eagle Medium
ELISA	Enzyme-linked immunosorbent assay
FBS	Fetal bovine serum
FDR	False discovery rate
LB	Luria-Bertani
LPS	Lipopolysaccharide
MIC	Minimum inhibitory concentration
MIP-1α	Macrophage inflammatory protein-1 alpha
MOI	Multiplicity of infection (macrophage to yeast ratio)
NCBI	National Center for Biotechnology Information
NTC	Nourseothricin
ORF	Open reading frame
PAMP	Pathogen-associated molecular pattern
PBMC	Peripheral blood mononuclear cell
PCR	Polymerase chain reaction
PI	Propidium iodide
PMA	Phorbol 12-myristate 13-acetate
PRR	Pattern recognition receptor
RFU	Relative fluorescence unit
ROS	Reactive oxygen species
RPKM	Reads Per Kilobase Million
RPMI	Roswell Park Memorial Institute medium

LIST OF ABBREVIATIONS

TB	Trypan blue
TLR-2	Toll-like receptor 2
TNF-α	Tumor Necrosis Factor- alpha
TPM	Transcripts Per Million
WHO	World Health Organization
WT	Wild type
YPD	Yeast extract peptone dextrose

CHAPTER 1: RESEARCH BACKGROUND

1.1 *CANDIDA* SPP. AS CAUSAL ORGANISM OF CANDIDIASIS

Candida (Berkh. 1923), is a fungal genus belonging to Division Ascomycota, Class Saccharomycetes, Order Saccharomycetales, and Family *Saccharomycetaceae*. *Candida* is considered the largest genus of medically important yeasts and is the most common cause of fungal infections worldwide (Brandt & Lockhart, 2012). This genus contains approximately 200 species and at least 30 species have been recognized as causes of human infection (Miceli et al, 2011).

Candida is a commensal organism in the skin and mucous membranes of the respiratory, gastrointestinal, and female genital tract of healthy individuals. However, in immunocompromised individuals, some species can invade mucosal surfaces and cause mucosal or systemic candidiasis. Candidiasis is one of the most common opportunistic fungal infections and systemic candidiasis is the fourth leading cause of nosocomial bloodstream infections, causing serious infections that can affect the blood, heart, brain, eyes, bones, and other parts of the body (Brown et al, 2012; Pfaller & Diekema, 2007). Mortality in patients with systemic candidiasis exceeds 40% even with antifungal treatment (Kullberg & Arendrup, 2015).

C. albicans is the most frequent cause of candidiasis (Pfaller & Diekema, 2007) and is widely researched among all *Candida* strains. However, the incidence of the disease caused by other species of *Candida* has increased drastically over the years. Non-*Candida albicans Candida* species (NCAC) such as *C. glabrata*, *C. parapsilosis*, *C. tropicalis*, *C. krusei*, and the emerging pathogen, *C. auris* have caused invasive infections worldwide (Lockhart et al, 2017; Tortorano et al, 2006). Figure 1-1 shows a maximum likelihood phylogeny based on 1,570 core genes among different species of *Candida.* The multidrug-resistant *C. auris* is closely related to the rarely observed and often multidrug-resistant species from the *C. haemulonii* clade and distantly related to the mostly studied *C. albicans* and *C. glabrata* (Muñoz et al, 2018; Sharma et al, 2016). Furthermore, draft genome comparisons revealed that more than 99.5% of the *C. auris* genomic reads did not align with the current draft genome sequences of *C. albicans, C. lusitaniae, C. glabrata,* and *Saccharomyces cerevisiae*, which suggest that *C. auris* is highly divergent at the whole genome level (Chaterjee et al, 2015). At the physiological level, *C. auris* has a unique stress resistance profile compared to other pathogenic *Candida* species. *C. auris* was more resistant to the chitin-binding dye calcofluor white and the β-1,3-glucan-binding dye Congo red than *C. albicans* and *C. dubliniensis*, suggesting that there are possible cell wall differences between these species (Day et al, 2018).

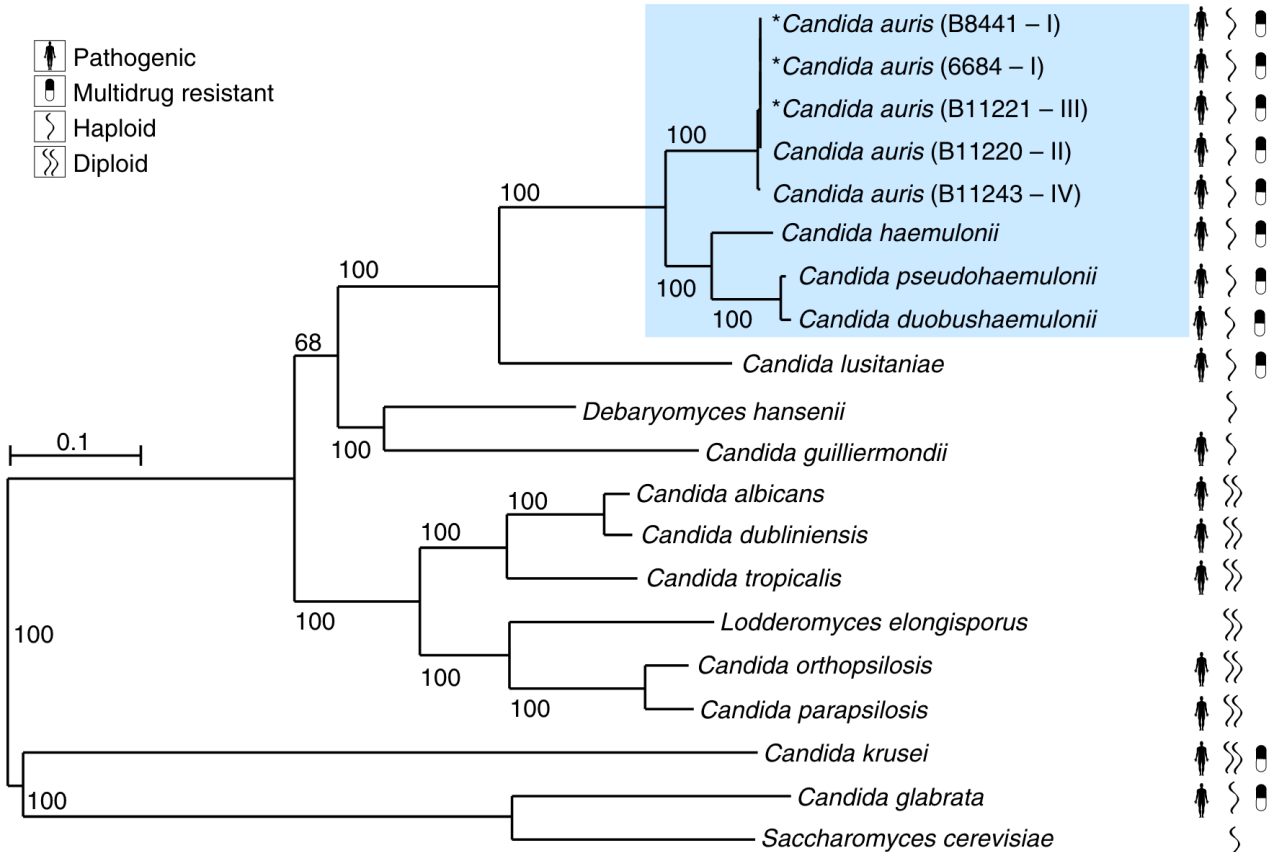

Figure 1-1. Maximum likelihood phylogeny using 1,570 core genes based on 1000 replicates, among 20 annotated genome assemblies, including *C. auris, C. haemulonii* (B11899), *C. duobushaemulonii* (B09383), and *C. pseudohaemulonii* (B12108), and closely related species. Branch lengths indicate the mean number of changes per site. Figure from Muñoz et al (2018).

1.2 *CANDIDA AURIS* AS AN EMERGING FUNGAL PATHOGEN

The emerging fungal pathogen, *C. auris,* is the first fungal pathogen to be designated as a global public health threat according to Lamoth and Kontoyiannis (2018). In the current report on antibiotic resistance threats in the United States, the Centers for Disease Control and Prevention (CDC) lists *C. auris* as a highest-level threat. Moreover, the World Health Organization (WHO) also lists *C. auris* as a critical priority fungal pathogen in their 2022 report.

C. auris is first discovered in the external ear canal of a female patient in Japan (Satoh et al, 2009). Years after its discovery in 2009, most *C. auris* isolates show high levels of resistance to three types of antifungal drugs such as azoles, polyenes, and flucytosine (Lockhart et al, 2017).

C. auris causes hospital outbreaks and is difficult to exterminate from hospital intensive care wards due to its resistance to commonly used cleaning agents and its ability to efficiently colonize the human skin, which supports easier transmission between hospital patients (Jeffery-Smith et al, 2017). According to a global surveillance report, *C. auris* has been found in 45 countries across all continents (Centers for Disease Control and Prevention, 2020). *C. auris* has been identified from many body sites including bloodstream, urine, respiratory tract, biliary fluid, wounds, and external ear canal, and invasive infections due to *C. auris* have a mortality rate of 60% (Lockhart et al, 2017). Even though *C. albicans* has always been considered the top causal agent of candidiasis, *C. auris* now accounts for nearly 20% of *Candida* bloodstream isolates in India, surpassing that of *C. albicans* (Mathur et al, 2018).

C. auris strains are divided into five clades, plus one recently discovered clade, based on whole genome sequencing (Suphavilai et al, 2023; Spruijtenburg et al, 2022; de Groot et al, 2020; Bravo Ruiz et al, 2019). Strains in each clade have highly plastic karyotype containing five to seven chromosomes. Susceptibility to antifungal reagents and survival from phagocytosis are also largely different among the first four clades (Muñoz et al, 2018; Lockhart et al, 2017). In terms of its general genomic characteristics, the *C. auris* genome has a size of 12.3–12.5 Mbp with a G+C content of 44.5%–44.8% (Chatterjee et al, 2015; Sharma et al, 2016).

Considering the relatively late discovery of *C. auris* compared to other known species, keyword searches for "*Candida auris*" in PubMed (https://www.ncbi.nlm.nih.gov/pubmed/) showed that the number of publications on this topic increased steadily starting in 2015 (Figure 1-2).

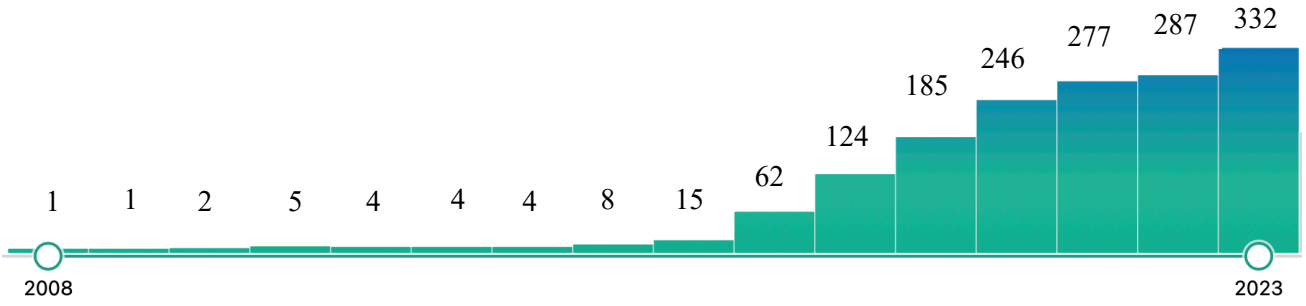

Figure 1-2. Number of publications per year with the keyword "*Candida auris*" on PubMed.

1.3 IMMUNE DEFENSE AGAINST *CANDIDA*

Cell walls of *Candida* sp. are composed of three main polysaccharides such as β-glucan, mannan, and chitin, that serve as pathogen-associated molecular patterns (PAMP). These PAMPs are specifically recognized by pattern recognition receptors (PRR) on the surface of immune cells like monocytes, macrophages, neutrophils, and dendritic cells (Perez-Garcia et al, 2011).

Figure 1-3 shows an illustration of how *Candida* species are recognized by PRRs through PAMPs.

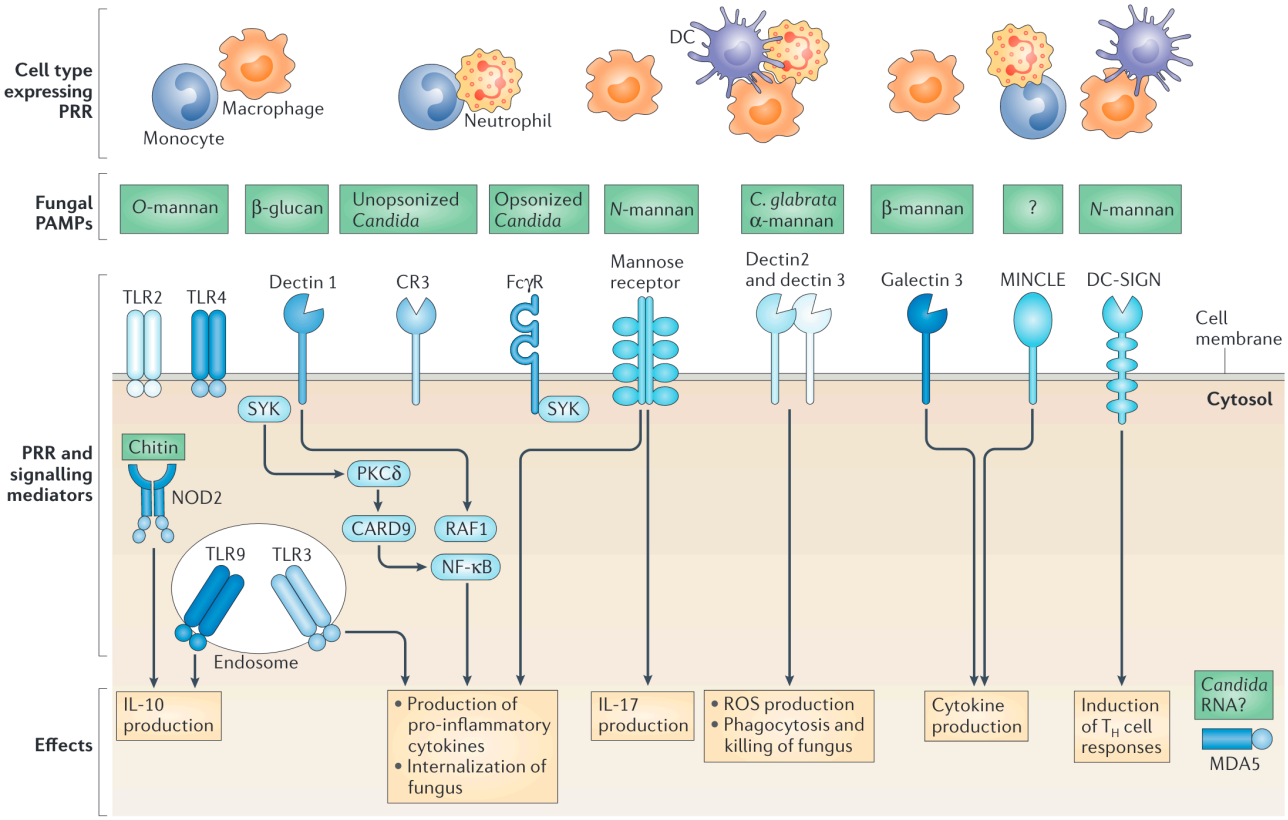

Figure 1-3. Recognition of *Candida* species by innate immune cells. Figure from Netea et al (2015).

β-glucans are recognized by the C-type lectin receptor Dectin-1 and Toll-like receptor TLR2. This recognition transduces intracellular signaling through several pathways thereby, triggering or regulating a wide range of cellular responses such as phagocytosis, ROS production, neutrophil extracellular trap development, inflammasome activation, and cytokine and chemokine synthesis. Furthermore, Dectin-1, like TLRs, can direct the development of adaptive immunity by boosting Th1- and Th17-type responses (Netea et al, 2015)

Even though all *Candida* species display PAMPs on the cell surface, Vendele et al (2020) clarified that the immune reactivity of fungal cell surfaces is not correlated with the relatedness of different fungal species. This means that previous findings on host-pathogen interaction studies mainly performed using *C. albicans,* may not be true for *C. auris*. Navarro-Arias et al (2019) support this statement by showing that the cell wall and innate immune recognition of *C. auris* are different compared to *C. albicans*.

Despite the medical relevance of *C. auris* and the priority level conferred by the CDC and WHO, the *C. auris*-immune effector interplay is still poorly understood. Understanding the relationship between environmental sensing and modulation of the host-*C. auris* pathogen interaction provides new opportunities for the development of innovative antifungal strategies.

1.4 OBJECTIVES OF THE STUDY

This research aims to address the following research questions:

1. Does *C. auris* exhibit changes in its cell wall when exposed to certain environmental stimuli? What are these conditions? What is the dynamics between cell wall β-glucan and mannan exposure in *C. auris*?
2. Does masking of β-glucan affect the innate immune response such as phagocytosis, cytokine production, and ROS production of macrophages?
3. Does masking of β-glucan impact the virulence of *C. auris* when injected into silkworm larvae?
4. What are the signaling systems or genes involved in the masking of β-glucan in *C. auris*?

CHAPTER 2: EFFECT OF ENVIRONMENTAL STIMULI ON BETA-GLUCAN SURFACE EXPRESSION OF *CANDIDA AURIS*

2.1 INTRODUCTION

Candida auris is a pathogenic yeast that is first discovered in the external ear canal of a female patient in Japan (Satoh et al, 2009). Years following its discovery in 2009, *C. auris* has been designated as a global public health threat (Lamoth and Kontoyiannis, 2018). According to the Centers for Disease Control and Prevention (2019), most *C. auris* isolates show high levels of resistance to three types of antifungal drugs such as azoles, polyenes, and flucytosine (Lockhart et al, 2017). Furthermore, *in vitro* studies have shown that more than 90% of *C. auris* isolates are resistant to the antifungal prophylactic drug fluconazole. Fortunately, the hosts such as human and animals have a natural way of overcoming invading pathogens to survive invasive infections.

The immune system recognizes fungal cells as foreign agents by detecting specific pathogen-associated molecular patterns (PAMPs). The three most common PAMPs in *Candida* species are β-glucan, chitin, and mannan (Calderone and Fonzi, 2001). Recent studies have shown that the most common *Candida* species, *C. albicans,* can mask β-glucan as a survival strategy when exposed to several environmental stimuli such as low oxygen concentrations, lack of iron, and high lactate concentrations. This poses a threat since masking of a major PAMP could lead to immune evasion, thereby allowing the pathogen to proliferate in the host (Pradhan et al 2019; Pradhan et al 2018; Ballou et al 2017).

Majority of PAMP masking studies on *Candida* have focused on *C. albicans* and not *C. auris.* Considering the predominant role of β-glucan in mediating the host-pathogen interaction and on host immune response (Hall, 2015), this chapter aims to determine if β-glucan masking phenomenon under certain environmental conditions is exhibited by a clinical isolate of *C. auris* and two type strains belonging to *C. auris* clade II and clade III. The influence of β-glucan masking in *C. auris* on the immune response was determined in the subsequent chapters.

2.2 MATERIALS AND METHODS

2.2.1 Yeast strains used

A clinical isolate of *Candida auris* from Indonesia (UI001) and type strains ATCC® MYA-5001™ (B11220) and ATCC® MYA-5002™ (B11221), as well as *Candida albicans* SC5314 for comparison purposes, were used in this study. All strains were stored as frozen stocks with 30% glycerol at -80°C and subcultured on YPD (1% yeast extract, 2% peptone, 2% glucose, 2% agar) plates. Yeast cells were inoculated in Minimal medium (0.67% BD Difco™ yeast nitrogen base with ammonium sulfate, 2% glucose) overnight at 37°C and 200 rpm. The Yeast Nitrogen Base used in this study contains all essential vitamins and inorganic salts necessary for the cultivation of yeasts except histidine, methionine, and tryptophan. The pH at 25°C is 5.4 ± 0.2. Cells were transferred to fresh Minimal media (OD_{600} = 0.2) and incubated for 5 h before analysis.

2.2.2 Culture conditions tested

To determine the effect of temperature, cells were grown at either 30°C or 37°C. To determine the effect of the presence of alternative carbohydrate sources such as lactate and glycerol, cells were grown in Minimal medium with 2% glucose (control) and varying concentrations of lactate (Nacalai Tesque, cat # 31604-95) and glycerol (Nacalai Tesque, cat # 17045-94), such as 0.25% lactate + 1.75% glucose, 0.5% lactate + 1.5% glucose, 1% lactate + 1% glucose, 2% lactate, 1% glycerol + 1% glucose, and 2% glycerol. There was an attempt to tease out the contributing effect of pH change during incubation. Different sets of Minimal media added with 50 mM MES buffer (Rane et al., 2019; Romanowski et al., 2012) were prepared and the pH of the media was adjusted to 5.50 before filter sterilization. The OD_{600} of all samples was measured after the 5-h incubation.

To further examine the effect of the initial amount of glucose vis-à-vis initial pH, Minimal media containing 1% or 2% glucose were prepared. The pH of both media was adjusted to 5.90 using 1 M NaOH to mimic the initial pH of the Minimal medium with 1% lactate. Both types of media were then filter-sterilized.

To determine the effect of oxygen level in β-glucan expression, cells were grown in hypoxic conditions (<0.1% O_2) using a hypoxia culture kit (Sugiyama-gen, cat. # nBIONIX-3) and without (poor aeration) or with shaking (normoxic) at 200 rpm. Nitrogen gas (Code 3-126-0491, Kenis, Japan) was injected before sealing the kit to accelerate oxygen removal.

To determine the effect of pH, different sets of buffered YPD (1% yeast extract, 2% peptone, 2% glucose, 3.57% HEPES) were prepared at varying pH (4.0, 5.5, 7.0, and 8.5).

To determine the effect of antifungal drugs, cells were grown in the absence or presence of sub-lethal concentrations of fluconazole (2-16 μg/mL; LKT Laboratories, cat # F4682), 5-fluorocytosine (16-500 ng/mL; Tokyo Chemical Industry Co., Ltd., cat # F0321), amphotericin B (31-188 ng/mL; Fujifilm Wako Pure Chemical Corporation, cat # 019-13364), and micafungin (1-40 μg/mL; Astellas, cat # 021360A). The shaker incubator was covered with foil during the 5-h incubation to ensure that light-sensitive drugs will not be inactivated by light. To determine if cells are still viable after drug exposure, 10 μL of 5-h-old cell culture suspension was spotted into the YPD plate. Growth was observed after incubation at 37°C for 24 h.

2.2.3 Surface staining of β-glucan

Cells were analyzed following the protocol of Ballou et al (2017) with slight modifications. Cells were collected (5000 rpm, 3 min, 4°C), washed with 1x phosphate-buffered saline (PBS) twice, and stained with 100 μL FACS buffer (1x PBS, 50 mM EDTA, 5% FBS) with 2.5 ng/μL Fc-hDectin-1a (Invivogen, cat. # fc-hdec1a) in the dark for 1 h at 4°C. Cells were washed twice with FACS buffer and stained with 100 μL FACS buffer with 1:500 Alexa Fluor 488®-conjugated AffiniPure Goat Anti-Human IgG_1 Fc_γ Fragment Specific (Jackson ImmunoResearch Laboratories, Inc., code # 109-545-098) in the dark for 1 h at 4°C. Cells were washed twice with FACS buffer and fixed with 100 μL 4% *p*-formaldehyde in 1x PBS in the dark for 15 min at 4°C. Cells were washed twice with FACS buffer and resuspended in 1x PBS prior to analysis. Controls such as unstained cells and cells stained with Alexa Fluor 488 only were used. For confocal microscopy observation, 5 μL of stained cell suspension were placed on a glass slide (Matsunami Superfrost Micro Slide Glass S2443), covered with micro cover glass (thickness no. 1, Muto Pure Chemicals Co. Ltd.), sealed with a nail polish, and kept in a closed container at 4°C until microscopy. Zeiss LSM780 upright confocal microscope was used to generate images.

2.2.4 Flow cytometry and statistical analyses

EC800™ Flow Cytometry Analyzer (Sony Biotechnology, Inc., Japan) with 488-nm laser in combination with FL1 (525/50) bandpass filter was used to analyze at least 100,000 cells from each sample. The gating strategy was kept constant in all analyses. To generate the histograms, FlowJo™ v10.8 Software (BD Life Sciences) was used.

The fold change is calculated as the mean of the median fluorescence intensities (MFI) of β-glucan::Alexa Fluor 488 in the experimental variable divided by the mean MFI of the control. Bar graphs were generated using GraphPad Prism version 9.4.0 for Windows, GraphPad Software, San Diego, California USA, www.graphpad.com. Means and standard deviations from at least three independent biological replicates (except data in Figure 2-5) were shown and the data were analyzed using t-test or one-way ANOVA with either Dunnett's multiple comparisons test or post-hoc Tukey HSD test (Figure 2-5B and D). A *P* value of at least 0.05 is considered significant (*$P < 0.05$, **$P < 0.01$, ***$P<0.001$, ****$P<0.0001$).

2.2.5 Specificity of Fc-hDectin-1a to β-glucan

Fc-hDectin-1a, which is expressed in CHO cells, is a soluble human Dectin-1 receptor constructed by fusing the C-terminal extracellular domain of human Dectin-1a (aa 67-247) to the C-terminus of an engineered human IgG1 Fc domain with a 10 amino acid linker (lifted from www.invivogen.com). This experiment was performed to confirm that Fc-hDectin-1a (Invivogen, cat. # fc-hdec1a), the reagent that was used in the β-glucan masking experiment, will only bind to β-glucan.

To determine the specificity of Fc-hDectin-1a to β-glucan, THP-1 (1.5×10^5 cells) was washed three times with a washing buffer (PBS + 2% FBS), blocked with 20 µL of 0.1% BSA for 5 min at RT, stained with 40 µL of 2.5 µg/mL Fc-hDectin-1a (InvivoGen) for 30 min at RT, followed by washing with washing buffer once and staining with 30 µL of AffiniPure Goat Anti-Human IgG_1 Fc_γ Fragment Specific (Jackson Immunoresearch) for 20 min at RT, washed with washing buffer once and analyzed using EC800™ Flow Cytometry Analyzer (Sony Biotechnology, Inc., Japan) with 488-nm laser in combination with FL1 (525/50) bandpass filter to analyze at least 25,000 cells from each sample. Unstained cells and Alexa Fluor 488 only stained cells were used as control.

2.3 RESULTS AND DISCUSSION

2.3.1 Specificity of Fc-hDectin-1a reagent to β-glucan

THP-1, a human monocytic cell line, was used because it does not have surface β-glucans. Based on Figure 2-1, the reagent used in the subsequent experiments, Fc-hDectin-1a, does not bind to non-β-glucans on the surface of a cell.

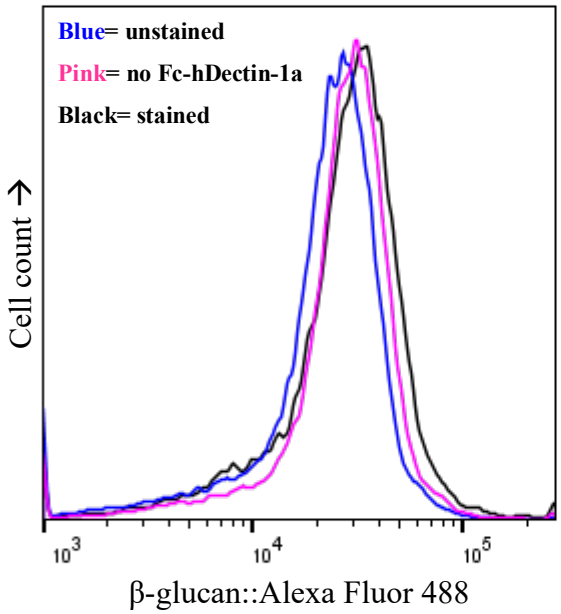

Figure 2-1. Flow cytometric analysis of THP-1 cells stained with Fc-hDectin-1a and Alexa Fluor 488-conjugated anti-Fc fluorochrome. Histogram shows that Fc-hDectin-1a does not bind to any molecule on the surface of THP-1. Figure shown is a representative of two independent experiments showing consistent results.

2.3.2 Effect of incubation temperature on β-glucan exposure

Recent articles showed that the temperature used to cultivate *C. auris* could either be 30°C (Mayr et al., 2020) or 37°C (Di Mambro et al., 2021). To confirm if growth temperature affects β-glucan expression in *C. auris*, β-glucan exposure level was measured after cells were grown at either 30°C or 37°C. Flow cytometric analysis of these cells revealed that there is no significant difference in β-glucan expression between yeast cells grown at 30°C and 37°C (Figure 2-2).

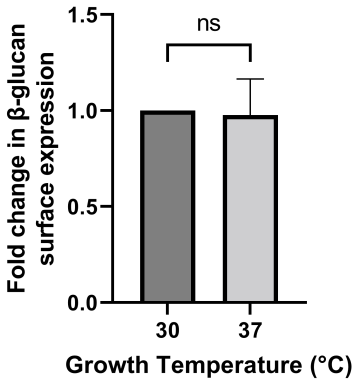

Figure 2-2. Effect of ambient temperature on the surface expression of β-glucan in *C. auris* after a 5-h incubation in Minimal medium with 2% glucose.

2.3.3 Effect of the presence of alternative carbon source on β-glucan exposure

The effect of presence of alternative carbon source, such as lactate and glycerol, in the expression of β-glucan in the surface of *C. auris* cells was determined. Lactate is abundant in the colon (Cummings, 1981) and is a significant physiological metabolite found in other *Candida* niches, such as the vaginal tract and blood, or produced by the host microbiota (Flint et al, 2012), with which *Candida* interact. Interestingly, Ene et al (2012) discovered that host carbon sources affect host-pathogen interactions such that in the presence of lactate, *C. albicans* becomes more resistant to antifungal drugs and osmotic and cell wall stresses.

Although the analysis of β-glucan masking in *C. albicans* has been extensively done previously, in this study, β-glucan masking experiments for *C. auris* was performed alongside *C. albicans* for comparison purposes. *C. auris* cells were grown in varying culture conditions and were subjected to β-glucan analysis by flow cytometry. The median fluorescence intensities of β-glucan::Alexa Fluor 488 in each sample were recorded and the fold change in β-glucan surface exposure relative to the control was computed. Figure 2-3 and Figure 2-4 show that in *C. auris* UI001, β-glucan masking is triggered in the presence of 0.5%, 1%, and 2% lactate (average fold change = 0.43, 0.32, and 0.56, respectively). A fold change value of less than or equal to 0.60 corresponds to β-glucan masking (Pradhan et al, 2018). To date, this is the first study to detect lactate-induced β-glucan masking in *C. auris*.

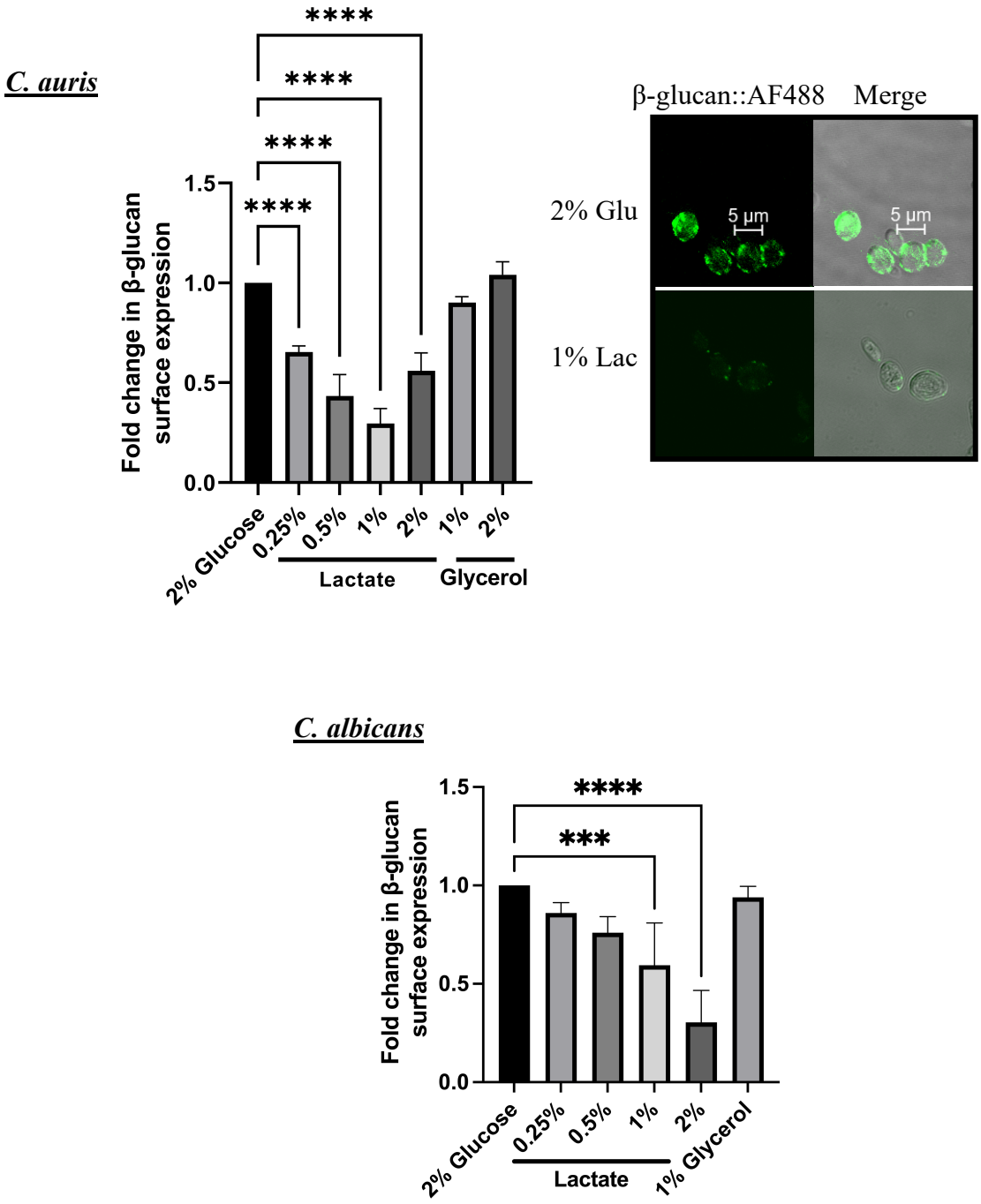

Figure 2-3. Effect of carbon source on the expression of β-glucan in the surface of *C. auris* UI001 (upper panel) and *C. albicans* SC5314 (lower panel). *C. albicans* did not grow in 2% glycerol.

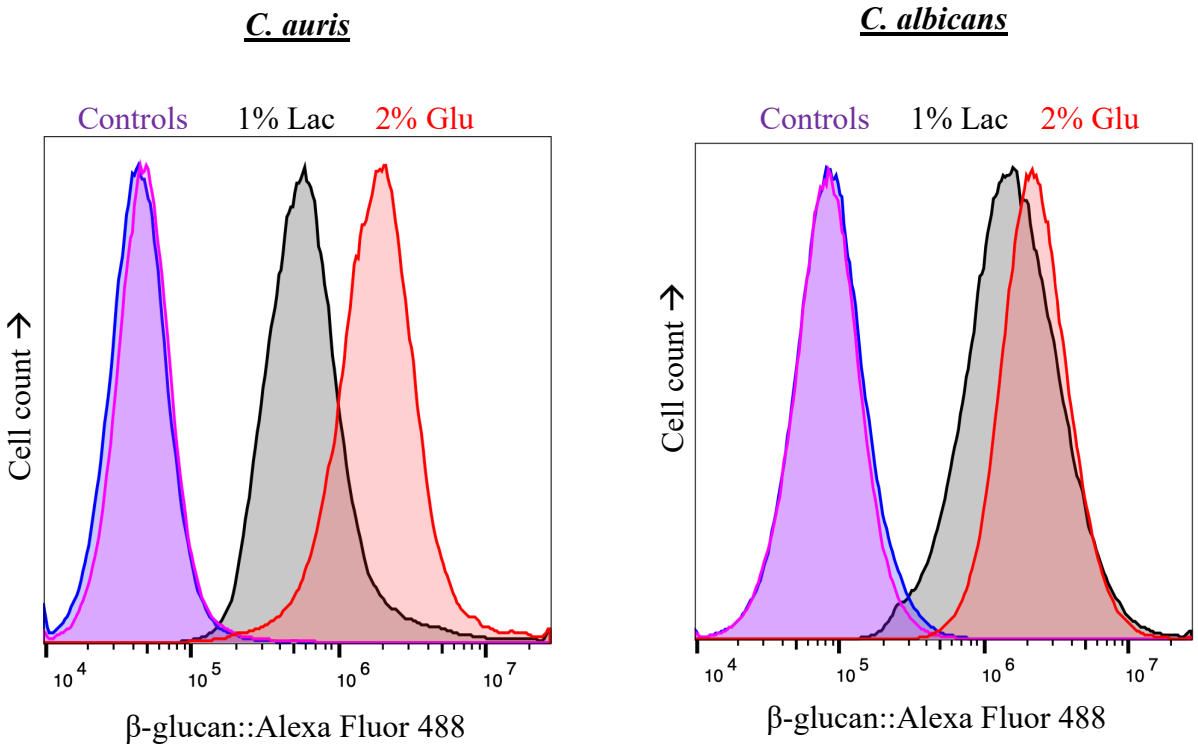

Figure 2-4. Flow cytometric analysis of lactate-grown *C. auris* (left) and *C. albicans* (right) stained with Fc-hDectin-1a and Alexa Fluor 488-conjugated anti-Fc fluorochrome. Histogram shows that there is reduction in β-glucan when cells are grown in 1% lactate. Figure shown is a representative of eight independent experiments showing consistent results.

Consistent with previous studies, β-glucan masking was observed when *C. albicans* is grown in 1% and 2% lactate, with a mean fold change of 0.60 and 0.30, respectively. To confirm whether this phenomenon is not due to differences in the pH of the medium, a biological buffer 50 mM MES (Wako et al, 2013), was added and the initial pH of the medium was adjusted to 5.5. Then, culture medium was filter-sterilized to avoid a change in pH during autoclaving. Both *C. auris* and *C. albicans* grew well in this medium. However, the control medium with 2% glucose is a bit yellowish compared to the others so the data collected might not be reliable.

Next, the effects of initial pH and glucose concentration on lactate-induced β-glucan masking in both *C. auris* (Table 2-1) and *C. albicans* (Table 2-2) were determined. Minimal medium plus 2% glucose (pH 5.86) was used to check if a slight difference in initial pH could affect β-glucan surface exposure in *Candida* and if the β-glucan masking effect observed in *C. auris* grown in 1% lactate (Figure 2-3) is due to difference in pH compared to the control. Minimal medium plus 1% glucose (pH 5.86) was used to check if the initial amount of glucose in the media affects β-glucan in the yeast cell wall.

Table 2-1. Lack of the contributing effect of initial pH and glucose concentration on lactate-induced β-glucan masking in *C. auris* UI001.

Carbohydrate Source	**Initial pH**	***Candida auris* UI001**		
		pH after 5-h incubation	$O.D_{600}$ after 5-h incubation (initial = 0.20)	Fold change in β-glucan surface expression vs. control^
2% glucose (control)	5.20	3.17 ± 0.04	0.72 ± 0.06	
2% glucose	5.86*	3.34 ± 0.06	0.80 ± 0.01	0.92 (N.S.)
1% glucose	5.86*	3.32 ± 0.04	0.79 ± 0.01	0.97 (N.S.)

*pH is the same as the medium with 1% lactate

^N.S. = not significant after t-Test analysis

Table 2-2. Lack of contributing effect of initial pH and glucose concentration on the lactate-induced β-glucan masking in *C. albicans* SC5314.

Carbohydrate Source	**Initial pH**	***Candida albicans* SC5314**		
		pH after 5-h incubation	$O.D_{600}$ after 5-h incubation (initial = 0.20)	Fold change in β-glucan surface expression vs. control^
2% glucose (control)	5.20	3.15 ± 0.02	0.82 ± 0.03	
2% glucose	5.86*	3.39 ± 0.00	0.79 ± 0.00	0.91 (N.S.)
1% glucose	5.86*	3.41 ± 0.03	0.78 ± 0.03	0.95 (N.S.)

*pH is the same as the medium with 1% lactate

^N.S. = not significant after t-Test analysis

Based on Table 2-1 and

Table 2-2, a slightly higher starting culture medium pH (5.20 versus 5.86) and the decrease in initial glucose concentration did not trigger β-glucan masking in *C. auris* and *C. albicans*. Therefore, for *C. auris* and *C. albicans,* the presence of lactate, not pH change, could trigger β-glucan masking.

In earlier experiments, both *C. auris* and *C. albicans* were incubated for 5 h before β-glucan analysis. To investigate whether β-glucan masking could occur at other time points, cells were grown in Minimal medium with 1% lactate from 1 h to 7 h. Figure 2-5A shows that for *C. auris,* there is a significant reduction ($P < 0.05$) in β-glucan after 5-h incubation. Figure 2-5B shows that an incubation of 5-7 h triggers a significantly lower β-glucan expression compared to an incubation of 1-3 h. On the contrary, there is a similar level of reduction in β-glucan expression in *C. albicans* grown in lactate for 1 h to 7 h (Figure 2-5C, Figure 2-5D) revealing that lactate-induced β-glucan masking occurs independently from the growth phase of *C. albicans*.

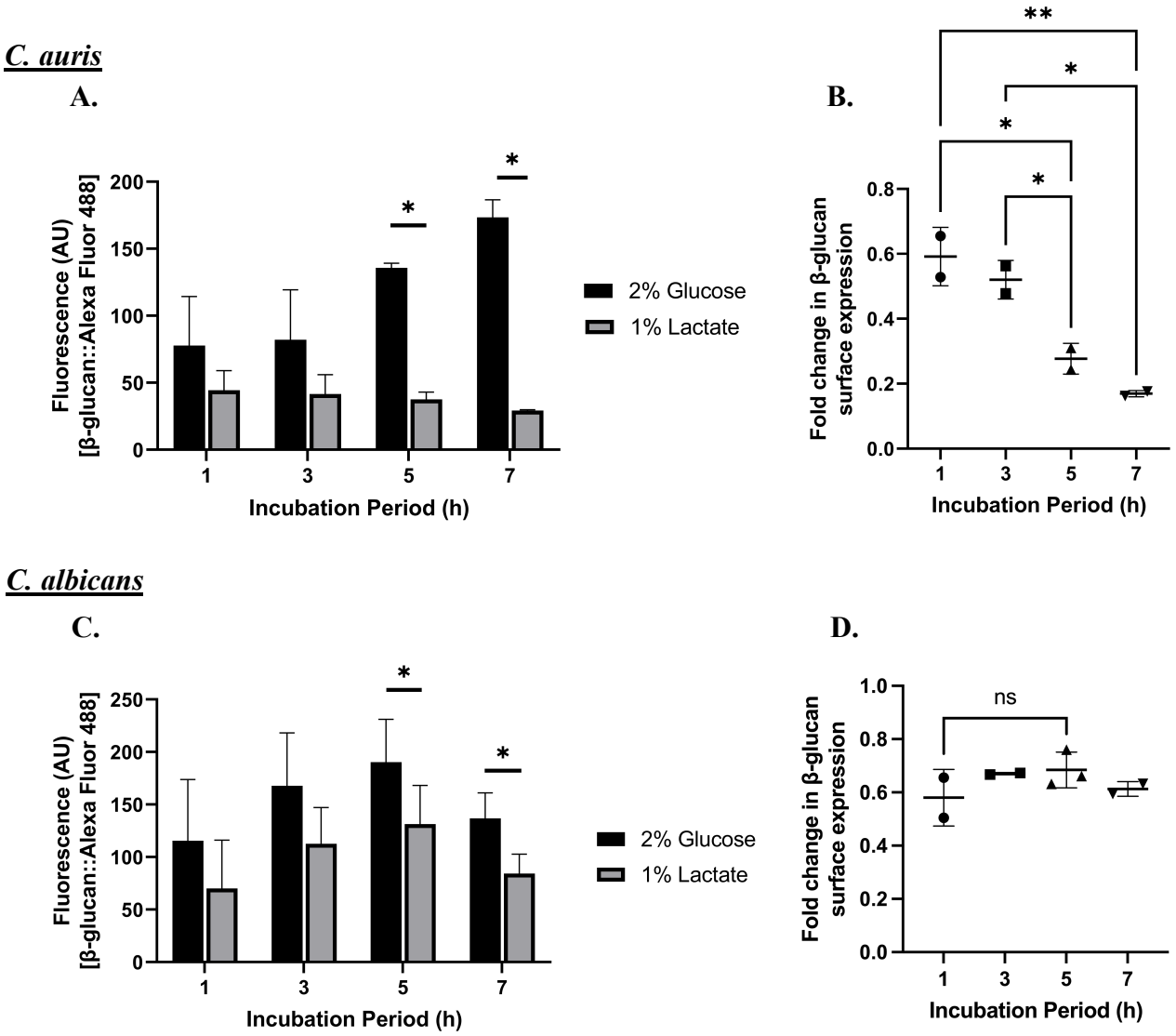

Figure 2-5. β-glucan exposures of *C. auris* (A and B) and *C. albicans* (C and D) after 1 h to 7 h incubation in Minimal media with lactate.

2.3.4 Effect of environmental oxygen level on β-glucan exposure

The effect of oxygen level in *C. albicans* β-glucan surface expression was first described by Pradhan et al (2018). Hypoxia is an important condition observed in the lower gastrointestinal tract (Rosenbach et al, 2010) and in inflamed tissues. For example, infiltration of polymorphonuclear leukocytes to the site of infection is shown to lead to hypoxic conditions (Lopes et al, 2018). Oxygen concentrations vary in normal tissues. For example, oxygen ranges from 0.5 to 7% in the brain; 1–5% in the eyes; 4–12% in the liver, heart, and kidneys; and 3–5 % in the uterus (Ivanovic, 2009; Panchision, 2009). As shown in Figure 2-6 and Figure 2-7, the oxygen level during cell growth also affects β-glucan expression in *C. auris,* where there is a 41% reduction in β-glucan during hypoxic growth and also 41% reduction in *C. albicans*. In a study by Pradhan et al (2018), *C. albicans* displayed a 52% reduction in β-glucan during hypoxia.

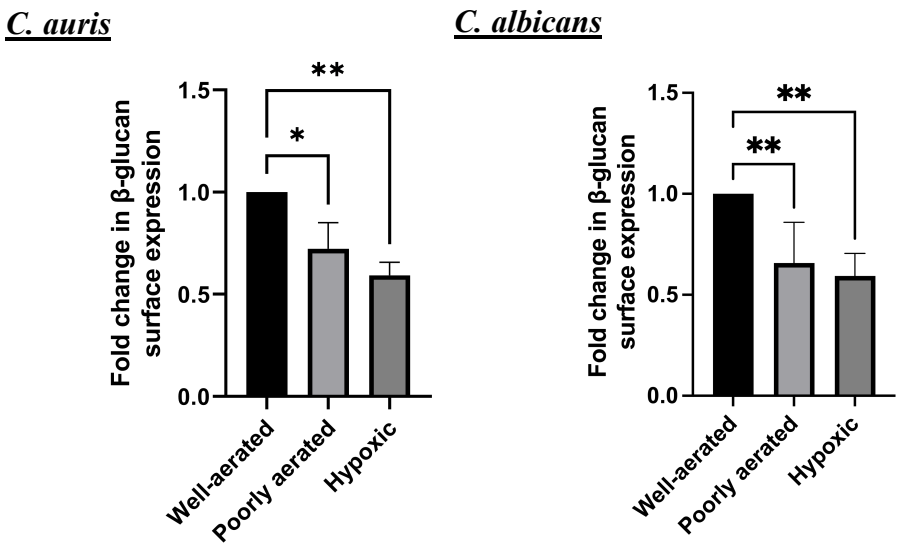

Figure 2-6. Effect of environmental oxygen level on the surface expression of β-glucan in *C. auris* (left) and *C. albicans* (right).

Results show that pathogenic *Candida* species show varying adaptations to hypoxic environments. In a study by Pradhan et al (2018), all strains of *C. albicans, C. krusei,* and *C. tropicalis* showed masking of β-glucan whereas clinical isolates of *C. auris*, as well as *C. parapsilosis* and *C. glabrata* isolates, showed variable results. All strains of *C. guilliermondii* do not exhibit β-glucan masking. This finding is validated by a subsequent article published in 2019, in which *C. albicans* grown under hypoxia exhibit a 50% reduction in exposed β-glucan (Pradhan et al, 2019).

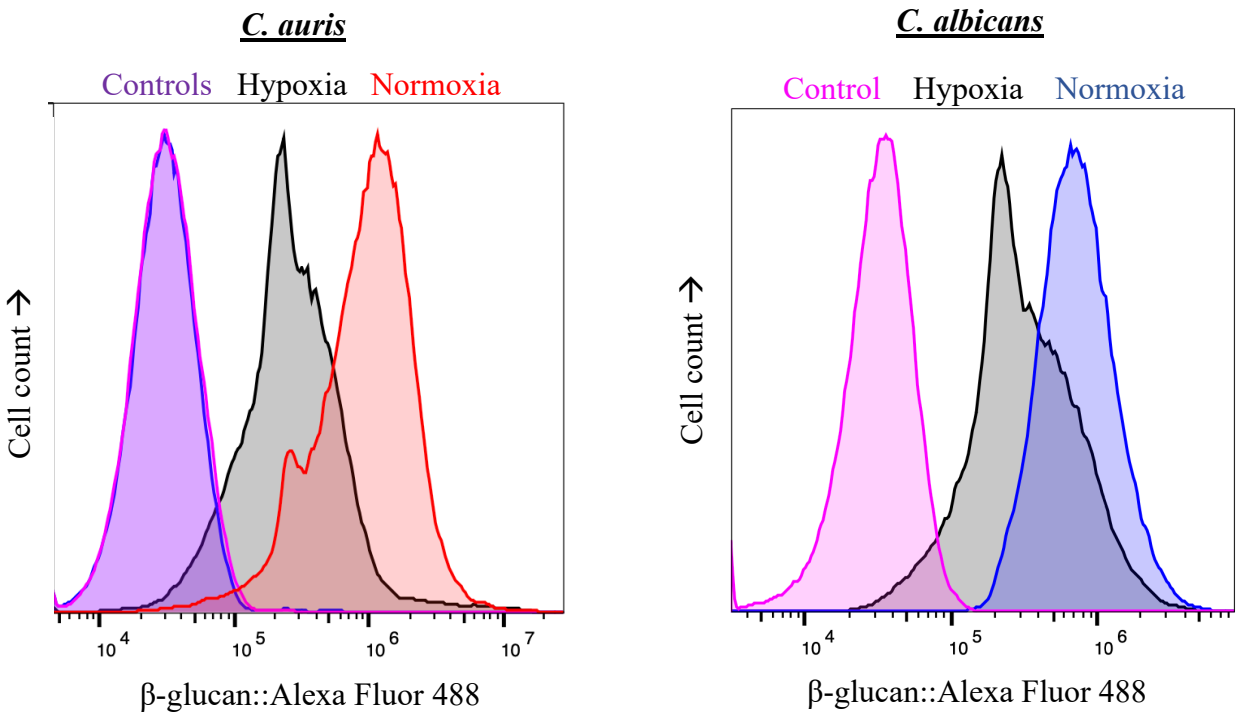

Figure 2-7. Flow cytometric analysis of hypoxia-grown *C. auris* (left) and *C. albicans* (right) stained with Fc-hDectin-1a and Alexa Fluor 488-conjugated anti-Fc fluorochrome. Histogram shows that there is reduction in β-glucan when cells are grown in hypoxic environment. Figure shown is a representative of at least three independent experiments showing consistent results.

2.3.5 Effect of pH on β-glucan exposure

The effect of a wide range of pH on the exposure levels of β-glucan was determined. To mimic the pH conditions in the gastrointestinal tract, yeast cells were grown in YPD with the following pH: 4, 5.5, 7, and 8.5. According to Surat (2018), the upper and lower stomach is around pH 4, the small intestine is close to pH 7.0 while the colon is approximately pH 8.5.

Cottier et al (2019) and Sherrington et al (2017) determined how *Candida* cell wall architecture is influenced by environmental pH. According to Sherrington et al (2017), acidic environments unmask β-glucan in *C. albicans* and *C. tropicalis* but not in *C. glabrata, C. parapsilosis, C. dubliniensis,* and *C. krusei*. In *C. albicans,* a significant difference in β-glucan is observed in cells grown in either a pH 4 or pH 6 YPD media but only within 2-5 h of culture. Relatively low ambient pH is associated with vulvovaginal niches, where certain *Candida* species are known to thrive. Furthermore, Cottier et al (2019) showed that the increase of β-glucan and chitin in clinical and laboratory strains of *C. albicans* and *C. dubliniensis* exposed in acidic environment is observed even after only 2 h of incubation. However, a “remasking” is observed

after 6 h. These observations were supported by Pradhan et al (2019) where it was shown that *C. albicans* grown at pH 4 displayed twice the amount of β-glucan on the cell surface compared with the cells grown at pH 5.5. β-glucan exposure also increases in cells grown at pH 8, compared to neutral pH, but not at significant levels. To date, there are little to no studies on pH-dependent β-glucan masking have been conducted in *C. auris*. Figure 2-8 and Figure 2-9 show that *C. auris* exhibits a similar β-glucan exposure profile to *C. albicans* when grown in a wide range of pH for 5 h. In both species, cells grown at pH 4 display increased β-glucan levels compared to pH 7.0. In *C. auris,* there is a six-fold increase in β-glucan while it is almost two-fold in *C. albicans.* In a study by Cottier et al (2019), a clinical strain of *C. auris* (strain name: JCH15448-1) did not show any pH- and time-dependent β-glucan and chitin masking.

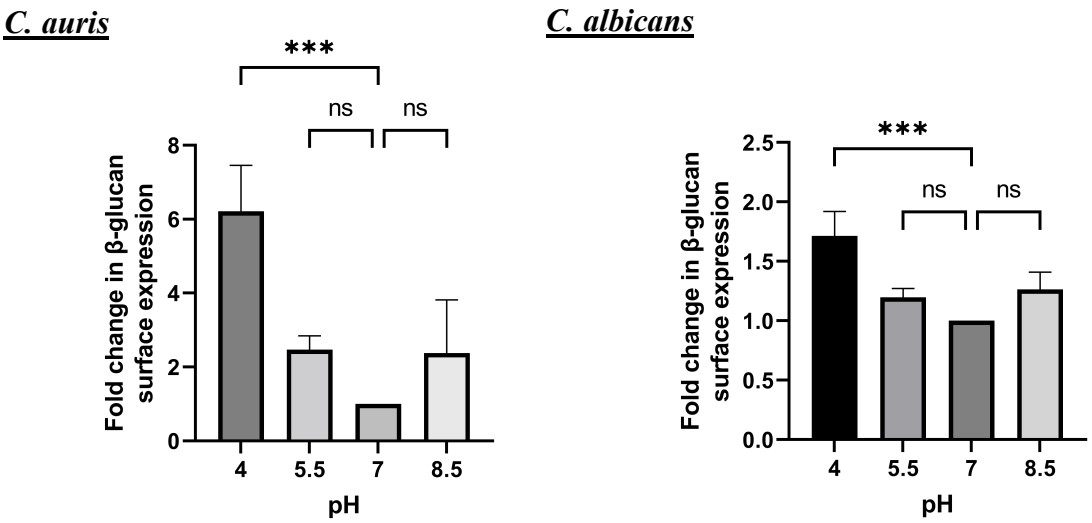

Figure 2-8. Effect of pH on the surface expression of β-glucan in *C. auris* (left and middle) and *C. albicans* (right).

From Figure 2-3 to Figure 2-8, it can be seen that the clinical strain of *C. auris* used in this study has a similar β-glucan expression profile to *C. albicans* SC5314 when grown in the different culture conditions tested in this study. A study by Navarro-Arias et al (2019) found that a clinical strain of *C. auris* isolated from India exhibits a highly similar cell wall composition and organization to *C. albicans* SC5314. The strain name of this clinical isolate is VPCI 479/P/13 and according to Yadav et al (2021), the strain belongs to clade I, the same as the clinical strain that was used in this research. This could explain why β-glucan exposure profile of C. *auris* UI001 is similar to *C. albicans* SC5314 in all conditions tested.

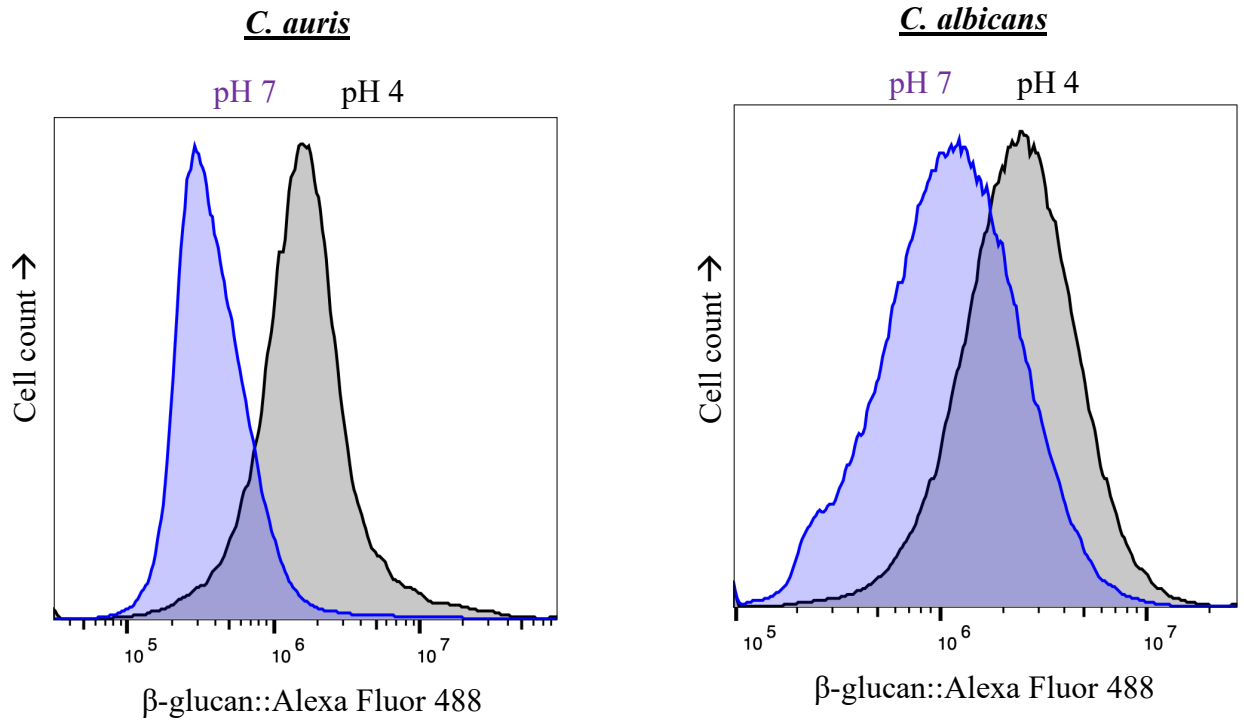

Figure 2-9. Flow cytometric analysis of *C. auris* (left) and *C. albicans* (right) grown in acidic and neutral pH and stained with Fc-hDectin-1a and Alexa Fluor 488-conjugated anti-Fc fluorochrome. Histogram shows that there is an increase in β-glucan when cells are grown in acidic pH. Figure shown is a representative of at least three independent experiments showing consistent results.

2.3.6 Effect of exposure to sublethal concentrations of antifungals on β-glucan exposure

According to a global surveillance report, 90% of *C. auris* clinical isolates are resistant to fluconazole (Lockhart et al, 2017), and a high percentage of isolates are resistant to at least two classes of antifungals. Previous studies have shown that antifungal drugs can elicit changes in the exposure of PAMPs, particularly β-glucan. This study aimed to determine whether a major PAMP in the cell wall of *C. auris* is affected when cells are exposed to sublethal concentrations of antifungals. The amount of antifungal added is considered "sublethal" since growth of cells are still observed despite the exposure to antifungals. A representative of each of the four different classes of antifungals - azole, echinocandin, polyene, and pyrimidine analog - was utilized. As shown in Figure 2-10, β-glucan masking occurs in *C. auris* in the presence of 16 μg/mL fluconazole (79% reduction) and 0.63 - 40 μg/mL micafungin (~42% reduction). There is also a slight reduction of β-glucan in the presence of 250 - 500 ng/mL 5-fluorocytosine (~26% reduction) but no change

in the presence of amphotericin B (AmB). The effect of dimethyl sulfoxide (DMSO), the solvent used to resuspend fluconazole and amphotericin B, was also determined. Both micafungin and 5-fluorocytosine were resuspended in sterile water.

Figure 2-10A (rightmost bar) shows that DMSO does not cause significant masking effects on cells. Therefore, the induction of β-glucan masking observed in the presence of 16 μg/mL fluconazole is only attributed to fluconazole, which disrupts the cell membrane by inhibiting the activity of lanosterol 14-α-demethylase (Hof, 2006). This result contradicts the data for the fluconazole-susceptible *C. albicans* SC5314*,* wherein exposure to a sublethal concentration of 0.25 μg/mL fluconazole triggers more β-glucan exposure (Pradhan et al, 2019). According to the CDC (2020), the tentative MIC breakpoint of fluconazole for resistant *C. auris* isolates is ≥ 32 μg/mL. So far, this is the first report of β-glucan masking in *C. auris* in the presence of sublethal concentrations of fluconazole. However, a concentration of 16 μg/mL fluconazole may not exist in patients. Pittrow and Penk (1997) determined fluconazole levels in human tissue and body fluids and there is approximately 1.26 μg/mL in the cerebrospinal fluid and 73 μg/g in the skin. Furthermore, according to a review article by Debruyne (1997), the maximum plasma drug concentration after a 100 mg oral dose is only 2 μg/mL. So, the concentration of fluconazole used in this study might not be present in actual patients of candidiasis.

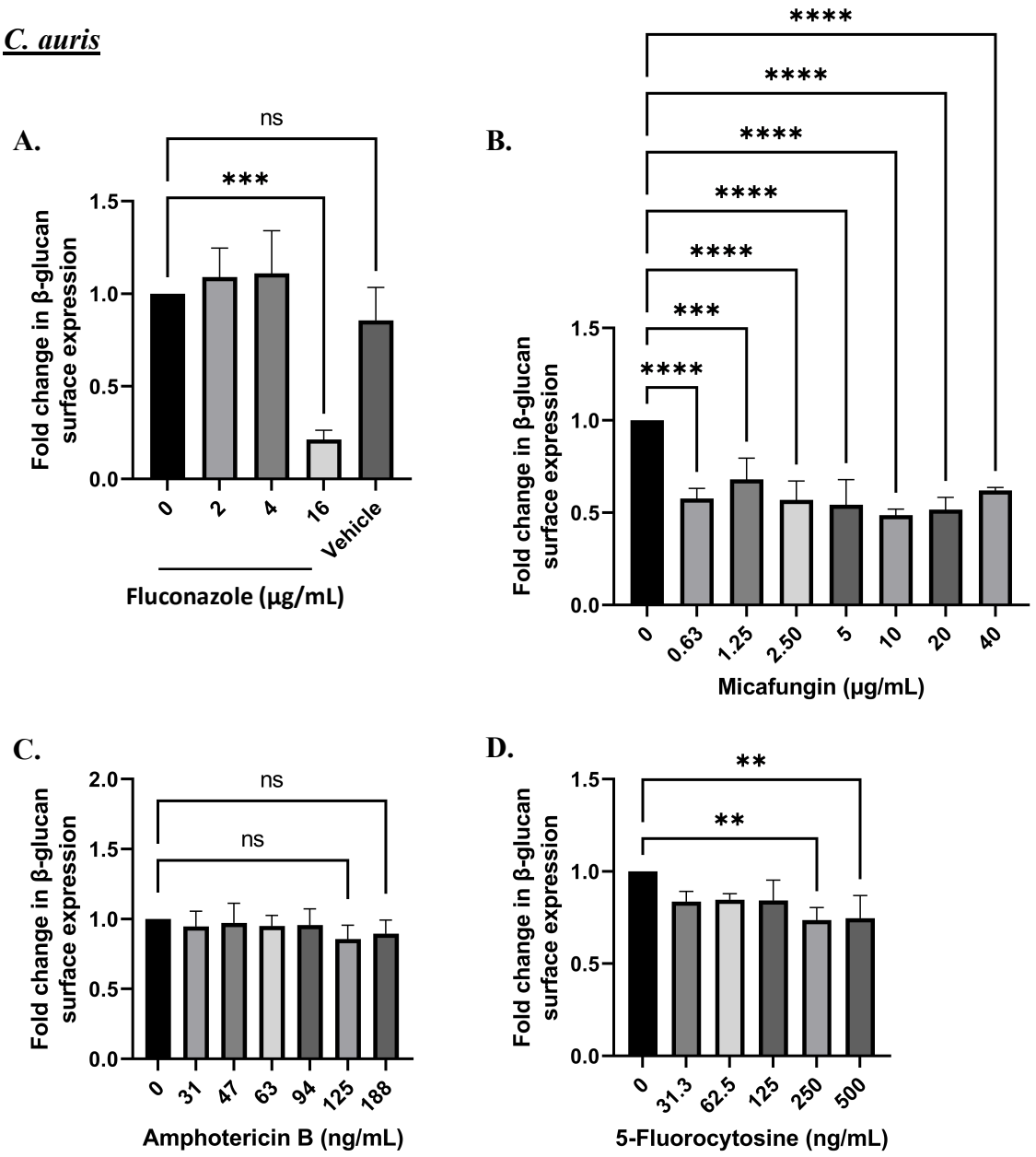

Figure 2-10. Effect of sublethal concentrations of Fluconazole (A), Micafungin (B), Amphotericin B and (C) and 5-Fluorocytosine (D) on the surface expression of β-glucan in *C. auris*. Fluconazole and Amphotericin B are resuspended in DMSO ("vehicle")

Figure 2-10B shows that sublethal concentrations of micafungin, which inhibits fungal 1,3-β-D-glucan synthase thereby interfering with fungal cell wall synthesis (Ikeda, 2003), could trigger β-glucan masking in *C. auris*. According to the CDC (2020), the tentative MIC breakpoint of micafungin for resistant *C. auris* isolates is ≥ 4 µg/mL; and the physiological concentration of micafungin is 4 µg/mL (Guembe et al, 2014). This study confirmed that β-glucan amount in *C.*

auris is decreased due to sublethal amounts of micafungin. To confirm whether yeast cells are still viable after 5 h incubation with antifungals, a 10 µL suspension was spotted on a YPD plate, which was then incubated at 37°C for 2 days. Growth was observed in all plates.

Exposure of *Candida* to antifungal drugs has previously been shown to affect the expression of proteins related to the cell wall. Chitinases such as *CHT2* and *CHT3* are markedly downregulated after exposure of *C. albicans* to micafungin (Kaneko et al, 2010), which is known to inhibit production of β-1,3-glucan. It is worth noting that during experimentation and based on visual inspection of the yeast cell suspension, *C. auris* cells grew poorly in the presence of low concentrations of micafungin (0.63 - 2.50 µg/mL) compared to when grown at high concentrations (20 - 40 µg/mL). This observation was consistent in all three independent replicates. Chamilos et al (2007) described this phenomenon as paradoxical growth, wherein resistant *Candida* sp. tend to grow more in a medium with higher concentration of an echinocandin, than in those with lower concentration.

Figure 2-11 shows that 250-1,000 ng/mL 5-fluorocytosine causes a slight reduction (~32%) in the cell wall β-glucan of the fluconazole- and micafungin-susceptible *C. albicans*. Although the statistical analyses showed that there are no significant differences between the cells grown with and without AmB, there is a slight increase in β-glucan when cells are grown in 94 - 188 ng/mL AmB (P = 0.2026). According to Pradhan et al (2019), sublethal concentrations of AmB led to increase in β-glucan amount on the surface of *C. albicans*.

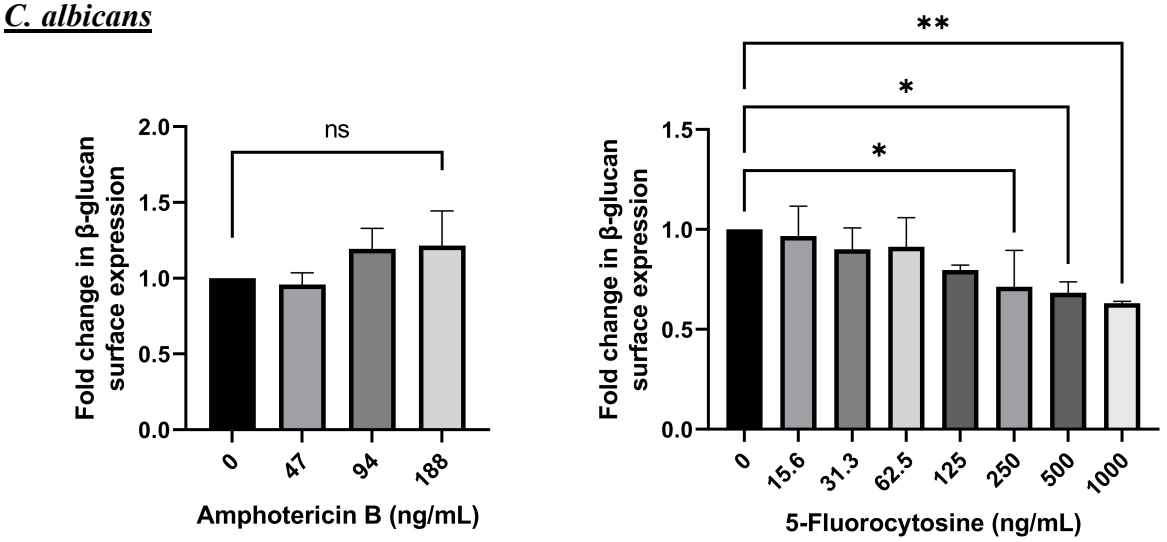

Figure 2-11. Effect of sublethal concentrations of Amphotericin B and (left) and 5-Fluorocytosine (right) on the surface expression of β-glucan in *C. albicans*.

Results of this study suggest that intake of inappropriate antifungals due to a misdiagnosed fungal infection may bring harm to a patient. In addition to the fact that most clinical isolates of *C. auris* are resistant to fluconazole, fluconazole could probably cause masking of an important PAMP, which could lead to evasion of immune surveillance (Lopes et al, 2018) thus reducing the immune response (Pradhan et al, 2019; Pradhan et al, 2018). This study reiterates how important it is to accurately identify the causative agent of systemic infection and to take antifungal drugs responsibly.

2.3.7 Effect of culture conditions on β-glucan exposure in other *C. auris* strains

To confirm if the β-glucan masking phenomenon observed in the clinical strain occurs in other isolates belonging to a different clade, the same experiments have been done in two ATCC strains such as MYA-5001 and MYA-5002. The former is also referred to as strain B11220, JCM 15448, CBS 10913, or DSM 21092 while the latter is also designated as strain B11221. Furthermore, MYA-5001 belongs to clade II and is isolated from the auditory canal of a patient in Japan, while MYA-5002 belongs to clade III and is isolated from the blood of a patient in South Africa (ATCC Product Sheet, 2020).

Figure 2-12 shows a summary of the β-glucan masking experiments performed. It is worth noting that, unlike UI001, lactate-induced β-glucan masking is not observed in both type strains whereas a low oxygen condition could trigger masking in *C. auris* MYA-5001 but not in MYA-5002. The expression profile of β-glucan towards a wide range of pH is different among strains of *C. auris.* The effect of antifungals on β-glucan was not experimented for these strains, as both strains do not show multidrug resistance.

In this study, a total of three *C. auris* isolates were tested, but cell wall remodelling due to lactate only occurred in one isolate (UI001). It is yet to be confirmed whether β-glucan masking is a general adaptation response of *C. auris*. Screening a larger panel of isolates would help identify whether cell wall remodelling occurs in different strains.

This study showed that different strains of *C. auris* have different cell wall responses to varying environmental conditions. Other studies have also observed differences between *C. auris* strains (Horton et al, 2024; Wang et al, 2022; Bruno et al, 2020). Therefore, we propose that mechanisms for environment-triggered cell wall remodelling may be different between strains regardless if they belong to the same clade. To date, there is no direct explanation about this phenomenon and thus serves as avenue for future research

***C. auris* ATCC:**

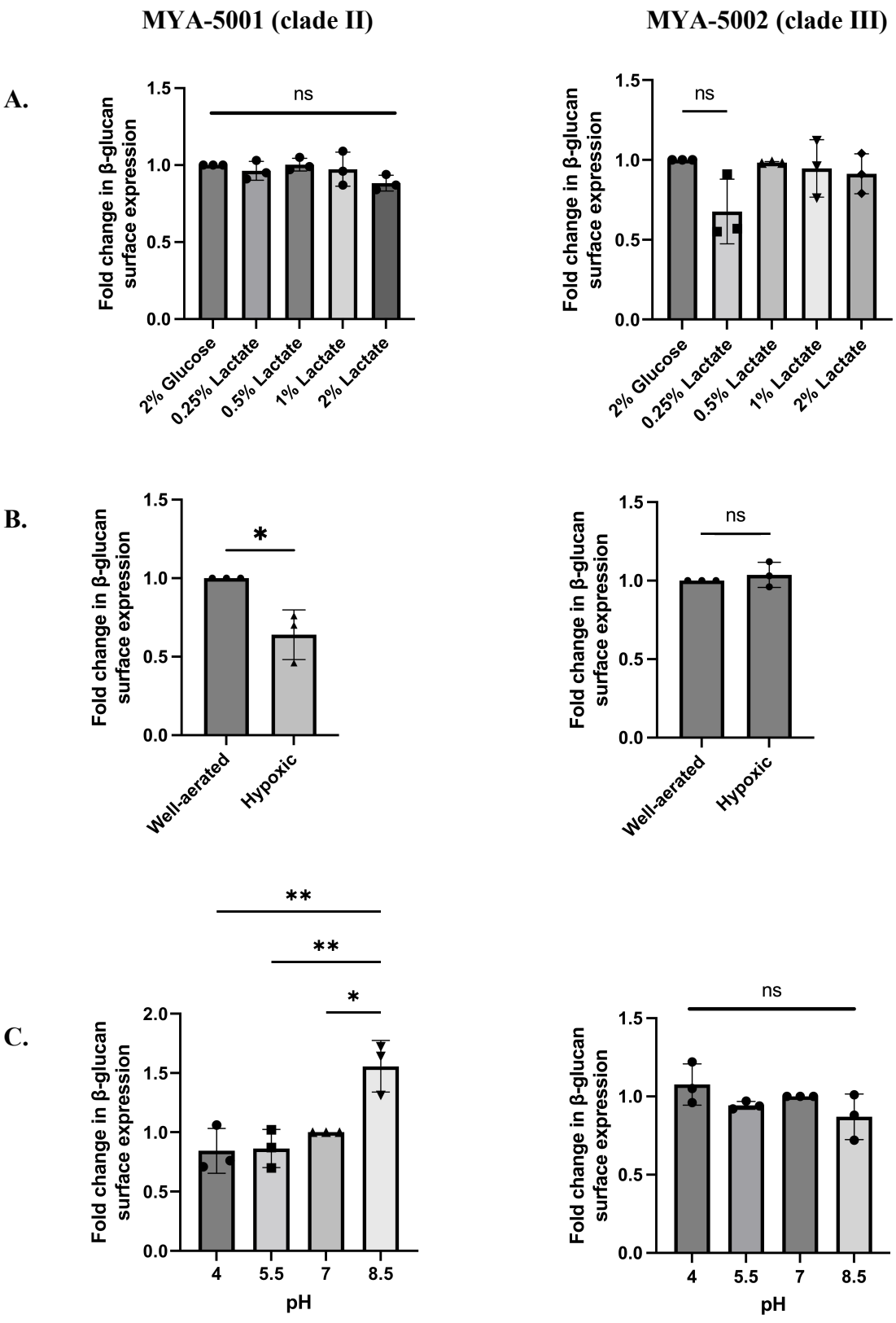

Figure 2-12. Effect of lactate (A), oxygen level (B), and pH (C) on β-glucan exposure in type strains of *C. auris*.

2.4 CONCLUSION AND RECOMMENDATION

This study provides evidence that β-glucan masking also occurs in the emerging fungal pathogen, *C. auris*. In particular, the following environmental stimuli triggered a decrease in β-glucan exposure: presence of lactate which is naturally found in the colon; lower oxygen levels that occur in some tissues of the body; and sublethal concentrations of antifungal drugs – fluconazole, micafungin, and 5-fluorocytosine. On the contrary, low pH triggers an increase in exposure levels of β-glucan. Further characterization of the lactate-induced β-glucan masking phenomena reveal that it is clade-specific and occurs during logarithmic growth (~5 h) of the cells. It is worth noting that the growth of *C. auris* strains used in this study is the same as the control under all environmental conditions tested except during low oxygen.

Determining the subsequent effect of this β-glucan masking phenomenon on the immune response against *C. auris* would be an interesting point of research. The results of this study shed light on the dynamics of β-glucan exposure in *C. auris* which could then help researchers understand more the immune response against various *C. auris* strains. Ultimately, this research aims to help develop novel strategies to combat the emerging pathogen, *C. auris.*

For future work, it will be worthwhile to check for β-glucan masking on physiological pH. Although this study is important to obtain a general picture of how dynamic β-glucan exposure is depending on varying conditions, it is essential to note that the glucose concentration that was used in the experiment is higher compared to the physiological blood glucose concentration. According to McMillin (1990), the glucose concentration in the blood is maintained at 80-120 mg/dL. The upper limit of this concentration is equivalent to 0.12% glucose. The culture medium used in this study is supplemented with at most 2% glucose, which is the standard glucose concentration in the yeast culture medium used in the laboratory.

It will also be interesting to find out if the masking observed is just a transient phenomenon, and if it is, how long will it be before unmasking occurs. Furthermore, it will be interesting to do the same set of experiments on a strain belonging to clades IV and V, to be able to show a probable clade-specific cell wall remodeling response of *C. auris* to varying environmental stimuli.

It is also recommended to check for chitin exposure levels across a wide range of pH, as unmasking of cell wall in *C. albicans* may induce non-protective hyperactivation of the immune system during growth in acidic environment

CHAPTER 3: CORRELATION BETWEEN BETA-GLUCAN AND MANNAN SURFACE EXPOSURE IN *CANDIDA AURIS*

3.1 INTRODUCTION

Cell walls provide cell rigidity and shape, confer protection from environmental stressors, and aid in metabolism and ion exchange. From the point of view of infection biology, the cell walls of fungal pathogens like *Candida* interplay with host defenses. The fungal cell wall contains relevant pathogen-associated molecular patterns (PAMPs) and epitopes for the immune response. These PAMPs are then recognized by the innate immune system of host cells via pattern recognition receptors (PRRs). A review article by Garcia-Rubio et al (2020) stated that the cell wall of the widely studied *Candida* species*, C. albicans,* is a two-layered structure. The main core is made up of a β-glucan-chitin skeleton (Figure 3-1), which is responsible for the strength and shape of the cell wall. Chitin is in the inner layer along with β-1,3-glucans, the most abundant molecule in the cell wall, which is then linked to β-1,6-glucans. The latter act as a linker molecule to bind different cell wall proteins to the β-1,3-glucan-chitin skeleton through glycosylphospatidyl inositol (GPI) proteins.

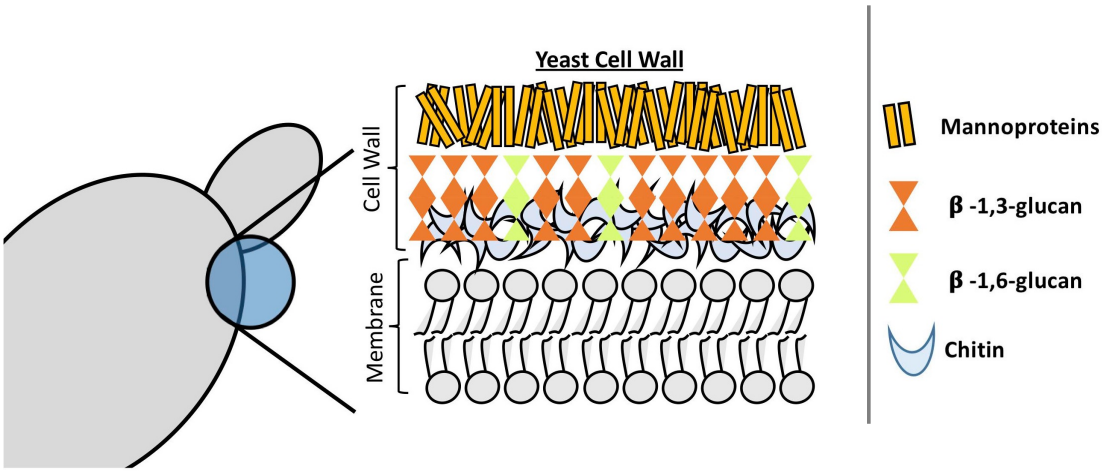

Figure 3-1. Structural organization and composition of *Candida albicans* cell wall. Figure modified from Garcia-Rubio et al (2020).

According to Shibata et al (2007), β-1,6-glucans are cross-linked to GPI-modified mannoproteins, which form the outermost layer of the cell wall. Distinct types of mannans are present. N-linked mannans are composed of α-1,6-mannose backbone with α-1,2-oligomannose sidechains capped with β-1,2- mono-, di-, tri-, or tetra mannans. On the other hand, O-linked

mannans, which are found to be associated with cell wall glycoproteins, are simple linear carbohydrates comprised of 1-5 residues of a series of α-1,2-linked mannose units (Hall and Gow, 2013).

Since mannans are found on the outermost part of the cell, Hernandez-Chavez et al (2017) argued that mannans affect exposure levels of β-glucan, thus affecting recognition of fungal pathogens by the host immune system. In fact, it has been shown that in *C. albicans,* nanoscale glucan exposure is controlled by mannan molecular substructures and that key enzymes like mannosyltransferases regulate the size and density of glucans in the nano scale level (Graus et al, 2018).

To show the potential inverse exposure levels of mannan and β-glucan, Tripathi et al (2020) revealed that *C. albicans* CAI4 grown in a medium without iron showed less β-glucan on the surface, which consequently also showed increased mannan. In contrast, the alteration of *C. auris* mannosylation genes, *PMR1* and *VAN1,* resulted in a decrease in mannose but an increase in the β-glucan content of the cell wall. A thinner mannan layer resulted in more exposed β-glucan residues (Horton et al, 2021).

With this information, it is interesting to find out if thickening of the mannan layer is the cause of the masking of β-1,3-glucan in *C. auris*. Even more so when *C. auris*-induced innate immune activation is elicited primarily by structurally unique *C. auris* mannoproteins (Bruno et al, 2020). In line with previous reports, β-glucan masking occurs due to cell wall remodeling. This chapter will address if β-glucan masking observed in *C. auris* has affected mannan surface exposure.

3.2 MATERIALS AND METHODS

3.2.1 Surface staining of mannan

Candida cells were cultured in the same way as described in Chapter 2. Cells were collected (5,000 rpm, 3 min, 4°C), washed with 1x PBS twice and stained with 100 µL 1x PBS with 50 µg/mL concanavalin A-tetramethylrhodamine (Thermo Fisher Scientific Inc., cat. # C860, 2 mg/mL stock solution in 0.1 M sodium bicarbonate) in the dark for 30 min at 4°C. Cells were washed twice with 1x PBS and fixed with 100 µL of 4% *p*-formaldehyde in 1x PBS in the dark for 15 min at 4°C. Cells were washed twice with 1x PBS and resuspended in 1x PBS prior to analysis. Unstained cells were used as control. For confocal microscopy observation, 5 µL of stained cell suspension were placed on a glass slide (Matsunami Superfrost Micro Slide Glass, S2443), covered

with micro-cover glass (thickness no. 1, Muto Pure Chemicals Co. Ltd.), sealed with nail polish, and kept in a closed container at 4°C until microscopy. Zeiss LSM780 upright confocal microscope was used to generate images.

3.2.2 Flow cytometry and statistical analyses

The EC800^{TM} flow cytometry analyser (Sony Biotechnology, Inc., Japan) with 488 nm and 561 nm lasers in combination with the FL2 (585/40) bandpass filter was used to analyse at least 100,000 cells from each sample. The gating strategy was kept constant in all analyses. To generate the histograms, FlowJo™ v10.8 Software (BD Life Sciences) was used.

The fold change is computed as the mean of the median fluorescence intensities (MFI) of mannan::TRITC in the experimental variable divided by the mean MFI of the control. The bar graphs were generated using GraphPad Prism version 9.4.0 for Windows (GraphPad Software, San Diego, California, USA, www.graphpad.com). Means and standard deviations from at least three independent biological replicates were shown and the data were analyzed using t-Test or one-way ANOVA with either Dunnett's multiple comparisons test or post-hoc Tukey HSD test. A *P* value of at least 0.05 is considered significant (*$P < 0.05$, **$P < 0.01$, ***$P<0.001$, ****$P<0.0001$).

3.3 RESULTS AND DISCUSSION

3.3.1 Comparison between the mannan content of *C. auris* and *C. albicans*

Mannans were quantified by staining the cells with concanavalin A conjugated with tetramethylrhodamine (TRITC). Concanavalin A selectively binds to α-mannopyranosyl and α-glucopyranosyl residues found in the cell wall of fungi and plasma membrane of mammalian cells (Chazotte, 2011). TRITC, on the other hand, is a bright orange-fluorescent dye that has excitation and emission wavelengths of 555 and 580 nm, respectively.

Several studies have been conducted to compare the abundance of cell wall components between *Candida* species. However, since *C. auris* is a relatively new species and is even considered an emerging pathogen, very little research has dealt with comparing the mannan of *C. auris* with those of the most studied, *C. albicans*. Chapter 2 showed that *C. auris* UI001 strain has a highly similar β-glucan masking profile with *C. albicans.* So, it would be interesting to find out if the mannan expression profile of these two species will also be similar. Figure 3-2 shows that *C. auris* UI001 has significantly less exposed mannans compared to *C. albicans* SC5314. This shows

that despite belonging to the same genus, differences in the abundance of cell wall components may be observed. A study by Navarro-Arias et al (2019) yielded a similar result when cell wall hydrolysates containing mannose and glucose were measured by high-performance anion exchange chromatography. Results show that a clinical strain of *C. auris* from India shows slightly lower mannan (30.8 ± 1.1% vs 36.1 ± 4.2) compared to *C. albicans* SC5314.

To confirm if this observation holds true regardless of the culture medium used to cultivate the cells, mannan exposure levels were measured in *C. auris* and *C. albicans* grown in either a minimal medium (Glucose Yeast Nitrogen Base) or a rich medium (Yeast extract Peptone Dextrose). Figure 3-2 shows that regardless of the type of medium, *C. albicans* have more exposed mannan. Whether these observed differences in the surface expression of pathogen recognition receptors would result to differences in the activation of downstream signaling leading to phagocytosis, cytokine release, and production of reactive oxygen species and nitric oxide remains to be investigated.

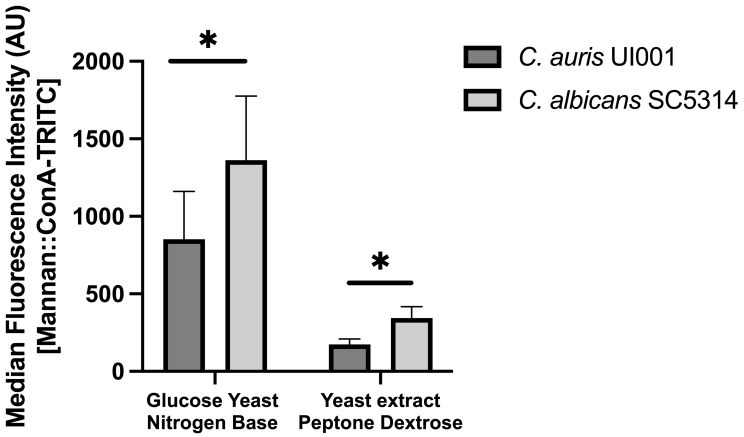

Figure 3-2. Comparison between mannan exposures of *C. auris* UI001 and *C. albicans* SC5314 grown in different culture media.

To give emphasis on the structural differences of mannans among *Candida* spp., Kogan et al (1988) showed that the mannan component of *C. krusei* cell wall is different from other *Candida* spp. based on branching and ratio of 1,2 and 1,6 side chains. Even mannans in clinical isolates of *C. auris* have also been shown to have unique structural features such as two distinct M-α-1-phosphate side chains determined by 2D COSY NMR spectroscopy analysis (Bruno et al, 2020).

3.3.2 Effect of environmental conditions on mannan exposure

This study attempts to shed light on to why β-glucan exposure is reduced in *C. auris* when exposed to certain environmental conditions. So far, little to no studies regarding the dynamics between β-glucan and mannan exposures has been performed on *C. auris*.

In Chapter 2, it was shown that lactate could trigger a significant reduction of β-glucan in both *C. auris* and *C. albicans.* Figure 3-3 shows that lactate has no effect on mannan exposure. The growth of *C. auris* strains used in this study is the same as the control under all environmental conditions tested except during low oxygen.

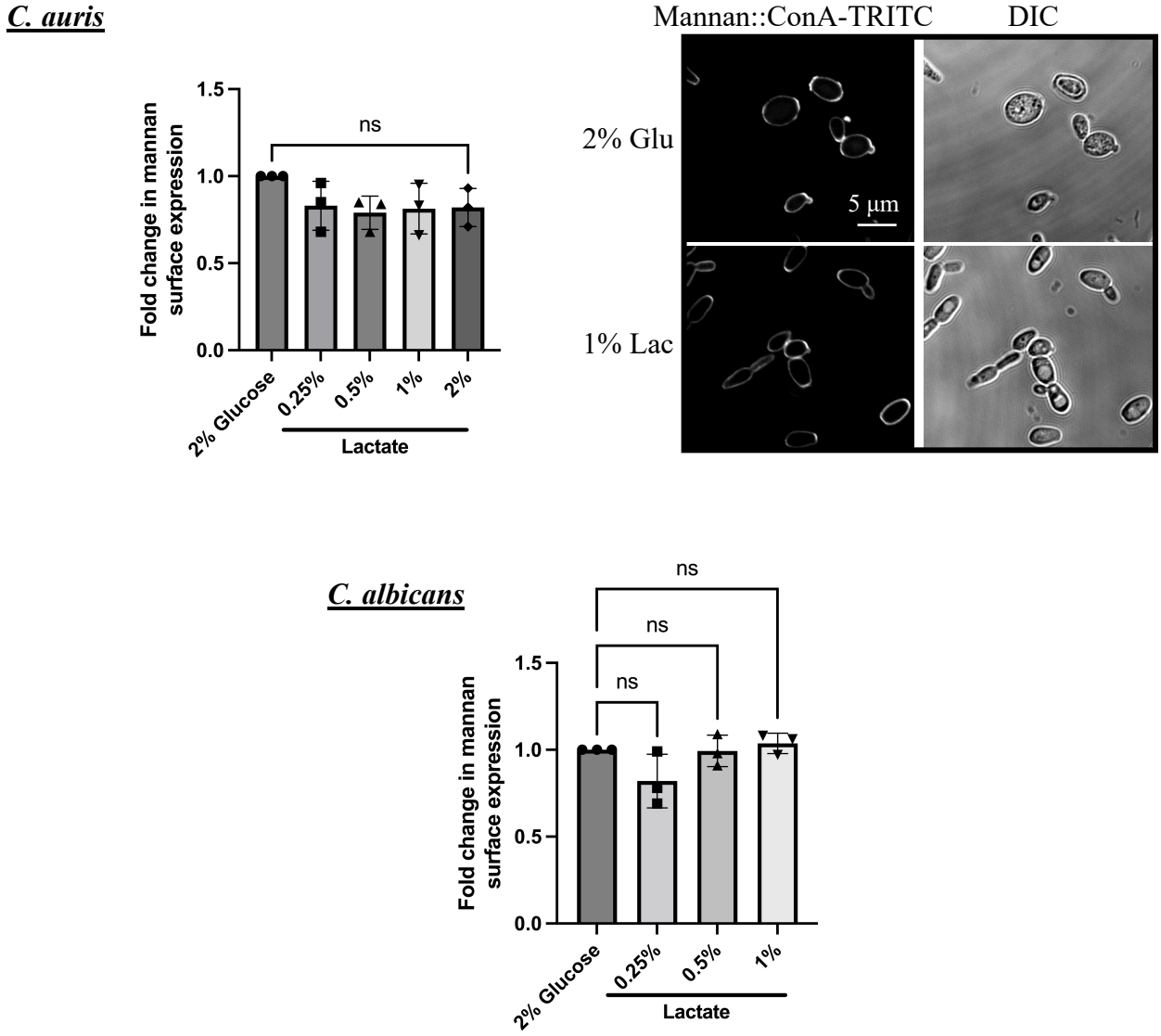

Figure 3-3. Effect of lactate on the surface expression of mannan in *C. auris* (upper panel) and *C. albicans* (lower panel).

This result is not in line with the hypothesis that increased mannan leads to masking of β-glucan. However, in confocal microscopy images published by Ballou et al (2017) and Childers et al (2020), lactate-grown *C. albicans* showed the same levels of mannan and less β-glucan compared to glucose-only grown cells. To confirm this result, both *C. auris* UI001 and *C. albicans* SC5314 were stained and viewed in a confocal microscope. It is clear from the microscopy images in Figure 3-3 that after a 5-h incubation in a medium containing 1% lactate, there is no change in mannan levels for both *C. auris* and *C. albicans*.

Several studies hinted about the possible non-inverse pattern between the exposure levels of cell wall β-glucan and mannan. Confocal microscopy images from Ballou et al (2017) showed that *C. albicans* CAI4 strain (wildtype) exhibited reduced β-glucan and mannan. In another study by Yang et al (2022), an *eng1* mutant strain of *C. albicans* showed higher exposure of β-glucan, due to the loss of an endoglucanase from *ENG1*, but mannan levels were unchanged. Lactate-induced β-glucan masking is mediated mainly through Eng1.

Next, the effect of hypoxia (Figure 3-4) and pH (Figure 3-5) on mannan exposure levels were determined. In Chapter 2, it was shown hypoxic conditions triggered 41% and 28% reduction in the β-glucan of *C. auris* and *C. albicans,* respectively. This time, *C. auris* showed a different pattern compared to *C. albicans*. In hypoxic environment, there is an insignificant 28% decrease in *C. auris* mannan and a significant 50% decrease in *C. albicans.* This observation is inconsistent with a previous study by Lopes et al (2018), where during hypoxic co-incubation of polymorphonuclear leukocytes with *C. albicans* for 2 h, there is no significant change in exposed β-glucan but an increase in exposed chitin and mannan.

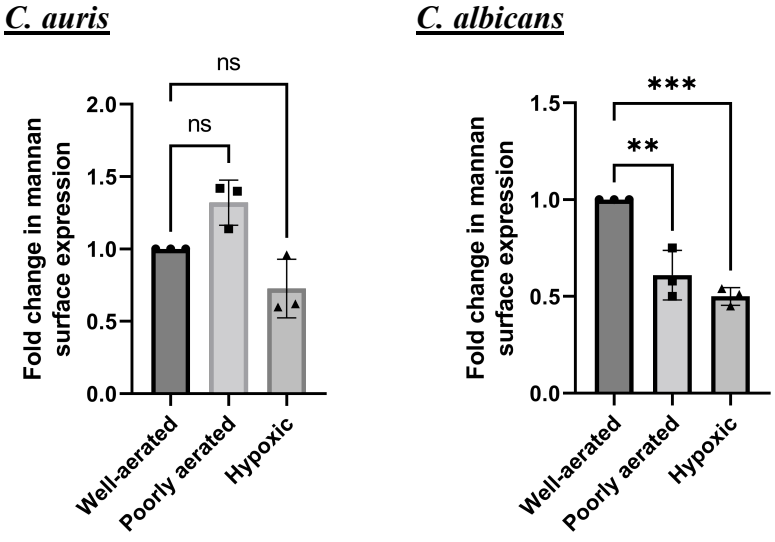

Figure 3-4. Effect of environmental oxygen level on the surface expression of mannan in *C. auris* (left) and *C. albicans* (right).

In Chapter 2, it was shown that in *C. auris,* there is a six-fold increase in β-glucan and almost two-fold increase in *C. albicans* when grown in low pH. For the mannan component, *C. auris* did not exhibit any changes throughout a wide range of pH. In *C. albicans,* acidic (pH 4) and basic (pH 8.5) environment triggered a 1.2x and 1.9x increase in mannan, respectively. Comparing this result with other studies, Sherrington et al (2017) determined how *Candida* cell wall architecture is influenced by environmental pH. It was shown that acidic environments (pH 4 versus pH 6) unmask β-glucan in *C. albicans* after 5 h of culture, but at this time point, there is an insignificant increase in mannan. So far, no studies have been done on *C. auris*.

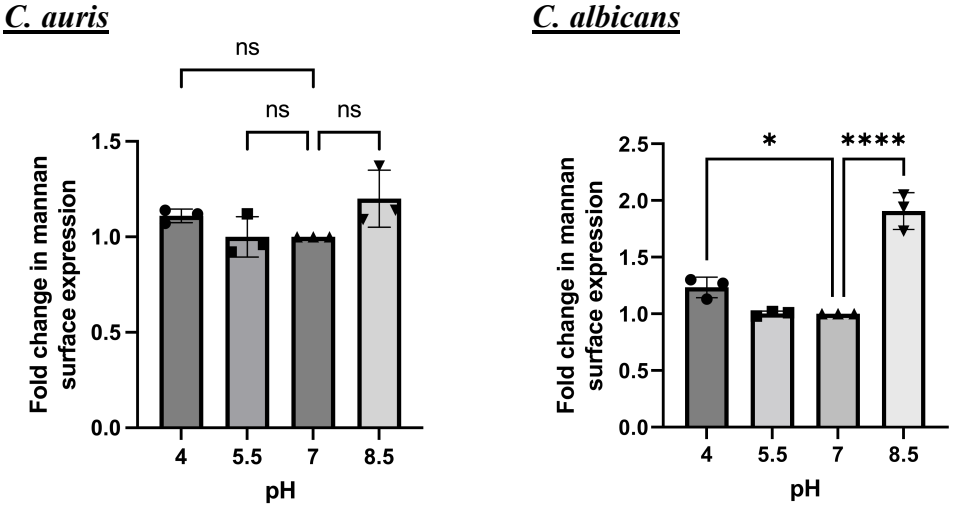

Figure 3-5. Effect of pH on the surface expression of mannan in *C. auris* (left) and *C. albicans* (right).

Next, the effect of β-glucan masking-inducing antifungals on mannan was determined. Figure 3-6 shows that there is no significant change in mannan in all antifungals tested. This supports our observation that β-glucan masking in both *C. auris* and *C. albicans* is not due to thickening of mannan.

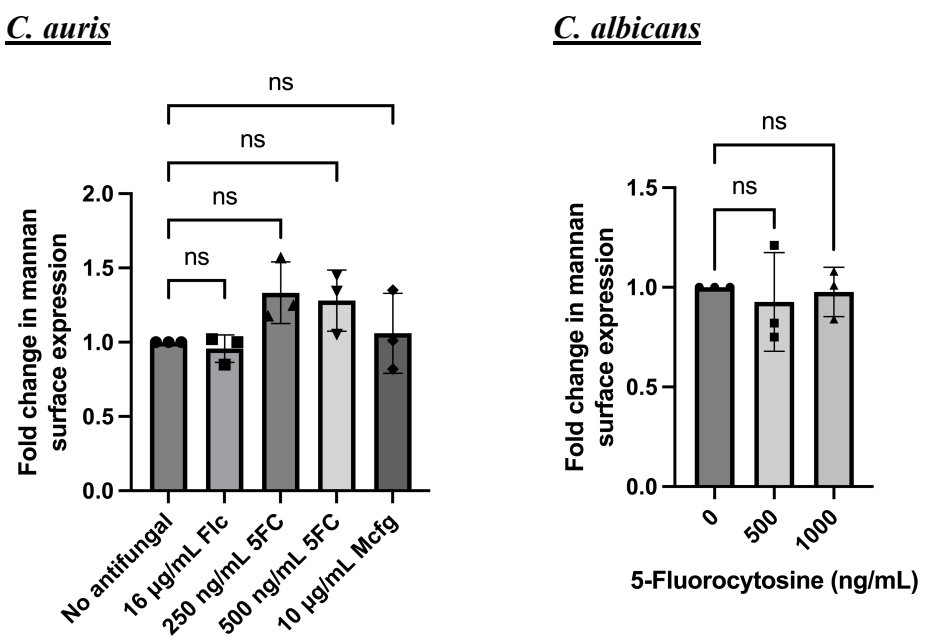

Figure 3-6. Effect of sublethal concentrations of antifungals on the surface expression of mannan in *C. auris* (left) and *C. albicans* (right).

To confirm if the mannan exposure levels observed in *C. auris* UI001 occur in other isolates belonging to a different clade, the same experiments have been done in two ATCC strains such as MYA-5001 and MYA-5002. Figure 3-7 shows that in the presence of up to 1% lactate, mannan levels remain unchanged in both type strains. Moreover, MYA-5001 grown in a hypoxic environment showed a 41% decrease in mannan, while β-glucan levels are reduced by 36% (Figure 2-12). For the effect of pH in MYA-5001, acidic (pH 4) and basic (pH 8.5) environment triggered a 1.3x and 1.7x increase in mannan, respectively. On the other hand, β-glucan was increased by 1.6x in pH 8.5 only (Figure 2-12).

To explain the variable mannan staining results between *C. auris* strains used in this study, Bruno et al (2020) revealed that two-dimensional COSY NMR spectroscopy analysis of mannans derived from clinical strains of *C. auris* belonging to clades I, II, and IV showed differences in structural features between and among strains.

3.4 CONCLUSION AND RECOMMENDATION

To date, there are no in-depth studies that determined the cell surface expression of mannan in *C. auris*, specifically by concanavalin A-TRITC staining and flow cytometry analysis. Results show that the initial hypothesis that the exposure levels of β-glucan and mannan occur in an inverse manner may be incorrect. However, it should be noted that concanavalin A is a nonspecific stain providing information only on the total amount of mannan and not the specific structure.

In this study, it was observed that thickening of mannan is not the cause of the reduction of β-glucan exposure in *C. auris*. Several studies have hinted at this and so, we hypothesize that although there is no direct correlation between β-glucan masking and mannan levels in *C. auris*, there is a possibility that a change in mannan structure led to less accessibility of β-glucan.

A summary of all staining experiments, as shown in Figure 3-8, reveals that mannan exposure levels are independent from β-glucan. It is also evident that each of the strains used exhibit different cell wall profiles depending on the environmental condition. This clearly supports the idea that the *Candida* cell wall is highly dynamic and diverse, and changes observed are strain-specific.

As a recommendation, microscopic imaging techniques such as fluorescence-based confocal laser scanning microscopy can be employed to complement all the flow cytometry-based experimental results generated in this study. Other studies performed transmission electron microscopy to measure the thickness of major PAMPs after growth in a certain environmental condition. However, Childers et al (2020) concluded in their study that there is no correlation between the thickness of the inner β-glucan-containing layer of the *C. albicans* cell wall and the degree of β-glucan exposure at the cell surface. For example, both hypoxia and iron limitation are strong triggers of β-glucan masking, but hypoxia leads to a thinner cell wall while iron limitation leads to a thicker cell wall.

***C. auris* ATCC:**

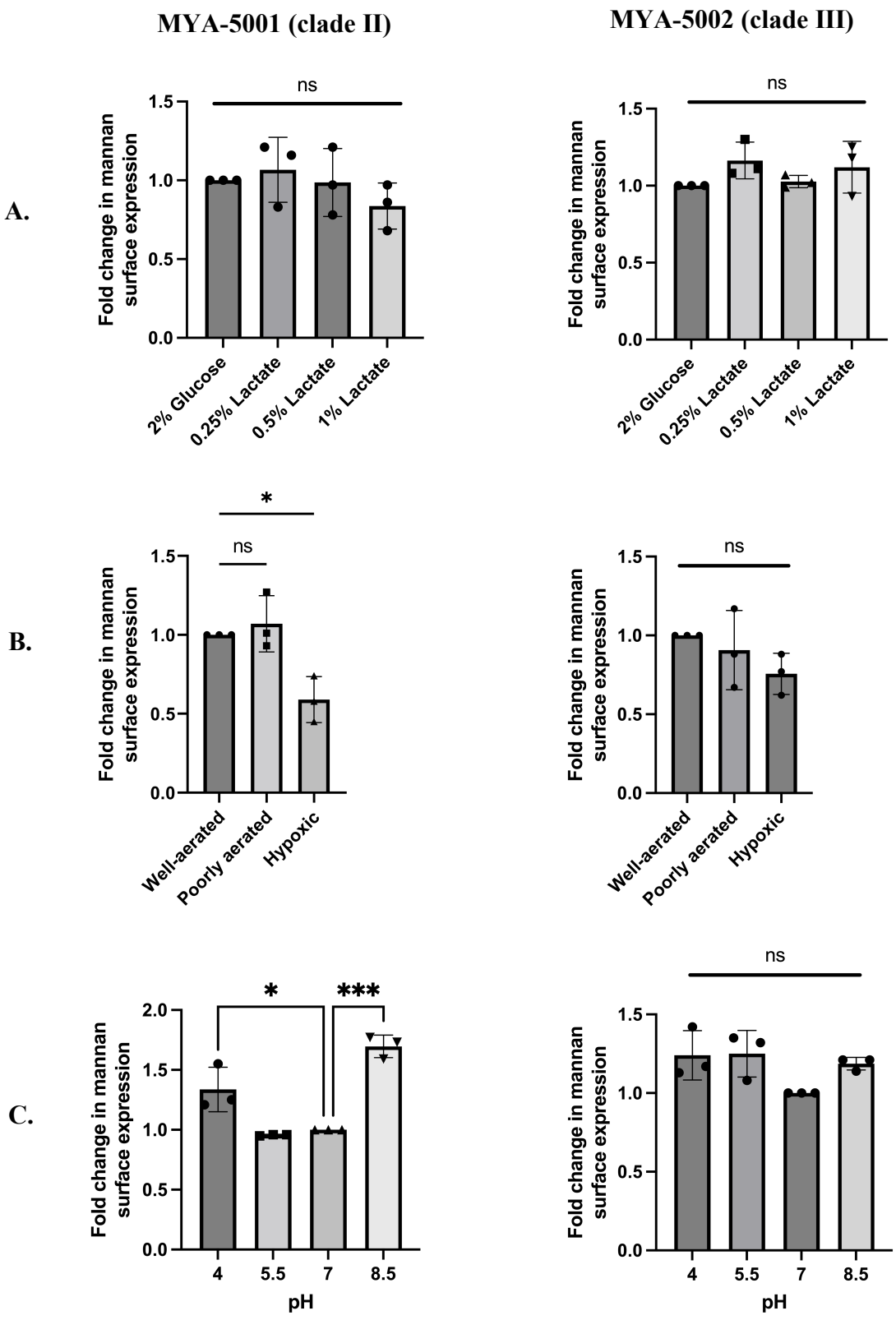

Figure 3-7. Effect of lactate (A), oxygen level (B), and pH (C) on exposure of mannan in type strains of *C. auris*.

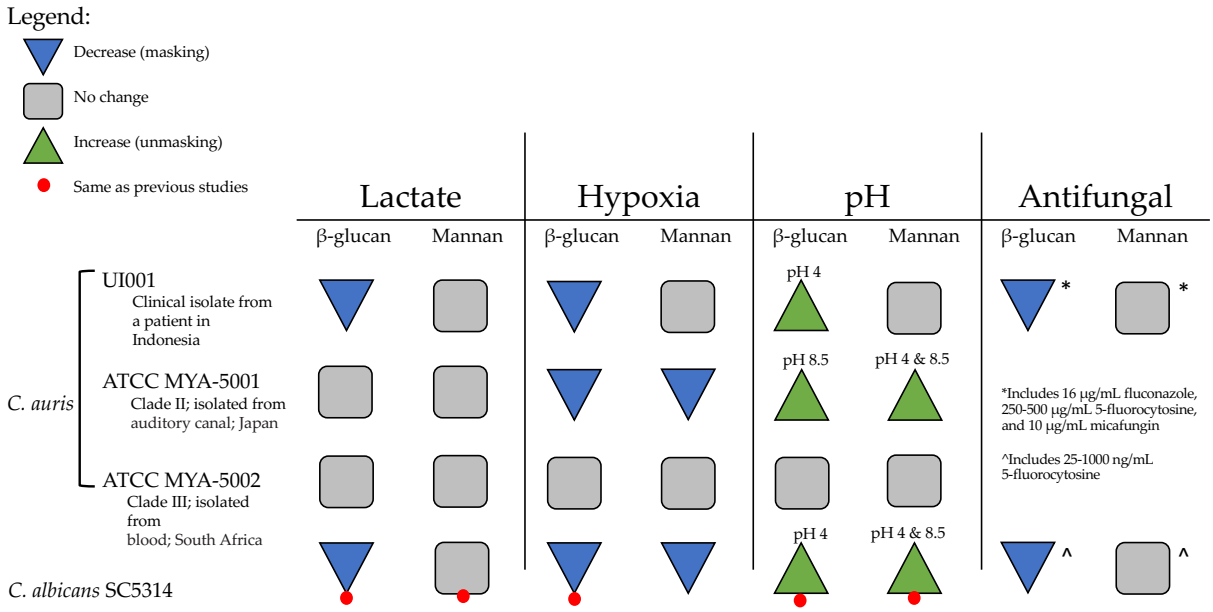

Figure 3-8. Summary of all the β-glucan and mannan staining performed on a clinical strain of *C. auris*, two American Type Culture Collection (ATCC) strains of *C. auris*, and *C. albicans* SC5314 grown for 5 h in different environmental conditions. Flc: Fluconazole; 5-FC: 5-Fluorocytosine; Mcfg: Micafungin.

CHAPTER 4: EFFECT OF BETA-GLUCAN MASKING IN *CANDIDA AURIS* ON THE HOST IMMUNE RESPONSE

4.1. INTRODUCTION

Candida auris is categorized as one of the four critical priority fungal pathogens by the World Health Organization. Despite this, the immune response against this emerging and often multi-drug resistant pathogen is still not well understood. *Candida* species, particularly the well-studied *C. albicans*, are commensal organisms that are naturally part of the human microbiome. However, several factors could trigger certain fungi to invade mucosal surfaces and cause mucosal or systemic candidiasis (Brown et al, 2012). Some *Candida* species developed effective immune evasion strategies to permit the colonization of an immunologically competent host.

As discussed in Chapters 2 and 3, *Candida* cell walls display three major PAMPs such as mannan, β-glucan, and chitin. These PAMPs are sensed by several PRRs on the surface of the host immune cells. A review article from Netea et al (2015) described the mechanisms for human immune defense against *Candida* infections. The major factor involved is the recognition of β-glucan by Dectin-1, which then results in the activation of myeloid cell signaling, fungal phagocytosis, and the production of proinflammatory cytokines. Several studies demonstrated that polymorphisms that impair Dectin-1 activity in humans are linked to aberrant cytokine responses, as well as a higher risk of recurrent mucocutaneous candidiasis and gut colonization. Other PRRs involved in the recognition of PAMPs in *Candida* are the C-type lectin receptors (CLR) such as dectin-2, macrophage mannose receptor (MMR), macrophage-inducible C-type lectin (Mincle), and dendritic-cell-specific intercellular adhesion molecule-3-grabbing non-integrin (DC-SIGN). Another major type of PRR is the Toll-like receptors (TLRs) such as TLR2 and TLR4, which recognize mannan-containing structures on the cell wall. These PRRs are described in Chapter 1.

Many studies have been done on *C. albicans.* However, Navarro-Arias et al (2019) concluded that current knowledge about *C. albicans* cell wall and its interaction with innate immune cells cannot be extrapolated to *C. auris* and other species like *C. tropicalis, C. guilliermondii,* and *C. krusei*. Indeed, Kean et al (2020) showed that neutrophils preferentially targeted *C. albicans* in mixed cultures with *C. auris* and that *C. auris* evaded neutrophil capture via neutrophil extracellular trap formation. Horton et al (2021) and Johnson et al (2018) also observed the same neutrophil evasion characteristic of *C. auris.* According to Horton et al, *C. auris* cell wall mannosylation helped the cell evade neutrophil attacks in a manner different from other species like *C. albicans* and *C. glabrata*. Neutrophils did not efficiently recognize and kill *C. auris*

and multiple strains of *C. auris* were shown to exhibit evasion of neutrophil phagocytosis. Despite this, Bruno et al (2020) said that *C. auris* is a more potent inducer of host immune response compared with *C. albicans* despite not being able to cause lysis of macrophage.

Among all the immune cells, macrophages were chosen to be used in this study since according to Netea et al (2015), macrophages are the main immune cell populations responsible for host defense against systemic candidiasis. In addition, Kean et al (2020) revealed that, unlike neutrophils, macrophages have the ability to recognize and phagocytose *C. auris*. Even though *C. auris* share the same genus with the well-studied *C. albicans,* differences in their abilities to elicit an immune response may also be observed. Cytokines produced by macrophages were measured in this study. This is important since immunomodulation with cytokines can enhance the antifungal activity of monocytes, macrophages, and neutrophils and upregulate protective T-helper type 1 adaptive immune responses (Antachopoulos & Roilides, 2005).

This chapter aims to determine the effect of lactate-induced β-glucan masking in *C. auris* on the uptake and subsequent phagocytosis of macrophages derived from the human monocyte cell line THP-1 and murine macrophage cell line RAW 264.7. Furthermore, the ability of these macrophages to kill *C. auris* cells was determined, and the amount of cytokines (MIP-1α, TNF-α, IL-10, and IL-6) and reactive oxygen species (ROS) produced by macrophages were quantified.

A thorough understanding of host-pathogen interaction is indispensable. Results from this study shed light on the interplay between *C. auris* and the host immune system, which will then open new opportunities for the development of possible innovative antifungal strategies.

4.2 MATERIALS AND METHODS

4.2.1 Staining of *Candida* species with acridine orange (AO)

C. auris and *C. albicans* were inoculated in a Minimal medium (0.67% BD Difco™ yeast nitrogen base with ammonium sulfate, 2% glucose) with shaking overnight at 37°C and 30°C, respectively. Cells were transferred to fresh Minimal media (OD_{600} = 0.2) and incubated for 5 h before staining. Cells were collected at 5,000 rpm for 3 min, washed twice with 1x PBS, stained with 10 μg/mL acridine orange (Sigma Aldrich, cat. # 318337-1G) for 20 min in the dark and in ice, washed twice with 1x PBS, and resuspended in PBS before flow cytometric analysis. The influence of the cell growth phase on the fluorescence intensity of acridine orange-stained *C. auris* was determined. Cells grown overnight were sub-cultured to a fresh medium (OD_{600} = 0.2) and grown in Minimal medium with 2% glucose for varying number of hours. Cells collected at certain

time points were washed twice with PBS and kept in PBS at 4°C until AO staining. Cells in the lag, logarithmic, and stationary phases are collected after 2 h, 8 h, and 24 h, respectively. All samples were stained at the same time and analyzed by flow cytometry. For each time point, the absorbance reading at 600 nm was determined by spectrophotometry. Moreover, cell concentration was determined by cell counting in a hemocytometer and serial dilution and spread plating in YPD.

For the flow cytometric analysis, EC800™ Flow Cytometry Analyzer (Sony Biotechnology, Inc., Japan) with 488-nm laser in combination with FL1 (525/50) and FL2 (585/40) bandpass filters were used to analyze cells from each sample. The gating strategy used was the same as the previous experiments described in chapters 2 and 3.

4.2.2 Phorbol 12-myristate 13-acetate (PMA) differentiation of THP-1

Following the protocol of Baxter et al (2020), 5 ng/mL PMA is added to THP-1 cells (ATCC TIB-202). After 24 h, the medium was removed and replaced with fresh RPMI with L-glutamine and phenol red (Nacalai Tesque, cat # 30264-85) supplemented with 10% FBS (Gibco) and 1% penicillin-streptomycin (Gibco, cat # 15140-122). The cells are incubated for 5 more days before analysis.

4.2.3 Co-incubation of stained *C. auris* and M0 macrophage and measurement of % phagocytosis

This protocol is adapted from Navarro-Arias et al (2019). AO-stained yeast cells resuspended in RPMI were added to PMA-differentiated THP-1 cells (3 x 10^5 cells/well in a 12-well plate). Plates were centrifuged for 10 min at 3,000 rpm and incubated for 2 h at 37°C and 5% CO_2. Cells were washed twice with cold 1x PBS, detached using 0.25% trypsin-EDTA (Gibco, cat # 25200-072), and incubated for 5 min at 37°C and 5% CO_2 with occasional mixing. Fresh RPMI was added and cells were transferred to a 1.5 mL microcentrifuge tube, centrifuged at 2,000 rpm for 2 min, washed twice with PEB buffer (1x PBS, 2.5 mM EDTA, 0.1% BSA), and resuspended in PEB buffer with 0.1% trypan blue. Because cells tend to clump, a cell strainer with a 40 µm mesh size (Funakoshi, cat. #HT-AMS-04002) was used before analysis. EC800™ Flow Cytometry Analyzer (Sony Biotechnology, Inc., Japan) with 488 nm and 561 nm lasers in combination with FL1 (525/50) and FL2 (585/40) bandpass filters were used to analyze at least 10,000 macrophage cells from each sample. The gating strategy was kept constant in all analyses. The early stage of the phagocytic event was analyzed from counted events in the green channel (FL1) whereas the late stage of the phagocytic event, wherein yeast cells are within acidified phagolysosomes, was

counted from the red channel (FL2). Macrophages without added yeast serve as the control. A phagocytosis assay was also performed using two reference strains of *C. auris.* ATCC MYA-5001 belongs to clade II and is isolated from the auditory canal of a patient in Japan, while ATCC MYA-5002 belongs to clade III and is isolated from the blood of a patient in South Africa (ATCC Product Sheet, 2020). To determine the effect of laminarin, yeast strains were grown in YPD for 4 h, collected, and used in the phagocytosis assay. A 100 µg/mL laminarin (InvivoGen, cat # tlrl-lam) was added to macrophages an hour before adding the yeasts.

4.2.4 Induction of macrophage lysis

To induce lysis of macrophages, 1% Triton X-100 was added to macrophage cultures until a final concentration of 0.5%. Plates were then kept at RT for 15 min with occasional mixing. Serial dilutions were prepared, and samples were spread-plated in YPD agar. After 48 h of incubation at 37°C, the number of viable yeast cells was determined by CFU counting. Controls consisting of yeast cells grown under the same conditions but without macrophages were used. The percentage of yeast cells killed by macrophages was calculated according to the following equation: % yeast killing = [(CFU of control well − CFU of test well) / CFU of control well × 100]. Wells containing yeast cells only serve as the control.

4.2.5 Quantitative determination of cytokines released by PMA-differentiated THP-1 upon co-incubation with *C. auris* for 24 h

Candida and M0 macrophages were co-incubated for 24 h at 37°C and 5% CO_2. Cell culture supernatant was collected, centrifuged at 5,000 rpm for 3 min to remove THP-1 and yeast cells, and then kept at -80°C before analysis. The concentration of cytokines (TNF-α, IL-10, IL-6, MIP-1α) was determined by sandwich ELISA following the manufacturer's protocol (DuoSet ELISA, R&D Systems). Corning® 96-well EIA/RIA Easy Wash™ Clear Flat Bottom Polystyrene High Bind microplate was used and the following reagents were manually prepared: PBS, wash buffer, reagent diluent, and stop solution. The substrate used was KPL SureBlue Reserve TMB Microwell Peroxidase (Sera Care, cat # 53-00-01). All the standards were analyzed in duplicates. The negative control is the cell culture supernatant in wells with THP-1 only (no yeast cells). Cytokine concentrations in the control and samples were computed following the equation of the line generated in the standard curve. The final cytokine concentration of the samples was computed by deducting the cytokine concentration of the negative control from the sample concentration.

Some wells were added with 250 ng/mL LPS (Fujifilm Wako Pure Chemical Corporation, 120-05131) to check for the ability of macrophages to release cytokines.

4.2.6 Detection of *TLR2* expression in PMA-differentiated THP-1

RNA from PMA-differentiated THP-1 was isolated using QIAGEN RNeasy Mini Kit following the manufacturer's protocol. Extracted RNA (Total RNA: 96 ng) was reverse transcribed and cDNA was synthesized using ReverTraAce qPCR RT Master Mix with gDNA Remover (Toyobo, Japan) following the manufacturer's protocol. Standard PCR using EmeraldAmp MAX PCR master mix (Takara Bio Inc.), following the manufacturer's recommended PCR conditions, was performed to confirm the amplification of the expected products. The primers used are shown in Table 4-1. Agarose gel electrophoresis was performed to view PCR products. The experiment was performed twice.

Table 4-1. Primers used in the detection of *TLR2* expression in PMA-differentiated THP-1 cells.

Target Gene	Forward and Reverse Primers (5' → 3' sequence)	PCR T_a (°C)	Amplicon Length (bp)	Primer Name	Source
β-actin	GCTCGTCGTCGACAACGGCTC	60	353	b-actin-F	Robles et al (2001)
	CAAACATGATCTGGGTCATCTTCTC			b-actin-R	
TLR2	GAGATGGGTGCTTACTCTGATG	50	140	TLR2_F	This study
	GTCTGAGAGTCCAAACCAGAAG			TLR2_R	

4.2.7 Determination of reactive oxygen species (ROS) levels in PMA-differentiated THP-1 co-incubated with glucose- and/or lactate-grown *Candida*

This protocol is adapted from Lopes et al (2018) and Wellington et al (2009) with slight modifications. Five-hour-old *Candida* cells, grown in Minimal medium with 2% glucose (referred to as "Glu") or 1% glucose + 1% lactate (referred to as "GluLac"), were collected, washed with PBS twice, and resuspended in phenol red-free RPMI. On the other hand, PMA-differentiated THP-1 cells were resuspended in RPMI without phenol red, stained with 50 µL of 10 µM CM-H_2DCFDA (Thermo Fisher Scientific Inc., cat # C6827) for 30 min in the dark at RT, and then washed with PBS. Yeast cells were co-incubated with the macrophage in a 1:3, macrophage to

yeast ratio, at 37°C and 5% CO_2 for at most 2 h. ROS production inside the macrophage was measured using a 488 nm laser and by quantifying fluorescence at 522 nm in a multi-well plate reader (Thermo Scientific Varioskan Lux VLBL00D0). To serve as controls, an unstained THP-1 was used to measure autofluorescence, and cells exposed to 1% H_2O_2 served as the positive control.

4.2.8 Phagocytosis assay using RAW 264.7 cells

This protocol is adapted from Cui et al (2016) but with slight modifications. Five-hour-old *Candida* cells, grown in Glu or GluLac, were collected, washed with PBS twice, and stained with 10 µg/mL acridine orange (Sigma Aldrich, cat # 318337-1G) for 30 min, similar to the phagocytosis assay using THP-1 cells. RAW 264.7 (ATCC TIB-71) macrophages were seeded (100 µL of 2 x 10^6 cells/mL) in each well of a black-walled, clear-bottom 96-well microtiter plate (Greiner Bio One µClear Black Cellstar®, REF 655090) in high glucose DMEM (Fujifilm Wako Pure Chemical Corporation, 043-30085) with 10% FBS and 1% penicillin-streptomycin. Plates were incubated for 2 h to let the cells adhere to the plates. Culture media was removed and 100 µL of the yeast suspension in DMEM was added. A macrophage-to-yeast ratio of 1:6 and 1:4 was followed for samples with *C. auris* UI001 and *C. albicans* SC5314, respectively. Phagocytosis was allowed to proceed at 37°C in 5% CO_2 for 1 h. The medium was removed and 100 µL of 0.1% trypan blue was added to quench the fluorescence of yeasts that were not internalized. After 1 min of incubation at room temperature, trypan blue solution was removed and the number of internalized yeasts was measured by measuring fluorescence at 520 nm in a multi-well plate reader (Thermo Scientific Varioskan Lux VLBL00D0). Using a 488 nm laser, the relative fluorescence unit (RFU) per well was measured and analyzed using the SkanIt v4.1 research edition software.

4.2.9 Statistical analysis

Graphs were generated using GraphPad Prism version 9.4.0 for Windows, GraphPad Software, San Diego, California USA, www.graphpad.com. Means and standard deviations from at least two independent biological replicates were shown and the data were analyzed using a t-test or one-way ANOVA with either Dunnett's multiple comparisons test or posthoc Tukey HSD test. A P value of at least 0.05 is considered significant (*P < 0.05, **P < 0.01, ***P<0.001, ****P<0.0001).

4.3 RESULTS AND DISCUSSION

4.3.1 Optimization of phagocytosis assay

Acridine orange staining of *Candida*

Yeast cells were stained with acridine orange (AO) before co-incubation with macrophages, following a protocol from Navarro-Arias et al (2019) and Hernandez-Chavez et al (2018). AO is a cell-permeable metachromatic dye that can stain DNA, RNA, and acid glycosaminoglycans. At low concentrations, it intercalates into DNA and precipitates RNA (Rost, 1992). AO is also used to analyze autophagy as it enters into acidic organelles in a pH-dependent manner. At neutral pH, AO gives a green fluorescence and in acidic conditions, it accumulates in acidic organelles giving a bright red fluorescence (Byvaltsev et al, 2019). Due to its properties, AO can be used in flow cytometry analysis, fluorescence microscopy, and cellular physiology-related experiments.

First, the optimal concentration of AO was determined. Cells were stained with either 1, 10, or 100 μg/mL AO, and resulting fluorescence intensities were analyzed in a flow cytometer. The resulting median FL1 and FL2 values are shown in Table 4-2. Cells stained with 10 or 100 μg/mL AO resulted in a high percentage of fluorescent cells with moderate fluorescence intensities compared to the unstained cells. However, the resulting cell pellet when 100 μg/mL AO is used looked extremely yellow and appeared inappropriate for use in the phagocytosis assay. So, 10 μg/mL AO was chosen as the appropriate concentration in staining cells for the phagocytosis assay.

Table 4-2. Median FL1 and FL2 values of *C. auris* UI001 stained with varying concentrations of acridine orange.

Parameter Tested:	**Unstained**	**1 μg/mL**	**10 μg/mL**	**100 μg/mL**
Median FL1 value	24.64	309.20	12,215.00	19,588.00
% fluorescent cells	(0.61)	(39.63)	(99.99)	(99.99)
Median FL2 value	4.83	36.93	850.53	2,962.65
% fluorescent cells	(0.54)	(40.86)	(99.63)	(99.98)

The next experiment was performed to confirm if the fluorescence intensity of AO-stained *C. auris* changes during cell growth (cells in lag *vs* logarithmic phase). This information is important to know if the fluorescence intensity between macrophages that phagocytosed *C. auris* cells grown in varying culture conditions is to be compared. First, a *C. auris* growth curve was generated to estimate the time points for the growth phases. Based on the growth curve, cells from the lag and logarithmic phases were collected after 2 h and 8 h, respectively. Results show that the same cells in the lag and log phases have similar fluorescence intensities. In other words, the fluorescence intensity stays the same whether the five-hr-old *C. auris,* grown in different β-glucan masking inducing conditions, collected for AO staining is still in the lag phase or already in the logarithmic phase. It is worth noting that cells in the stationary phase and death phase were not collected. Only five-hr old *C. auris* cells were used in the phagocytosis assay. So, the cells are only either in the lag phase or logarithmic phase.

PMA-differentiation method for THP-1

Macrophages are classified into pro-inflammatory (M1), non-activated (M0), and anti-inflammatory (M2) subsets that play distinct roles in the initiation and resolution of inflammation (Orekhov et al, 2019). This study used M0 macrophages only. One of the protocols used to trigger the differentiation of THP-1 monocytes into these three types is shown in Figure 4-1.

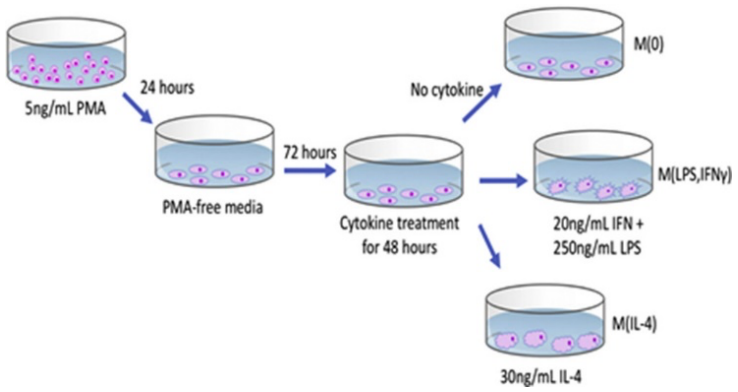

Figure 4-1. Graphical abstract of the standardized protocol for differentiation of THP-1 cells to macrophages with distinct M (IFNγ + LPS), M (IL-4), and M (IL-10) phenotypes. Figure from Baxter et al (2020).

The protocol to differentiate THP-1 monocytes using PMA used in this study was optimized. Compared to the protocol presented by Baxter et al (2020), the protocol followed by Tucey et al (2018) uses a higher concentration of PMA and a shorter incubation period (24 h) before the collection of macrophages. Figure 4-2 and Figure 4-3 show that there is a significant difference between the ratio of differentiated THP-1 cells collected following the protocol of Baxter et al (2020) and therefore, was followed in succeeding experiments in this study. To further support the protocol chosen in this study, according to Daigneault et al (2010), allowing a 5-day rest in a PMA-free medium will lead to an increase in cytoplasmic to nuclear ratio and mitochondrial and lysosomal numbers, as well as an altered differentiation-dependent cell surface markers in a pattern similar to monocyte-derived macrophages (MDM). These 5-day rested cells retained a high phagocytic capacity for latex beads and expressed a cytokine profile similar to MDM in response to TLR2 (Daigneault et al, 2010). Furthermore, Riendeau and Kornfeld (2003) showed that PMA-differentiated THP-1 cells mimic the response of primary macrophages and can be used in phagocytosis experiments.

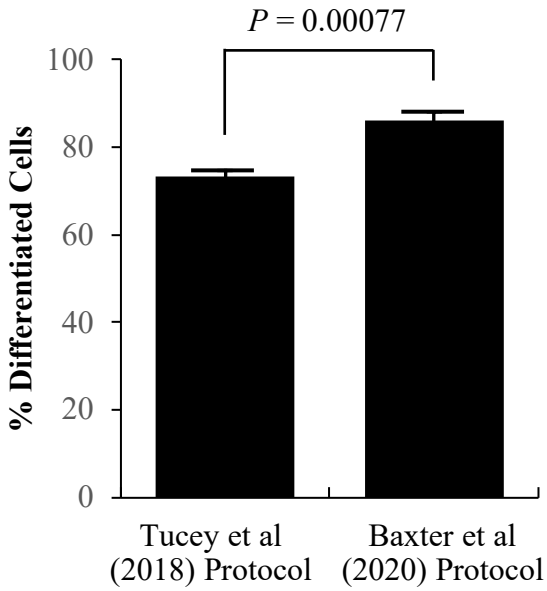

Figure 4-2. Percentage of PMA-differentiated cells generated following the protocols of Tucey et al (2018) [without a 5-day rest period; using 185 ng/mL PMA] and Baxter et al (2020) [with 5-day rest period; using 5 ng/mL PMA].

Tucey et al (2018) Protocol
(1-day incubation with 185 ng/mL PMA)

Baxter et al (2020) Protocol
(using 5 ng/mL PMA; with 5-day rest period)

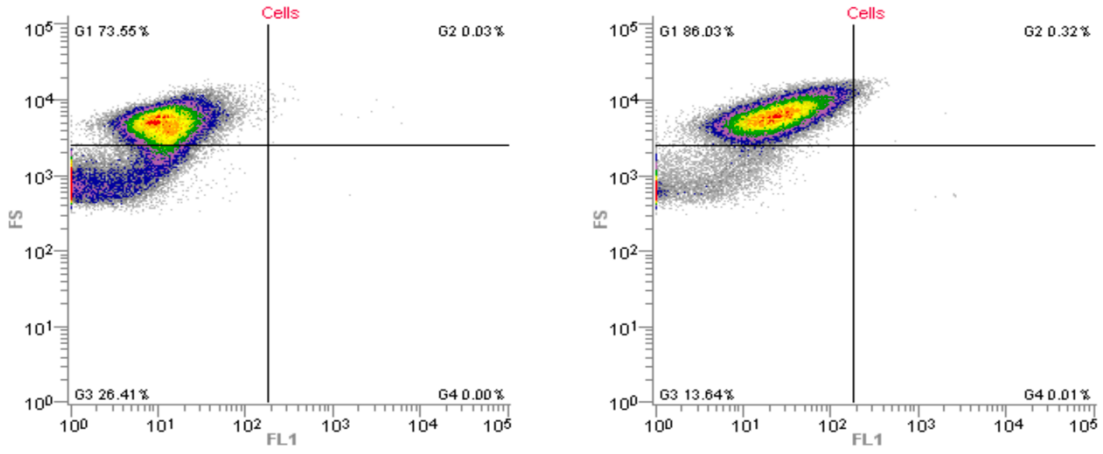

Figure 4-3. Flow cytometer FL1 vs FS dot plot used for gating macrophages generated following the protocol of Tucey et al (% differentiated THP-1 cells = 73.55%) and a protocol by Baxter et al (% differentiated THP-1 cells = 86.03%). Quadrants were kept constant in both analyses. Dot plot is a representative of three replicates with consistent results.

Macrophage to yeast cell ratio determination

Since there are few to no publications that use differentiated THP-1 cells for phagocytosis assay involving *C. auris*, determination of the optimized ratio between macrophage and fungal cells during co-incubation is needed. Several ratios (host : fungus) ranging from 1:2 up to 1:6 were experimented. Based on Figure 4-4, a ratio of one macrophage to five *C. auris* cells produced the highest fluorescence intensity, and adding more fungal cells seemed to saturate the macrophage. Also, up to some level, macrophages that phagocytosed more fungal cells have higher fluorescence intensity compared to macrophages that phagocytosed fewer fungal cells. With these data, a 1:5 ratio was used in all subsequent experiments.

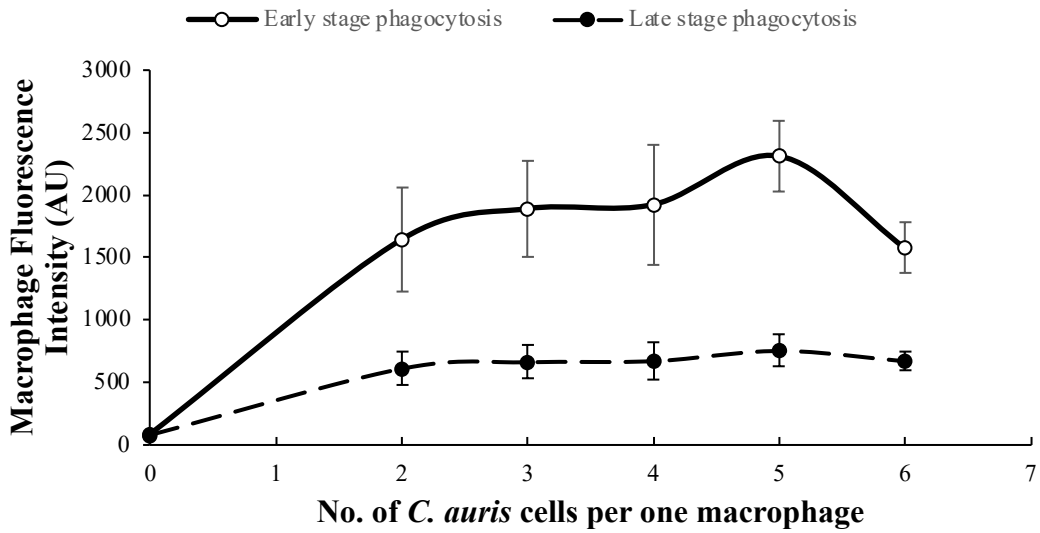

Figure 4-4. Fluorescence intensity of PMA-differentiated THP-1 co-incubated with increasing numbers of *C. auris* cells for 2 h.

Effect of trypan blue on the fluorescence intensity of stained *C. auris*

The final step in performing the phagocytosis assay is to resuspend samples in PEB buffer (PBS, 2.5 mM EDTA, 0.1% BSA) with 0.1% trypan blue (TB) before the flow cytometric analysis. TB serves as a quencher, a substance that absorbs excitation energy from a fluorophore thereby removing or decreasing its detected fluorescence. So, TB will only quench the fluorescence of *Candida* cells that are attached but not phagocytosed by the macrophage (Bruno et al, 2020; Navarro-Arias et al, 2019; Lopes et al, 2018; Santos et al, 2015). This experiment was carried out to make sure that the fluorescence signal detected by the flow cytometer is due to *C. auris* cells phagocytosed by the macrophage and not the cells that are attached only to the macrophage. Figure 4-5 shows the histogram generated by flow cytometric analysis of macrophages co-incubated with unstained or stained *C. auris* resuspended in a buffer with or without TB. Results show that TB can decrease the fluorescence of acridine orange by 99% in the FL1 band pass filter (median fluorescence of 5,257 a.u. vs. 39 a.u.) and 98% in the FL2 band pass filter (median fluorescence of 331 a.u. vs. 5 a.u.).

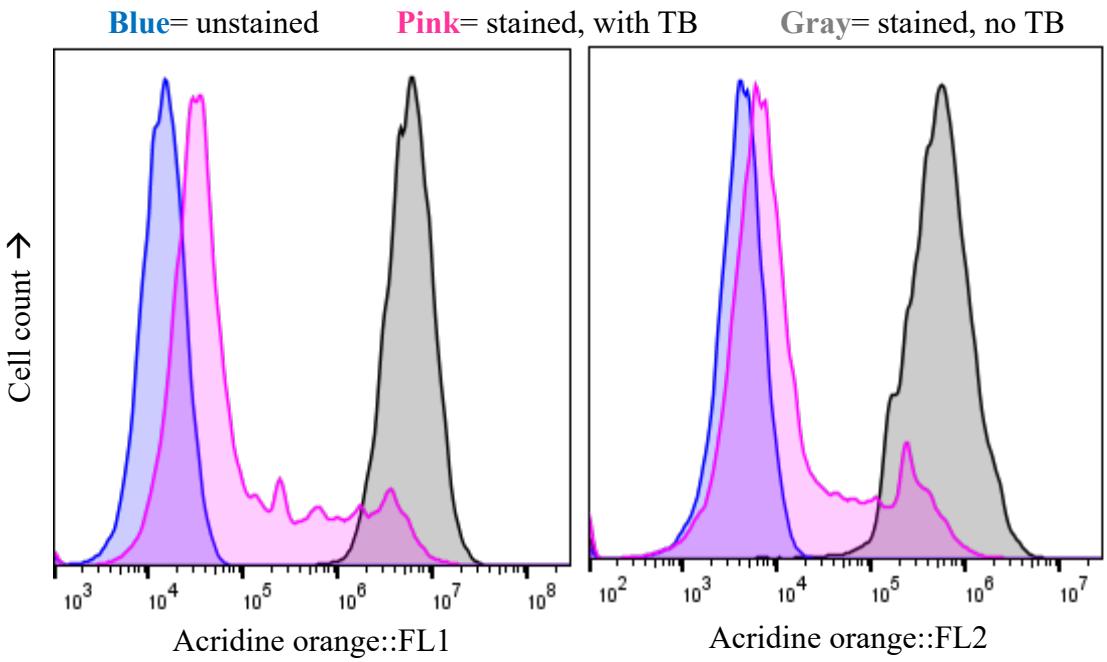

Figure 4-5. Effect of resuspending samples in trypan blue (TB) in the flow cytometry-based analysis of phagocytosis of *C. auris* by PMA-differentiated THP-1 macrophage. Histogram shown is a representative of two independent replicates showing consistent results and is generated using FlowJo™ v10.8 Software (BD Life Sciences).

4.3.2 Effect of lactate-induced β-glucan masking on phagocytosis of *C. auris*

Glucose-only and lactate-grown *C. auris* were stained and separately co-incubated with unstained macrophages for 2 h. Macrophages were then collected and analyzed through flow cytometry. The negative control, which is composed of macrophages that are not exposed to *Candida*, was used. The percentage of phagocytosis (Figure 4-7A) was calculated based on the percentage of fluorescent macrophages gated against the negative control. The stages of phagocytosis are determined based on the emission wavelength of AO. AO is a cell-permeable metachromatic dye that exhibits excitation/emission spectra of 502/525 nm and 475/590 nm when bound to dsDNA and when under acidic conditions, respectively (Han and Burgess, 2010). In addition, AO could also detect cellular autophagy (Thomé et al, 2016). Early-stage phagocytosis is detected through the FL1 bandpass filter (525/50) while late-stage phagocytosis, in which *Candida* cells are within acidified lysosomes of the macrophage, is detected through the FL2 bandpass filter (585/40). Based on the result, lactate-induced β-glucan masking in *C. auris* UI001 triggered a 45-84% and 30-75% reduction in both early-stage and late-stage phagocytosis, respectively. Growth in increasing amounts of lactate led to more reduction in phagocytosis. The fold change in the ratio of phagocytosed fungal cells grown in lactate relative to cells grown in

glucose only, as well as the median fluorescence intensity of phagocytosing macrophages, is shown in Figure 4-7B and Figure 4-7C. To aid in the interpretation of Figure 4-7C, a cartoon (Figure 4-6) demonstrating that an increase in the number of phagocytosed yeast cells in a macrophage will lead to increased fluorescence is shown. There was an attempt to record a video and take confocal images of the co-incubated macrophage and fungi. However, the protocol for these has not been successfully optimized. It is worth noting that glucose-only and lactate-grown *C. auris* have the same morphology and do not form a hypha upon incubation in a serum-containing RPMI medium.

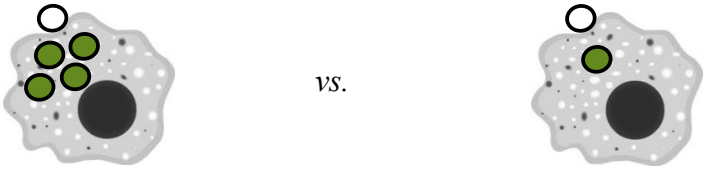

Higher fluorescence
Macrophage + *C. auris*
pre-cultured in 2% Glucose

Lower fluorescence
Macrophage + *C. auris*
pre-cultured in Glucose-Lactate

Figure 4-6. Cartoon used to visualize macrophages and *Candida* cells during the phagocytosis assay.

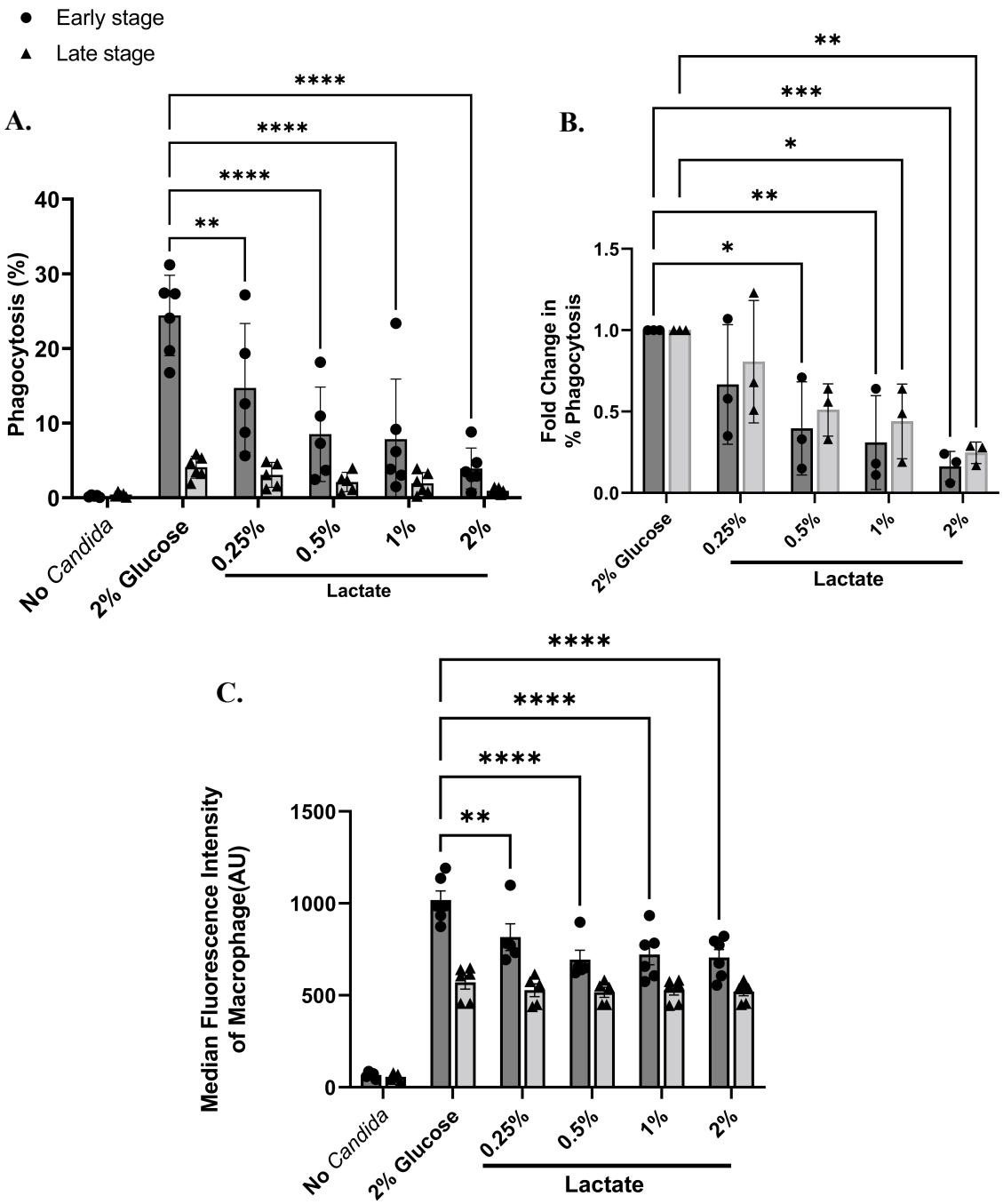

Figure 4-7. Percent phagocytosis (A), fold change in % phagocytosis (B), and median fluorescence intensity of phagocytosing macrophages (C) co-incubated with glucose- and lactate-grown *C. auris* for 2 h

Candida species interact with macrophages in different ways. Some strains could be effectively phagocytosed by macrophages leading to fungal death. Unlike *C. albicans*, *C. glabrata* is shown to be able to survive and replicate inside macrophages, for long periods of time eventually leading to macrophage lysis due to fungal load (Galocha et al, 2019). *C. glabrata* can survive inside macrophages by suppression of ROS production in macrophages, alteration of phagosomal compartments leading to non-acidification of resulting phagolysosome and other effective metabolic and stress adaption to the phagosomal environment leading to low damage and cytokine release (Kasper et al, 2015). So, in this study, the ability of macrophages to kill *C. auris* cells was determined.

The difference in the killing ability of macrophages against *C. auris* precultivated in Glu or GluLac was investigated. After co-incubation for 2 h, macrophages were lysed with the addition of 0.5% Triton X-100. Lysis of macrophages by 0.5% Triton X-100 was observed in a microscope and the remaining fungal cells were diluted and spread on agar plates. Colonies were counted after a 2-day incubation. Colony-forming units (CFU) per mL of sample was calculated, considering plates with 10 - 150 colonies only. Percent killing was calculated following the equation below:

$$\%\ killing = 10\ \text{x}\ \frac{\frac{CFU}{mL}control - \frac{CFU}{mL}sample}{\frac{CFU}{mL}control}$$

Results in Figure 4-8 show that macrophages were not able to kill most of the fungal cells grown in a media with lactate. This data explains that the reduction of β-glucan in the cell wall of lactate-grown *C. auris* led to a reduction in the chance of phagocytosis.

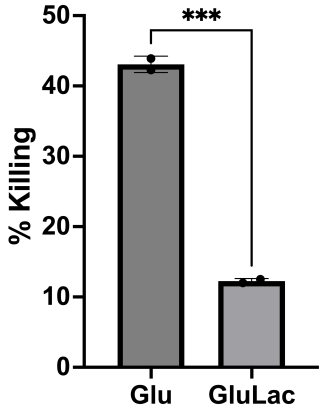

Figure 4-8. Percentage of glucose only- and lactate-grown *C. auris* killed by PMA-differentiated THP-1 after co-incubation for 2 h.

4.3.3 Effect of pre-exposure to antifungal agents on the phagocytosis of *C. auris*

Based on the β-glucan masking experiment performed in *C. auris* UI001, sublethal concentrations of antifungals (16 μg/mL fluconazole, 250-500 ng/mL 5-fluorocytosine, and 0.63-40 μg/mL micafungin) could trigger masking of β-glucan. A phagocytosis assay was performed to determine the effect of pre-exposure to these antifungals on the phagocytosis of *C. auris*. In a practical sense, it would be interesting to know if having residual concentrations of antifungals on the body of a person infected with *C. auris* could have some effects on the phagocytic activity of macrophages.

The ratio of phagocytosis, fold change in phagocytosis relative to cells grown with no antifungals, and the median fluorescence intensity of phagocytosing macrophages are shown in Figure 4-9. Results show that *C. auris* cells pre-grown in Minimal media containing 16 μg/mL fluconazole and 10 μg/mL micafungin, which are exhibiting β-glucan masking, are phagocytosed well by the macrophages. This result is the opposite of the pattern observed in lactate-grown *C. auris*. To date, studies that dealt with *C. albicans* showed that cells undergoing β-glucan masking have a decreased chance of being phagocytosed by macrophages (Childers et al, 2020; Pradhan et al, 2018, 2019). However, few studies show that the efficiency of phagocytosis depends on the cultivation condition of *Candida* and the type of macrophage. Similarly, in a study by Cui et al (2016), enhanced phagocytosis efficiency of murine macrophage cell line RAW 264.7 was observed when *C. albicans* CAF2-1 (genotype: Δ*ura3*::imm434/URA3) was exposed to sublethal concentrations of caspofungin. Furthermore, in a study by Yang et al (2022), BMDMs co-incubated with *C. albicans* cultured in YPD with 0.06 μg/mL caspofungin for 3 h or in YPD with 10 μg/mL fluconazole overnight, produced more TNF-α as detected by ELISA. Although quantification of cytokines released after co-incubation with fungi pre-exposed to antifungals was

not performed in this study, increased phagocytosis of fungal cells pre-grown in these antifungal agents may be correlated to results observed in the study of Yang et al (2022).

For *C. auris* cells pre-grown in a media with amphotericin B, it was observed that after co-incubation for 2 h, consistently fewer macrophages (13,000 cells on average versus 23,000) were detected during flow cytometry analysis. Whether the macrophages died or burst during co-incubation remains to be investigated.

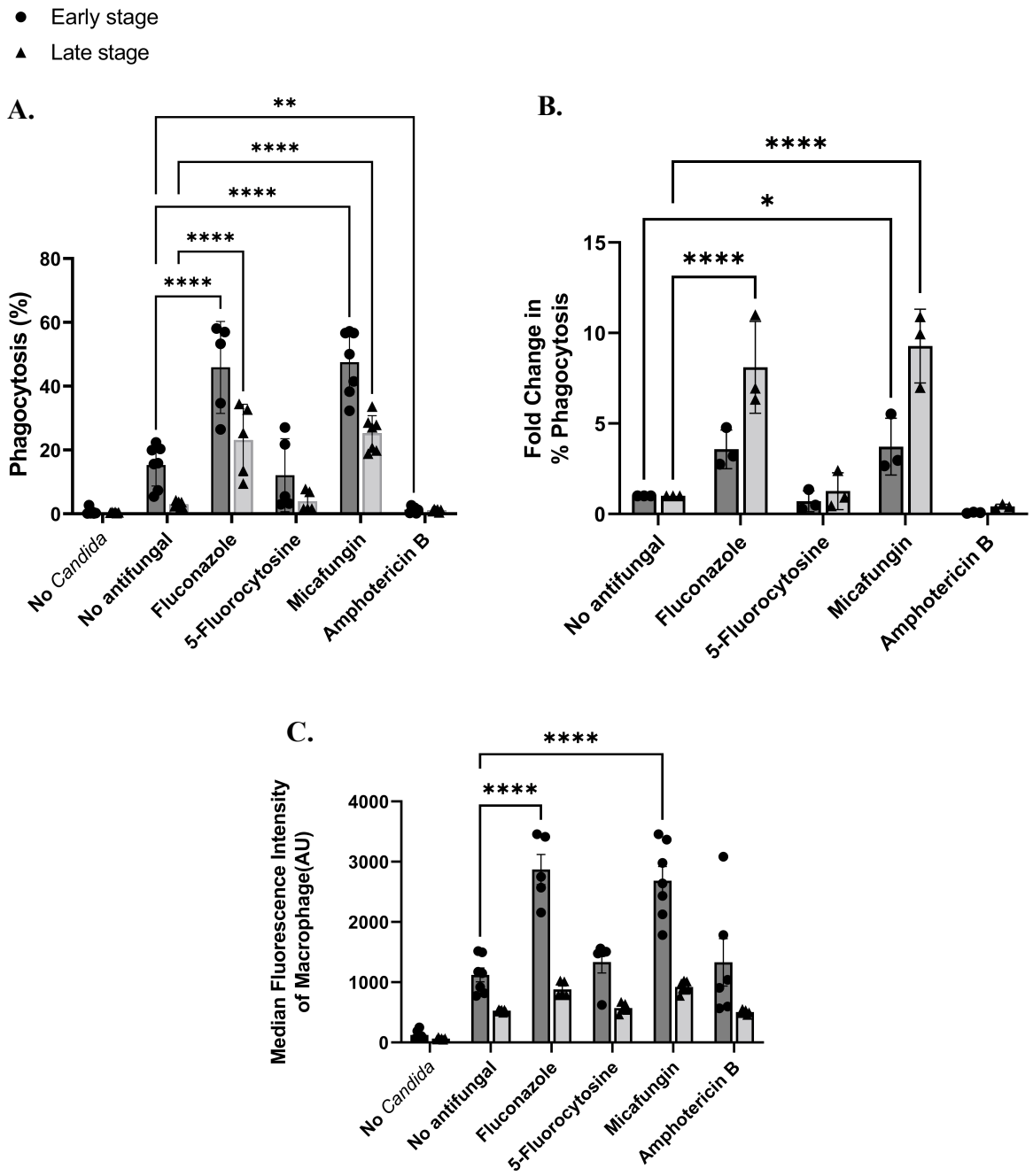

Figure 4-9. Phagocytosis ratio (A), fold change in % phagocytosis (B), and median fluorescence intensity of phagocytosing macrophages (C) co-incubated with *C. auris* UI001 pre-grown in YPD with antifungal agents.

4.3.4 Quantitative determination of cytokines released by PMA-differentiated THP-1 upon co-incubation with *Candida* for 24 h

The effect of changes in the cell wall architecture of *C. auris* on the immune factor production of macrophages was investigated. *C. auris* was cultivated in a lactate-containing media, collected, and used in the phagocytosis assay involving M0 macrophages derived by PMA differentiation of THP-1. The cell supernatant was collected after 24 h of co-incubation and used in the quantification of cytokines by ELISA. Macrophage inflammatory protein (MIP)-1α, also referred to as chemokine (C-C motif) ligand 3 (CCL3), is an inflammatory chemokine produced by cells during infection or inflammation. CCL3/MIP-1α-expressing cells are usually found in areas of inflammation and bone resorption as it plays an important role in recruiting various cells such as macrophages, lymphocytes, and eosinophils via the CCR1 or CCR5 receptor (Bhavsar et al, 2015).

Figure 4-10A shows the CCL3/MIP-1α production of macrophages incubated with *C. auris* UI001 grown with glucose and/or lactate. *C. auris* grown in the media with at least 0.5% lactate, where this strain exhibits a 57% reduction in β-glucan, triggered an 84% reduction in CCL3/MIP-1α production (87 pg/mL vs. 14 pg/mL). Since the quantity of detected cytokine is low, LPS was used as a positive control for confirming the ability of macrophages to produce cytokines. Figure 4-10B shows that upon the addition of LPS with or without *Candida*, CCL3/MIP-1α production increased by 11-fold (87 pg/mL vs. 915 pg/mL). In addition, there is no significant difference in CCL3/MIP-1α production for samples with or without the added yeast. Like this study, Ballou et al (2017) showed that human M1-activated monocyte-derived macrophages stimulated less CCL3/MIP-1α ($P < 0.0001$) and less TNF-α ($P = 0.0005$) after infection with lactate-grown *C. albicans* compared to glucose-grown cells.

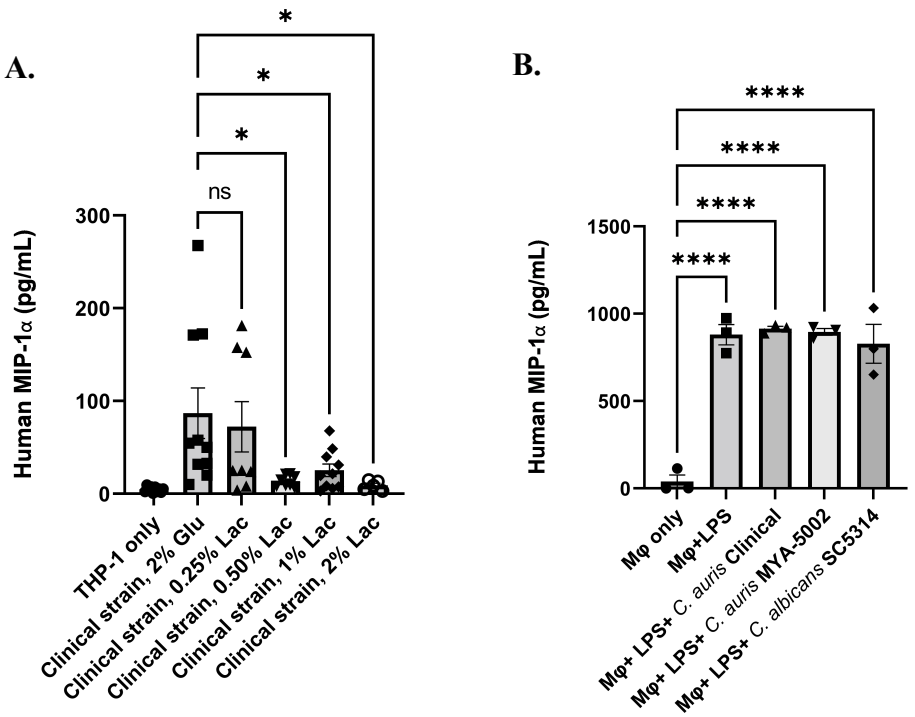

Figure 4-10. Quantification of CCL3/MIP-1α produced by PMA-differentiated THP-1 co-incubated with *C. auris* UI001 previously grown in Minimal media with glucose only or with varying amounts of lactate (A) and the effect of LPS on CCL3/MIP-1α production (B). Mφ = macrophage

TNF-α production was determined next. Tumor Necrosis Factor (TNF) is a pro-inflammatory cytokine that plays a major role in host defense and regulation of the immune response. During fungal infection, TNF-α stimulates the expression of chemokines and leukocyte adhesion molecules leading to the recruitment of polymorphonuclear leukocytes and enhanced phagocytosis and killing of fungi (Cannom et al, 2002). In addition, the role of TNF-α in the development of protective Th1 responses was demonstrated in animal models of candidiasis (Antachopoulos & Roilides, 2005).

As shown in Figure 4-11A, there is no significant difference in TNF-α produced by macrophages co-incubated with glucose only and lactate-grown *C. auris.* Also, detected levels are only approximately 11 pg/mL, but production is increased by 101 times upon the addition of LPS (11 pg/mL vs. 1108 pg/mL) as seen in Figure 4-11B. Furthermore, *C. auris* UI001 triggered more TNF-α production than *C. albicans* (1108 pg/mL vs. 855 pg/mL; $P = 0.1192$). The observed low amounts of TNF-α are also observed by Park et al (2007), whereby negligible to no TNF-α was secreted by differentiated THP-1 in the absence of LPS stimulation. In addition, Brzicova et al (2019) showed that PMA-differentiated THP-1 exposed to LPS could only produce 1,100 pg/mL TNF-α, similar to what was detected in this study.

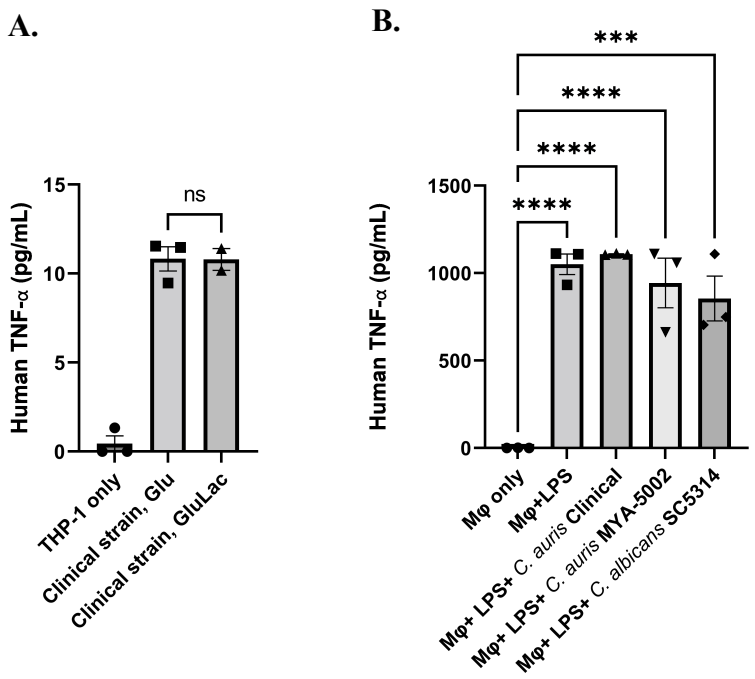

Figure 4-11. Quantification of TNF-α produced by PMA-differentiated THP-1 co-incubated with *C. auris* UI001 previously grown in Minimal media with glucose only "Glu" and glucose-lactate "GluLac" (A) and the effect of LPS on TNF-α production (B). Mφ = macrophage

IL-10 production was determined next. In contrast to TNF-α, IL-10 is an anti-inflammatory cytokine that reduces the inflammatory response by down-regulating the secretion of pro-inflammatory cytokines (Wagener et al, 2014). IL-10 also plays an important role in regulating the development of T helper cells and innate immune response (Antachopoulos & Roilides, 2005). As shown in Figure 4-12A, there is no significant difference in IL-10 produced by macrophages co-incubated with glucose only and lactate-grown *C. auris.* Also, detected levels are only approximately 7 pg/mL, but the production is increased by only 12-fold upon the addition of LPS (7 pg/mL vs. 85 pg/mL) as seen in Figure 4-12B. Among the tested *Candida* strains, ATCC MYA-5002 triggered the highest IL-10 production (141 pg/mL).

Another pro-inflammatory cytokine, IL-6, is involved in the immune response against fungal pathogens (Antachopoulos & Roilides. 2005). There was an attempt to measure IL-6 production, but ELISA analysis showed that the M0 macrophage used in this study does not produce IL-6 upon co-incubation with *C. auris*, regardless of how *C. auris* was cultivated before the phagocytosis assay. However, upon the addition of LPS, an average amount of 515 pg/mL IL-6 was produced (Figure 4-12C). Overall, LPS triggered an increase in IL-6 and IL-10 production, but not as much as in CCL3/MIP-1α and TNF-α.

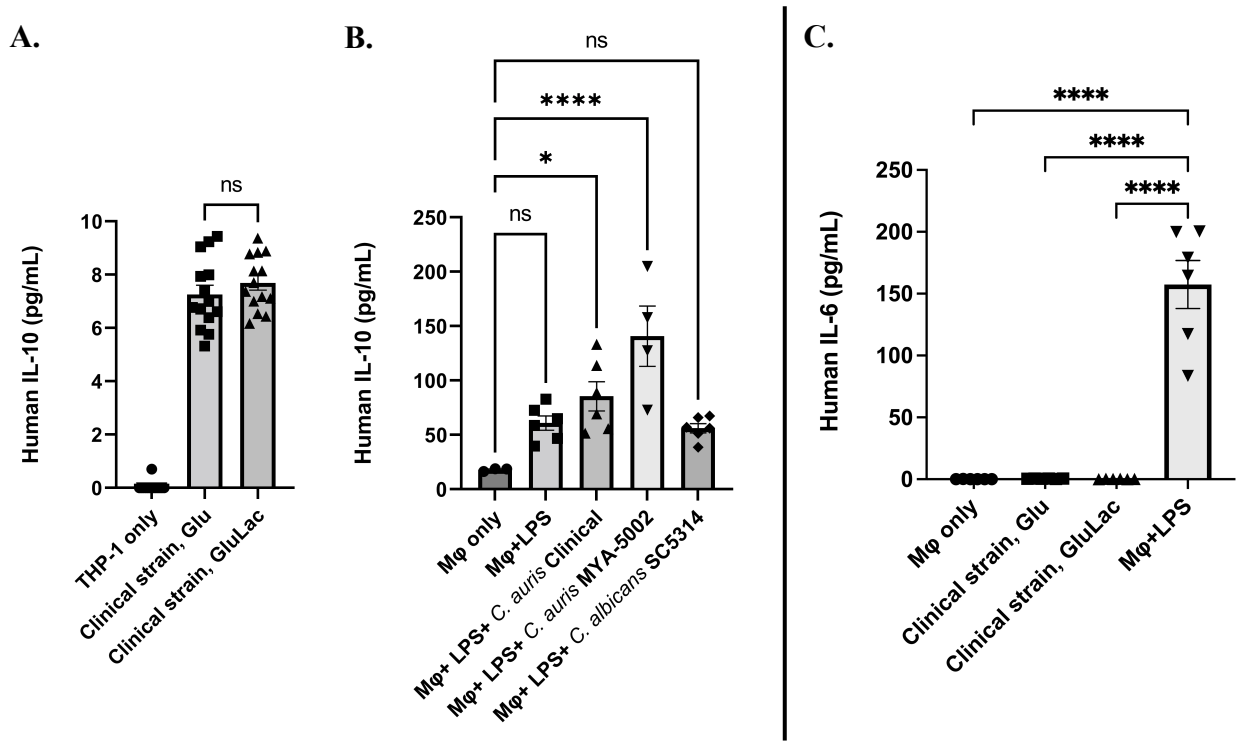

Figure 4-12. Quantification of IL-10 (A) and IL-6 (C) produced by PMA-differentiated THP-1 co-incubated with *C. auris* UI001 previously grown in Minimal media with glucose only "Glu" or glucose-lactate "GluLac" and the effect of LPS on IL-10 production (B). Mφ = macrophage

To support the low levels of cytokines detected in this study, Kean et al (2020) demonstrated that peripheral blood mononuclear cells (PBMCs) fail to induce a potent pro-inflammatory cytokine response against *C. auris*, while other species such as *C. tropicalis*, *C. guilliermondii*, and *C. krusei* induced production of TNF-α, IL-6, and IL1-β in PBMC co-cultures. Despite this, the same study showed that human monocyte-derived macrophages can recognize and phagocytose *C. auris.*

The effect of lactate-induced reduction in β-glucan on cytokine production of phagocytosing macrophages was reported and studies, mainly on *C. albicans*, showed that lactate-induced β-glucan masking led to a significant reduction in the production of TNF-α and IL-6 (Childers et al, 2020). To gain more insights into the opposite phenomenon, which is an increase in β-glucan due to low pH, the same methodology was performed using *C. auris* UI001 grown in YPD with either pH 4 or pH 7. In Chapter 2, it was shown that cells in pH 4 exhibit a six-fold increase in β-glucan compared to cells grown at neutral pH. Figure 4-13 shows that there is no significant difference in CCL3/MIP-1α, TNF-α, and IL-10 production in *C. auris* cells pre-grown in acidic and neutral media. This contrasts with a study by Sherrington et al (2017) where *C. albicans* grown at pH 4, which have more exposed β-glucan ($P < 0.05$) than cells grown at pH 6, illicit higher TNF-α and IL-6 from PBMC after 24 h of co-incubation.

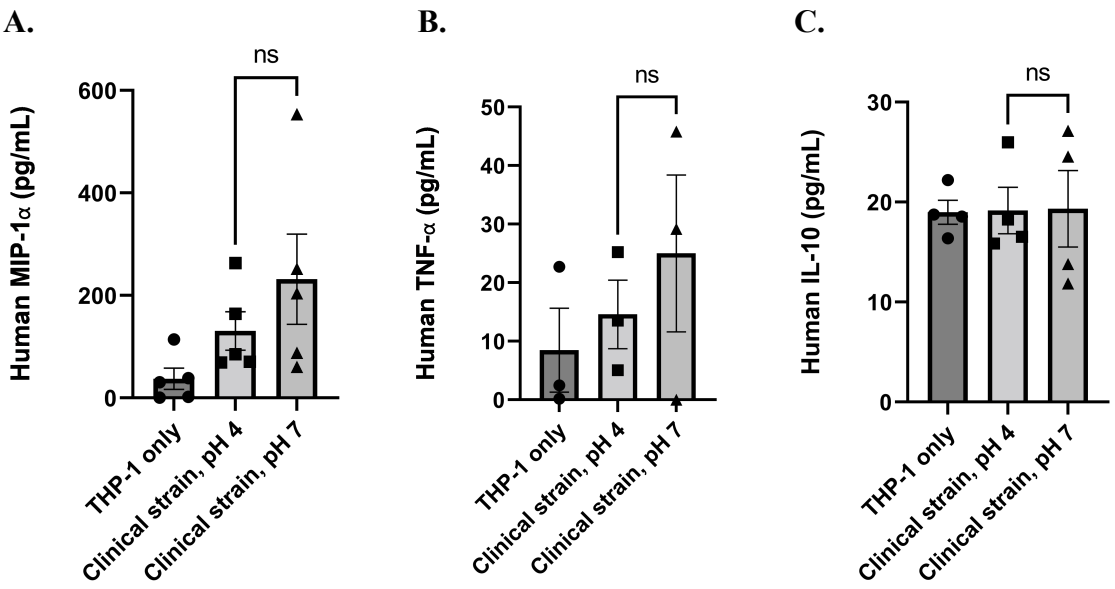

Figure 4-13. Quantification of CCL3/MIP-1α (A), TNF-α (B), and IL-10 (C) produced by PMA-differentiated THP-1 co-incubated with *C. auris* UI001 previously grown in YPD with varying pH.

A few studies showed that masking of PAMPs in *Candida* does not always result in a decrease in phagocytosis by macrophages. *C. albicans* SC5314 exposed to caspofungin showed an increase in β-glucan exposure but the phagocytosis by J774.1 murine macrophages and TNF-α production decreased. Meanwhile, *C. tropicalis* exposed to caspofungin exhibit increased β-glucan exposure but the phagocytosis rate is reduced and TNF-α production is increased (Walker and Munro, 2020). In addition, Pradhan et al (2018) showed that *C. albicans* SC5314 cells grown in hypoxic conditions exhibit reduced β-glucan exposure leading to reduced phagocytosis. However, ELISA analyses of cytokines revealed that there is no significant difference in the amount of TNF-α and CCL3/MIP-1α. In another study by Pradhan et al (2019), *C. albicans* SC5314 cells grown in a medium without iron, which has reduced β-glucan on the cell wall, stimulated the same levels of IL-10 with the fungal cells grown in a media with iron. However, a significant difference between these two samples is observed in TNF-α, IL-6, and CCL3/MIP-1α production by human macrophages. To have a full picture of the effect of PAMP exposure levels on the immune response, chitin levels can also be determined as reduced cell wall chitin is shown to affect late-phase cytokine response in *C. albicans* (Wagener et al, 2014).

4.3.5 Effect of laminarin on the uptake of *Candida*

To investigate whether β-glucan and Dectin-1 interaction is indispensable for the uptake of *C. auris* cells by macrophages, laminarin was added to macrophages before co-incubation with the yeast. Laminarin, a soluble β-glucan from brown seaweed (*Laminaria digitata*), is a low molecular weight Dectin-1 ligand composed of linear β(1-3)-glucan with β(1-6)-linkages. With this, laminarin acts as a Dectin-1 antagonist (Smith et al, 2018) where it can bind to Dectin-1 without stimulating downstream signaling and can therefore able to block binding of yeast cell wall β(1-3)-glucan to Dectin-1 (Goodridge et al, 2011). THP-1 monocytes and their corresponding PMA-differentiated macrophages have a significantly high presence of human Dectin-1a isoform on the cell surface (Fischer et al, 2017), which are shown to be highly responsive to laminarin (InvivoGen Review, 2013).

The effect of the addition of laminarin on the cytokine production of macrophages upon phagocytosis was not tested, but a similar study by Navarro-Arias et al (2019) showed that pre-incubation of human PBMCs with laminarin for 60 min did not affect the ability of live *C. albicans* and *C. auris* to stimulate cytokine production.

Figure 4-14 shows the effect of laminarin on the phagocytosis of three strains of *C. auris* belonging to different clades. Figure 4-14C shows that the addition of laminarin was able to significantly reduce the uptake of *C. auris* UI001. This means that β-glucan is necessary for the recognition and subsequent uptake of fungal cells. However, phagocytosis was not completely prevented, which implies that other PAMPs or PRRs may also be involved. Interestingly, both the ATCC strains may not be recognized well by THP-1 macrophages since the phagocytosis ratio is very low. There is a slight reduction only in the early-stage phagocytosis of *C. auris* ATCC MYA-5002. There is also entirely no effect in both early and late-stage phagocytosis of *C. auris* ATCC MYA-5001. These results also show the inherent differences, not only in β-glucan and mannan expression but also in the efficiency of phagocytosis of *C. auris* strains belonging to different clades.

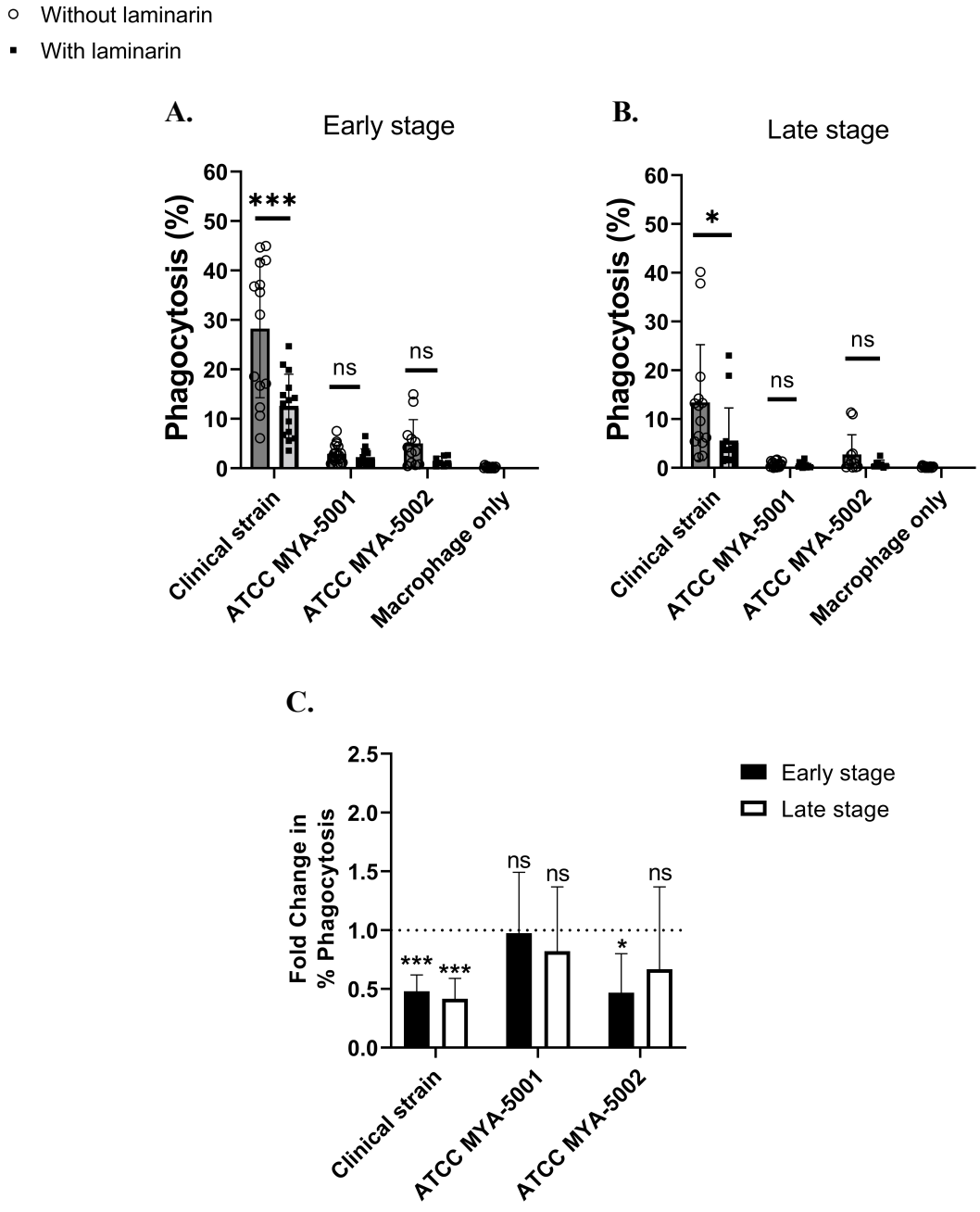

Figure 4-14. Effect of laminarin on the early stage (A) and late stage (B) % phagocytosis and the computed fold change in phagocytosis (C) of a clinical strain and two type strains of *C. auris*.

As shown in Chapter 1, other PRRs found on the surface of immune cells like macrophages could contribute to the recognition and uptake of fungal cells. Signaling via Toll-like receptor 2 (TLR2), a PRR that plays an important role in the innate immune response, can also be activated by yeast β-glucan (Van der Graaf et al, 2005). TLR2 is expressed on the surface of monocytes, macrophages, and dendritic cells. Recognition of a pathogen triggers a cascade of signaling events

that could lead to the production of pro-inflammatory cytokines and chemokines (Goodridge et al, 2011). To check for the expression of *TLR2* in the specific batch of PMA-derived THP-1 macrophages used in this study, the extracted RNA from these macrophages was reverse transcribed and *TLR2* cDNA was detected by PCR.

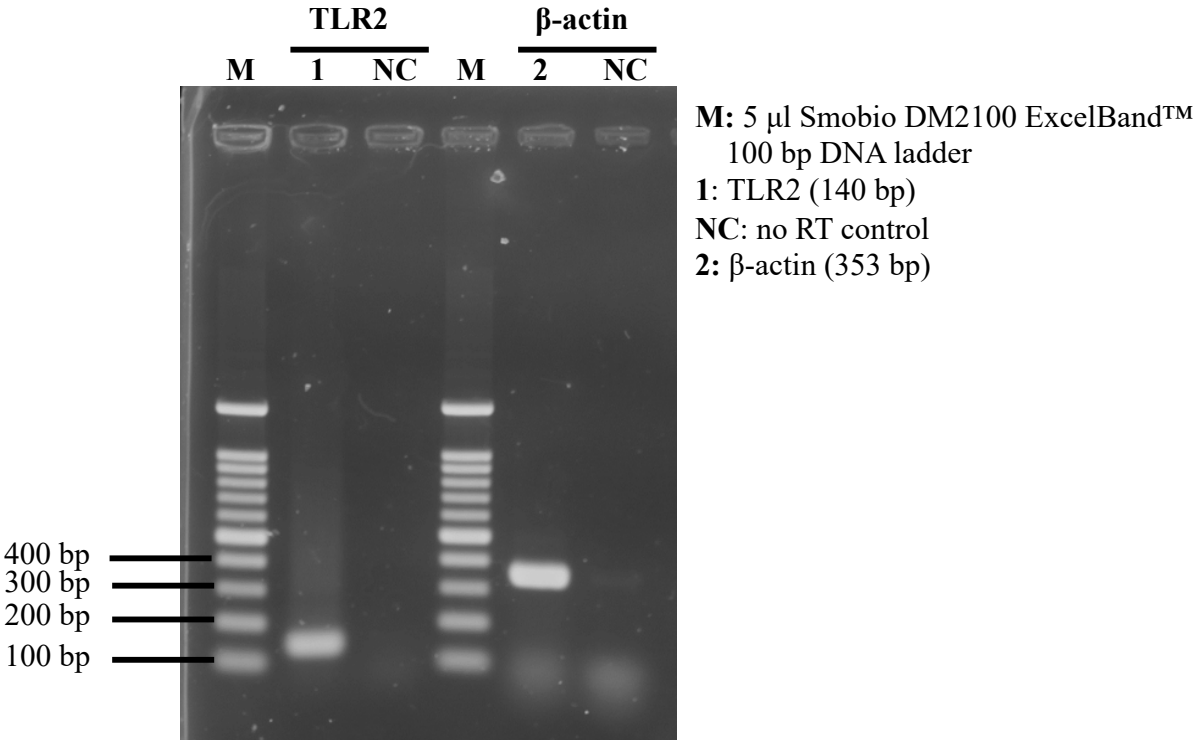

Figure 4-15. Detection of *TLR2* expression in M0 macrophage derived from PMA-differentiation of THP-1 monocyte. Electropherogram is a representative of two replicates with consistent results.

Figure 4-15 shows that macrophages used in this study express *TLR2.* Although β-glucan and Dectin-1 interaction is the main trigger for immune response, other PRRs like TLR2 and other PAMPs such as mannan and chitin and their respective receptors might have contributed to the phagocytosis and subsequent release of cytokines measured in this study. Conversely, it is also possible that TLR2 is not involved like in the study of Li et al (2009) where insoluble β-glucan from the cell wall of *C. albicans* can activate immune responses in THP-1 monocytes through Dectin-1 but not TLR2.

4.3.6 Determination of ROS levels in PMA-differentiated macrophage co-incubated with glucose only and glucose-lactate-grown *Candida*

To further characterize the immune response of macrophages against *C. auris,* ROS production of macrophages upon infection was measured. When myeloid phagocytes such as macrophages, dendritic cells, and neutrophils recognize fungal cell walls, the formation of ROS in the phagolysosome is initiated following phagocytosis (Goodridge et al, 2011). In *C. albicans*, it was shown that increased β-glucan exposure could lead to increased ROS production and cytokine secretion at 4 h post-infection (Galán-Díez et al, 2010).

In this study, a general oxidative stress indicator was used. CM-H_2DCFDA, a chloromethyl derivative of H_2DCFDA, is a cell-permeant indicator for ROS in cells. CM-H_2DCFDA passively diffuses into cells, where its acetate groups are cleaved by intracellular esterases and its thiol-reactive chloromethyl group reacts with intracellular glutathione and other thiols. Subsequent oxidation yields a fluorescent adduct that is trapped inside the cell, thus facilitating long-term studies.

Figure 4-16 shows the level of ROS produced by macrophages after adding *Candida* cells cultured in Minimal media with either glucose only (Glu) or glucose-lactate (GluLac). Generally, the ROS level had a steep increase within 30 min, regardless of the species and culture condition of fungal cells. Although more in-depth experiments must be performed, this result may suggest that although β-glucan exposure levels on the surface of fungal cells affect the rate of phagocytosis, it may not affect the level of ROS produced by macrophages. Oxidative burst through rapid release of ROS is one of the mechanisms used by macrophages to kill phagocytosed fungal cells. Results in this study suggest that mechanisms other than oxidative burst may be involved in the increased killing of glucose-only grown *C. auris*, observed in Figure 4-8.

4.3.7 Phagocytosis assay using RAW 264.7 cells

The effect of β-glucan masking phenomenon on the phagocytic capacity of murine macrophage cell line RAW 264.7 was experimented. This is performed to ensure that the observed reduction in phagocytosis is exhibited regardless of the type of macrophage. RAW 264.7 cells are a macrophage-like, Abelson leukemia virus-transformed cell line derived from BALB/c mice (*Mus musculus*). This cell line is a commonly used model of mouse macrophages for the study of cellular responses to microbes and their products (ATCC Product Sheet, 2022).

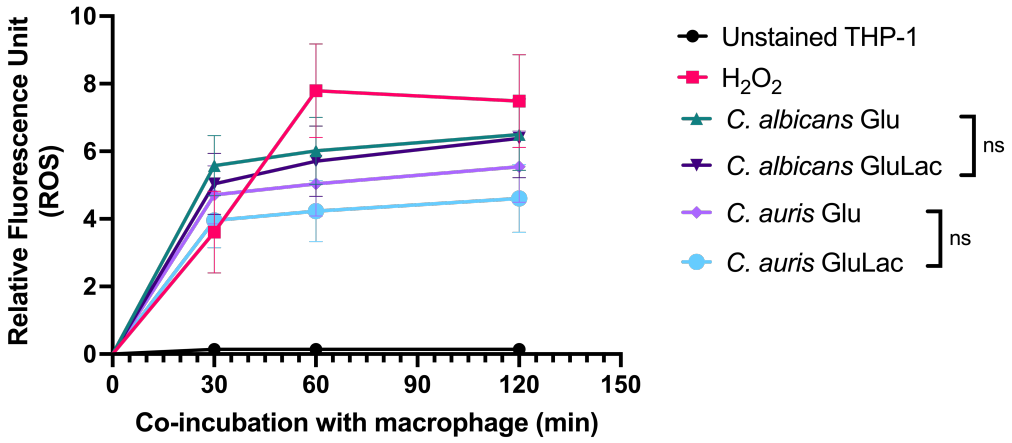

Figure 4-16. ROS production in PMA-differentiated THP-1 co-incubated with *Candida* previously grown in Minimal media with glucose only (Glu) or with lactate (GluLac). Line graph plots the mean and SEM from two independent biological replicates each with 4-6 technical replicates. Differences between Glu and GluLac samples within the same species is analyzed by unpaired t-test. ns= not significant.

The phagocytosis assay protocol was optimized by first determining the appropriate multiplicity of infection (MOI) for both *C. auris* and *C. albicans*. *Candida* is grown in Minimal media for 5 h before AO staining, and varying numbers of fungal cells were co-incubated with the macrophage. Based on the result shown in Figure 4-17, the appropriate MOI to be used for *C. auris* is 1:6 (macrophage : fungal cell). For *C. albicans*, the RFU becomes unstable beyond 1:4 MOI. *C. albicans* yeast cells transitioned to hyphae due to the presence of FBS in DMEM. To date, there are few studies that used *C. auris* and RAW 264.7 cells. Based on previous studies for *C. albicans,* the MOI ranged from 1:1 (Marcil et al, 2008) to 1:5 (Lohse and Johnson, 2008), 1:6 (Uwamahoro et al, 2014), and as high as 1:10 (Strijbis et al, 2013; Cui et al, 2016) but the length of co-incubation is usually 1 h.

The effectiveness of trypan blue in removing the fluorescence of bound and non-phagocytosed *Candida* was also tested. Based on the result shown in Figure 4-18, there is a 99.7% reduction in the fluorescence of samples stained with trypan blue compared to unstained samples.

Next, the effect of lactate-induced β-glucan masking of *Candida* cells to phagocytosis by RAW 264.7 murine macrophages was determined. *Candida* cells pre-cultured in either glucose only (Glu) or glucose-lactate (GluLac) were stained with AO and co-incubated with RAW 264.7 macrophages for 1 h. The efficiency of phagocytosis was determined by measuring the fluorescence of internalized yeast cells in the plate reader. The fold change in the RFU was calculated using this formula:

$$\text{Fold change} = \frac{RFU\ of\ sample}{RFU\ of\ 2\%\ glu\ (control)}$$

Figure 4-19 shows that RAW 264.7 murine macrophages were not able to phagocytose lactate-grown *Candida* cells efficiently. There is a 65% and 32% reduction in the phagocytosis of *C. auris* and *C. albicans*, respectively, pre-cultivated in a lactate-containing Minimal media. This result is similar to that in PMA-differentiated THP-1 macrophages.

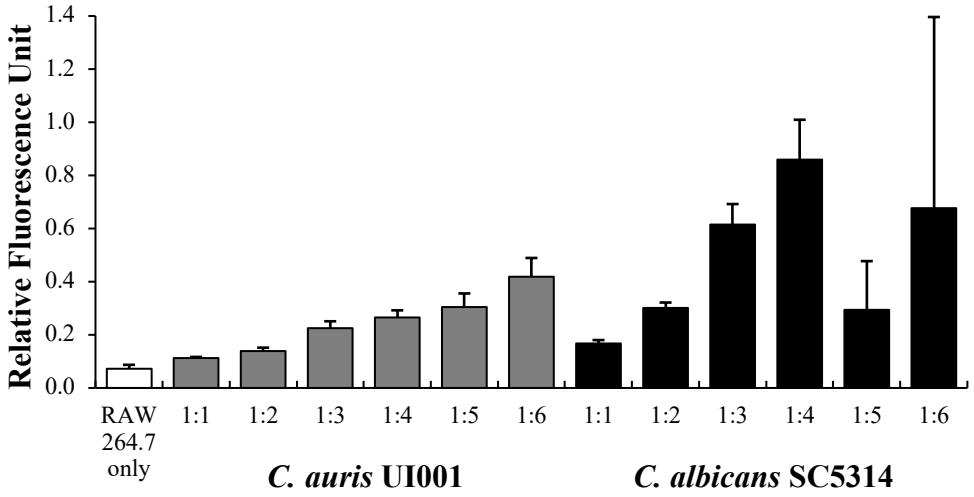

Figure 4-17. Relative fluorescence of RAW 264.7 macrophages co-incubated with increasing numbers of *C. auris* UI001 and *C. albicans* SC5314.

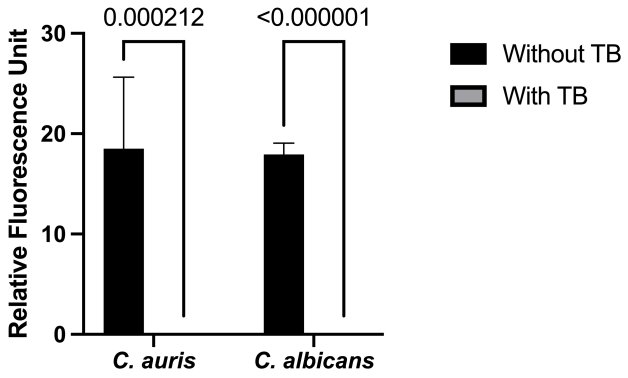

Figure 4-18. Effectiveness of trypan blue (TB) in removing fluorescence of fungal cells stained with acridine orange.

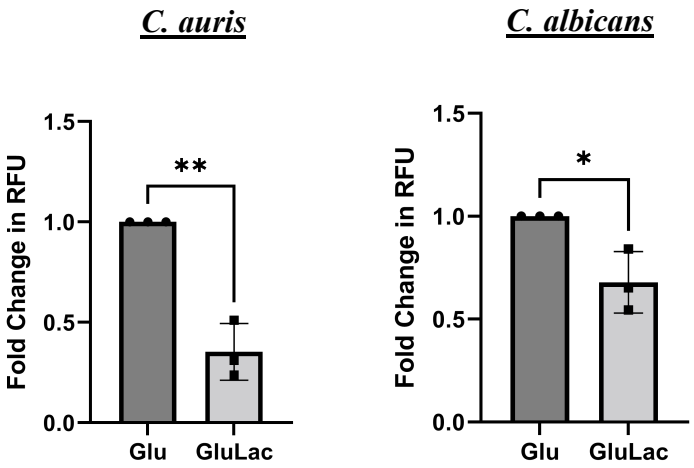

Figure 4-19. Fold change in the phagocytosis of *C. auris* UI001 (left) and *C. albicans* SC5314 (right) by murine macrophage cell line RAW 264.7.

4.3.8 Phagocytosis assay for *C. auris* type strains

To confirm if the reduction in phagocytosis rate observed in *C. auris* UI001 occurs in other strains belonging to a different clade, the same experiments were performed in two ATCC strains such as MYA-5001 and MYA-5002.

Figure 4-20 shows the effect of pre-culture under certain environmental conditions on the phagocytosis of two *C. auris* strains by PMA-differentiated THP-1 macrophages. In the previous chapters, it was shown that unlike UI001, 2% lactate did not induce changes in β-glucan but a 134% increase in mannan occurs in the MYA-5002 strain. As shown in Figure 4-20A, there was a ~50% decrease in both early and late-stage phagocytosis of *C. auris* MYA-5002 pre-cultured in Minimal medium with 2% lactate. MYA-5001 strain does not show any changes in β-glucan and mannan in the presence of lactate and so, was not used in this experiment. On the other hand, the *C. auris* MYA-5001 grown under hypoxic conditions exhibits a reduction of 36% and 41% in β-glucan and mannan, respectively. Figure 4-20B shows that this reduction in PAMP triggered a ~50% decrease in early and late-stage phagocytosis. MYA-5002 does not show any changes in β-glucan and mannan in hypoxic conditions and so, was not used in this experiment. In the case of varying pH, *C. auris* MYA-5001 grown under low pH conditions showed no changes in β-glucan but a 134% increase in mannan, compared to cells grown at neutral pH. Figure 4-20C shows that MYA-5001 grown under low pH conditions was phagocytosed twice as much as the cells pre-cultured at neutral pH. Cottier et al (2019) also checked the effect of pre-culture in low pH on the phagocytosis rate of *C. albicans.* Results show that cells harvested from a pH 4 medium, which

triggers the unmasking of β-glucan, were phagocytosed more by macrophages but could survive longer inside neutrophils.

The growth in 2% lactate and low pH, which both triggered an increase in mannan in one of the type strains, resulted in opposite outcome for phagocytosis. At this point, more experiments must be performed to further clarify the effect of these environmental stimuli on the succeeding phagocytosis by macrophages. Mannans are found to be fundamental for orchestrating the *C. auris*-specific host response at a 24-h time point (Bruno et al, 2020). The activity of Dectin-2 may also need to be checked to determine the contribution of mannan in the phagocytosis of *C. auris* strains.

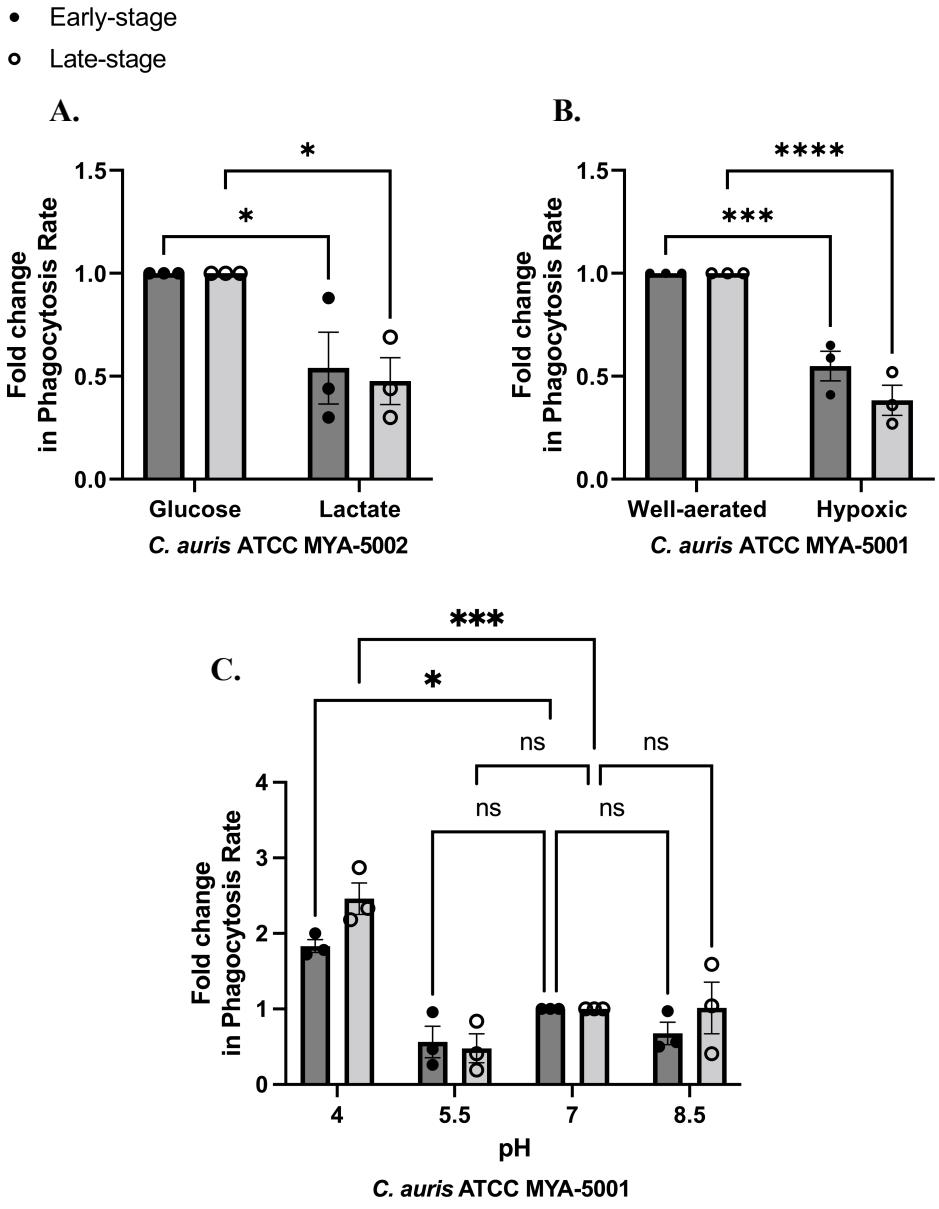

Figure 4-20. Fold change in the phagocytosis of type strains of *C. auris* pre-cultured in the presence of 2% lactate (A), in hypoxic condition (B), and varying pH (C). Data not shown in this Figure means that corresponding experiment was not performed.

4.4 CONCLUSION AND RECOMMENDATION

This chapter showed that changes in the cell wall architecture, particularly the masking of cell wall β-glucan in *C. auris*, affect the immune response against the pathogen. Lactate-induced β-glucan masking in *C. auris* triggered up to 84% (early stage) and up to 75% (late stage) reduction in phagocytosis by PMA-differentiated THP-1 macrophages. The same pattern was observed when murine macrophage cell line RAW 264.7 was used, where there is a 65% reduction in early-stage phagocytosis. In addition, it was observed that pre-culture in increasing amounts of lactate led to more reduction in the number of phagocytosing macrophages at 2 h post-infection. Consequently, the killing of lactate-grown cells decreased four-fold compared to that of glucose-only grown cells. Contrastingly, β-glucan masking due to sublethal concentration of antifungal agents such as fluconazole and micafungin increased the phagocytosis rate. Although considered non-canonical, this phenomenon is indirectly supported by other studies. To investigate whether β-glucan and Dectin-1 interaction is necessary for the uptake of *C. auris* cells by THP-1 macrophages, a Dectin-1 antagonist was used. The addition of laminarin an hour before the infection assay using *C. auris* UI001 resulted in 50% less phagocytosis. This means that recognition of β-glucan by Dectin-1 is important but not necessary for phagocytosis to occur, as other PAMPs or its corresponding PRR could also play an important role in sensing and phagocytosis of *C. auris.*

To determine if the immune response against *C. auris* is strain specific, two ATCC strains belonging to different clades were used. MYA-5001 strain, which exhibits a ~40% reduction in both β-glucan and mannan in a hypoxic environment, triggered a ~50% decrease in both early and late-stage phagocytosis. However, the growth in 2% lactate and low pH, which both triggered an increase in mannan in the type strains, resulted in an opposite outcome for phagocytosis. At this point, more experiments must be performed to further clarify the effect of these environmental stimuli on the succeeding phagocytosis by macrophages.

To have a full picture of the effect of PAMP exposure levels on the immune response, chitin levels can also be determined. The contribution of Dectin-2, the receptor for mannan, to the phagocytosis of *C. auris* strains can also be clarified. Also, to complement the phagocytosis assay result, PBMCs derived from the blood of healthy human volunteers can be used. For the quantification of ROS production, a rapid and sensitive luminescent assay that can measure the real-time ROS from the immediate start of infection up to several hours is recommended. In this study, ROS levels at only three time points - 30 min, 1 h, and 2 h post addition of yeast cells, were measured. Furthermore, it will be interesting to determine if *C. auris* can cause lysis of macrophages.

CHAPTER 5. EFFECT OF BETA-GLUCAN MASKING IN *CANDIDA AURIS* ON ITS VIRULENCE ON DOMESTIC SILKWORM (*Bombyx mori* Linnaeus, 1758)

5.1 INTRODUCTION

The use of experimental animals is deemed valuable in testing for fungal pathogenesis and virulence, as well as developing innovative treatments for fungal diseases. The larvae of some insects have been successfully used as models of fungal pathogenesis due to many reasons such as low cost of rearing, rare ethical issues, low requirement for biosafety measures, and having a sufficient size that allows injection of standardized fungal inoculum and studies of drug pharmacodynamics. Furthermore, using insects and other invertebrates (see Table 5-1) make it possible to conduct *in vivo* examinations of phagocytic cell function (Chamilos et al, 2007; Goldman and Osmani, 2007).

Table 5-1. *In vivo* infection models with invertebrate animals and mice (lifted from Matsumoto and Sekimizu, 2019 and Ishii et al, 2016).

Animals	Cost of Rearing	Space for Rearing	Permission from the Ethics Committee	Requirement for Biosafety Measures	Quantitative Injection of Samples with a Syringe
Silkworm (larva) [*Bombyx mori*]	Low	Small	Not necessary	Low	Easy
Fruit fly (adult) [*Drosophila melanogaster*]	Low	Small	Not necessary	High	Difficult
Nematode [*Caenorhabditis elegans*]	Low	Small	Not necessary	Low	Difficult
Greater wax moth (larva) [*Galleria mellonella*]	Low	Small	Not necessary	Low	Easy
Mouse [*Mus musculus*]	High	Large	Necessary	High	Easy

Several infection studies in which *Candida* sp. was injected into invertebrate hosts such as silkworm (Matsumoto and Sekimizu, 2019; Hamamoto et al, 2004), fruit fly (Binggeli et al, 2014), nematode (Lopes et al, 2018), and greater wax moth (Cottier et al, 2019) have been carried out. In

terms of assessing fungal virulence, infection experiments could be performed to verify the effect of yeast cell wall remodeling on the innate immune response against the pathogen. For example, Cottier et al (2019) used *G. mellonella* larvae to determine the effect of low pH-induced unmasking of β-glucan in *C. albicans* on the immune response of the greater wax moth. The results showed that yeast cells pre-grown at pH 4 for 2 h are more virulent to *G. mellonella* larvae compared to cells pre-grown at pH 6. Virulence of *Candida* sp. and other yeast species like *Aspergillus fumigatus* and *Cryptococcus neoformans* can be assessed by melanization and eventual death of the larvae (Pereira et al, 2018) and changes in hemocytes, the immune cells of invertebrates. Results are comparable to using mammals since the immune system of *G. mellonella* shares several structural and functional similarities with the mammalian innate immune system (Kavanagh et al, 2004). Infection experiments using *C. auris* have recently been performed using the greater wax moth (Garcia-Bustos et al, 2022; Smith et al, 2022) and nematode (Lima et al, 2020; Day et al, 2018) but to date, little to no research have been done using silkworms.

According to Matsumoto and Sekimizu (2019) and Ishii et al (2016), the use of silkworms offers several advantages compared to other invertebrates. Silkworms are larger than fruit flies and nematodes, so it is easier to inject an accurate amount of fungal suspension using a tuberculin syringe. Furthermore, the use of silkworms over greater wax moths allows accurate intra-hemolymph and intra-midgut injection. Both routes of injection can be easily differentiated and employed as distinct sites of inoculation in silkworms, with the former serving as a similar system to intravenous injection and the latter to oral delivery in humans. Silkworms also allow the investigation of molecular mechanisms of infection by human fungal pathogens (Hanaoka et al, 2005, 2008). *B. mori* larvae require a temperature of 29°C for growth and maintenance but can still thrive at mammalian physiologic temperature (37°C), which allows for the expression of relevant temperature-regulated virulence factors (Ishii et al, 2016).

Another advantage of using silkworms is that fungal cell wall components such as mannan and β-glucan can activate the immune system. The β-1,3-glucan recognition protein (βGRP) found on the surface of silkworm hemocyte binds to β-1,3-glucan leading to activation of the prophenoloxidase cascade (Ashida, 2004; Ochiai and Ashida, 2000) resulting in the production of quinones and melanin, which then manifests as blackening of the injected larvae. On the other hand, a C-type lectin receptor BmMBP is shown to bind mannan thereby triggering an immune response (Ohta et al, 2006; Watanabe et al, 2006).

In this study, silkworm larvae were used to determine the effect of lactate-induced β-glucan masking in *C. auris* UI001 on the innate immune response against the pathogen. Survival curves of larvae injected with either glucose-only grown or glucose-lactate grown *C. auris* were generated and compared.

5.2 MATERIALS AND METHODS

5.2.1 Fungal strains used in this study

All yeast strains used in this study are shown in Table 5-2. *C. albicans* TUA6 was obtained from the National Institute of Infectious Diseases in Japan. *C. auris* UI001 is a clinical isolate from a patient in Indonesia while *S. cerevisiae* S288C was obtained from the Institute of Fermentation in Japan.

Yeast strains that served as control were cultured overnight by inoculating in YPD medium (1% yeast extract, 2% peptone, 2% glucose) and cultured with shaking at 200 rpm. The culture temperature is 37°C for *C. albicans* and *C. auris* and 30°C for *S. cerevisiae.* Overnight cells were transferred to fresh YPD in a 1:50 ratio, then cultivated until the mid-logarithmic phase (OD_{600} = 0.5-0.8). For *C. auris,* cells were cultured in a Minimal medium with either Glu (2% glucose) or GluLac (1% glucose plus 1% lactate) the same method in Chapter 2. The cultured yeasts were collected, washed with 0.6% saline, and then resuspended in 0.6% saline up to the desired concentration. The concentration was adjusted so that the number of cells to be inoculated per silkworm was present in 100 μL of the fungal solution.

Table 5-2. Fungal strains used in this study.

Species	Strain	Genotype	Source
C. albicans	TUA6	*ura*3Δ::*imm434*/*ura3*Δ::*imm434* *arg4*Δ::*hisG200*/*ARG4 RP10*::p3HA-ACT1(*URA3*)	Hanaoka et al (2005)
C. auris	UI001	wildtype	University of Indonesia
S. cerevisiae	S288C	*MATα* prototroph *SUC2 gal2 CUP1 flo1 mal2 flo8-1 hap1*	Mortimer & Johnston (1986)

5.2.2 Infection assay using silkworm

Rearing of silkworms

Silkworm infection experiments were performed as described previously (Hamamoto et al, 2004) but with slight modifications. Third instar larvae of *Bombyx mori* (Fuyo x Tsukubane), purchased from Ehime Sanshu (Ehime, Japan), were fed with the antibiotic-containing SilkMate 2S (Nihon Nosan Kogyo Corporation, Yokohama, Japan) until they developed to fifth-instar larvae. Silkworms were put on a plastic food pack with Kimwipes (Kimtech Science™) at the bottom and secured by a rubber band. One to two plastic food packs were placed inside a carton wrapped in Saran wrap and laid with Kimtowels for easier cleaning. Silkworms were bred in an incubator (Eyelatron, model FLI-301N, Rikakikai Co., Ltd, Japan) set at 27°C, and with a fluorescent lamp that is set to be turned on for 12 h and turned off for 12 h in one day. A beaker with sterile water was placed inside the incubator for added moisture. Rearing boxes were cleaned every day. After seven days of feeding with SilkMate 2S (Nihon Nosan Kogyo Co. Ltd., Yokohama, Japan), the silkworms were fed with an antibiotic-free feed (10% mulberry leaf powder [Healthy Company, Japan], 10% soybean flour [Kadoya Beikoku], 2.5% agar) for one day. This artificial feed was formulated by Paudel et al (2020). Larvae were then starved for one day before injection.

Intra-hemolymph injection

The silkworm larvae used for injection were those that had grown to a weight of 1.9 to 2.3 g and had no wounds. Intra-hemolymph injection, where the injection was made parallel to the silkworm body and at an angle close to where the half-moon crest is present, was performed. Prior to injection, the silkworm's body was wiped using a Kimwipe sprayed with 70% ethanol. Yeast suspension (100 µL) containing 5 x 10^6 yeast cells was injected into each larva using a 1 mL tuberculin syringe and a 27G × 3/4″ needle (Terumo Medical Corporation, Tokyo, Japan). The same volume of saline was injected as the control. Injected larvae were not fed and kept in an incubator set at 27°C. Mortality was checked every 24 h for three days. Dead silkworms were removed and soiled Kimwipes were replaced after each observation period. A silkworm was judged dead if its head, thoracic legs, and tail legs do not move autonomously when touched with a finger. After the experiment, all larvae whether alive or dead were autoclaved at 121°C for 15 min. Used carton boxes were sprayed with 70% ethanol and UV-sterilized after each trial.

5.2.3 Statistical analysis

The infection assay was independently performed thrice. In each replicate, ~15 larvae were injected with *C. auris* grown in each condition while 10 larvae were injected with each of the control yeast strains. Survival data were evaluated by Kaplan-Meier analysis, and statistical significance was calculated using a log-rank test. Calculated p values were adjusted following the Benjamini-Hochberg method using the "survminer" (Kassambara et al, 2019) package in R (R Core Team, 2020).

5.3 RESULTS AND DISCUSSION

The purchased third instar silkworm larvae were fed for one week with SilkMate 2S (Figure 5-1A), an antibiotic-containing feed used in several infection assay experiments (Matsumoto et al, 2022; Kurakado, Matsumoto, and Sugita 2021; Hanaoka et al, 2008). To eliminate the possible effect of antibiotics in the infection assay, larvae were fed two days pre-injection with an antibiotic-free artificial diet (Figure 5-1B) which was manually prepared, autoclaved at 121°C for 15 min, and stored in a 4°C refrigerator before use.

A. **B.**

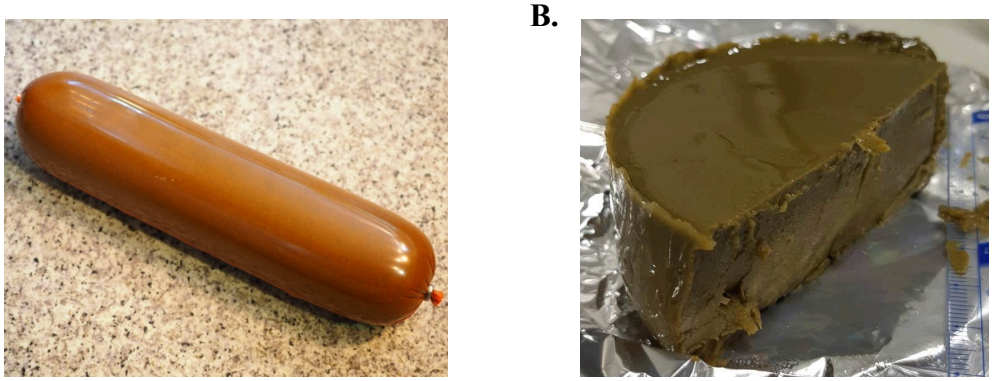

Figure 5-1. Silkworm feed with antibiotic (A) purchased from Ehime Sanshu and a manually prepared antibiotic-free artificial feed (B).

Before starting the infection assay, a practice injection was performed wherein a red food-grade dye (Figure 5-2A) was injected into the hemolymph of the silkworm. A successful intra-hemolymph injection would result in the diffusion of the red dye throughout the silkworm hemolymph resulting in the appearance of red legs (Figure 5-2B).

A. B.

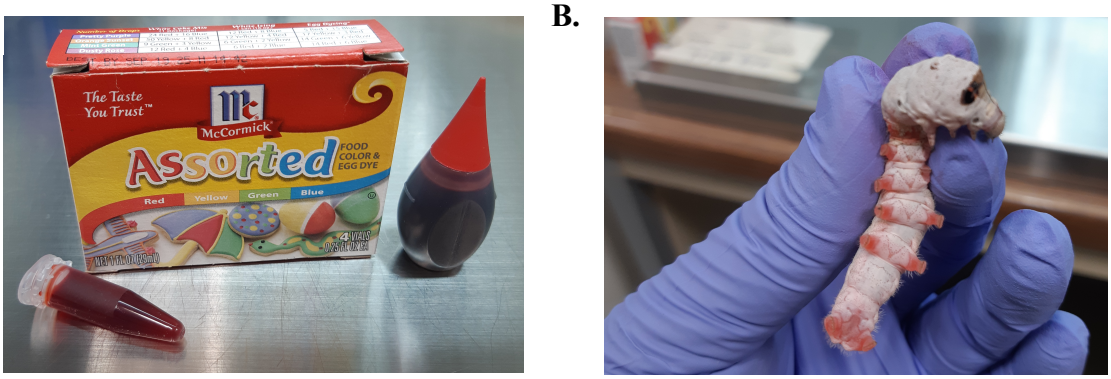

Figure 5-2. Red food color used in the practice injection (A) and injected larva with red legs as observed 15 min post-intra-hemolymph injection.

Infection experiments were then independently performed thrice. A Kaplan-Meier survival analysis (Kaplan & Meier, 1958) was conducted to compare survival times among silkworm larvae injected with different strains of yeast. *C. albicans* TUA6 and *S. cerevisiae* S288C serve as positive and negative control, respectively based on previous experimental results. The resulting survival curve representing all three independent biological replicates is presented in Figure 5-3. After the 72-hour observation period, all uninjected silkworm larvae, as well as those injected with 0.6% saline, survived. A log-rank test was used to determine if there were differences in the survival of silkworm larvae injected with different fungal strains. The survival distributions were statistically significantly different, $\chi 2(2) = 38.6$, $P = 3x10^{-7}$. Pairwise comparisons wherein *P* values were adjusted following the Benjamini-Hochberg method (Benjamini & Hochberg, 1995) were conducted. Results show that there is a difference in the survival of larvae injected with *C. auris* pre-cultured in glucose only vs the same strain but pre-cultured in glucose-lactate ($P = 0.042$) where median survival is 48 h and 24 h, respectively.

The infection experiment result complements the data presented in Chapter 4, where lactate-induced β-glucan masking in *C. auris* UI001 triggered a significant reduction in phagocytosis by human monocyte cell line THP-1 and murine macrophage cell line RAW 264.7. The phagocytic ability of these types of macrophages may not be the same as the immune cells of silkworms but considering that silkworms can recognize β-1,3-glucan via the β-1,3-glucan recognition protein (βGRP) found on the surface of silkworm hemocyte, we hypothesize that masking of β-glucan lead to immune evasion, thus leading to increased virulence of *C. auris*.

In a study by Lopes et al (2018), hypoxia-induced β-glucan masking in *C. albicans* lead to increased virulence in a *C. elegans* infection model. Conversely, Cottier et al (2019) showed that an increased level of PAMP exposure in low pH-grown *C. albicans* correlates with higher pathogenicity.

Overgrowth of *C. auris* due to immune evasion may have caused the death of the larvae. According to Matsumoto and Sekimizu (2019), the growth of fungi contributes to the silkworms' death since antifungal drugs can be successfully used to treat silkworms in silkworm infection models with pathogenic fungi.

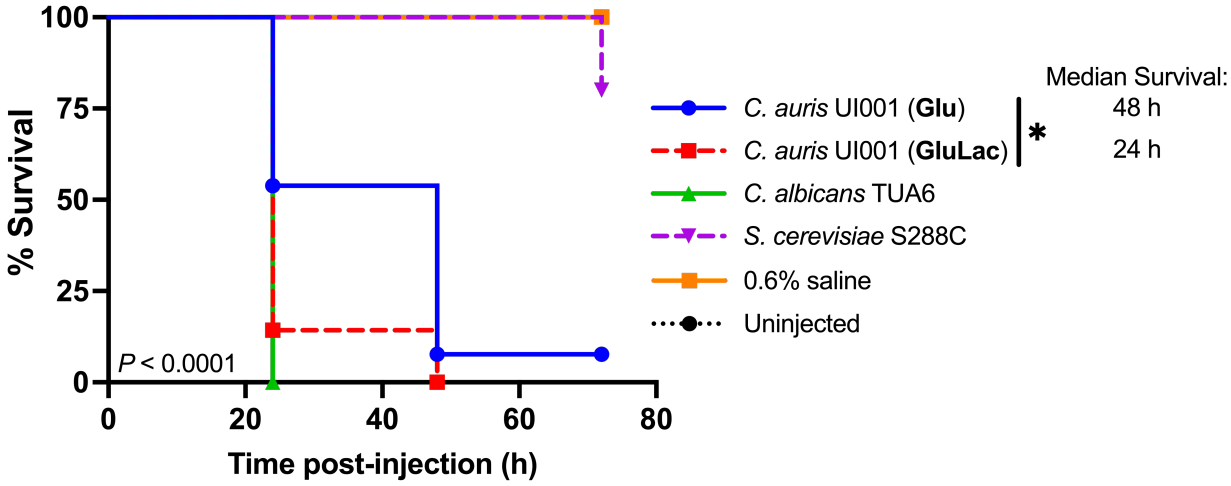

Figure 5-3. Kaplan-Meier survival curve for silkworm larvae following infection with 5 x 10^6 cells of indicated strains. The graph represents data from three independent biological replicates. Statistical significance was calculated using a log-rank test followed by BH correction of *P* values: * $P < 0.05$.

Several studies compared the virulence level of *C. auris* and *C. albicans.* In a study by Garcia-Bustos et al (2022), *C. auris* showed remarkably higher immunogenic activity in a *G. mellonella* infection model and induces a greater inflammatory response than *C. albicans* reference strain SC5314 and *C. parapsilosis* reference strain 22019. Compared to this study, different strains were used which could explain why *C. albicans* TU6 was observed to be more virulent than *C. auris*. In another study by Bruno et al (2020), *C. auris* is less virulent than *C. albicans* in an experimental model of murine disseminated candidiasis.

During the infection experiments, it was observed that silkworms injected with *C. auris* were starting to turn black at 24 h post-injection. This blackening is due to melanin, a common fungal virulence factor that could promote oxidative stress resistance, mammalian immune response evasion, and antifungal peptide and pharmaceutical inactivation. In a study by Smith et al (2022), all experimented with *C. auris* isolates belonging to Clade I were able to produce melanin that protected the fungus from oxidative damage. However, an *in vitro* analysis using

BMDM showed that melanin does not protect *C. auris* against macrophage killing. Furthermore, an *in vivo* analysis showed that melanin does not affect *C. auris* virulence during *G. mellonella* infection.

5.4 CONCLUSION AND RECOMMENDATION

Considering the low experiment cost and lack of ethical concerns, silkworm is an ideal animal model that can be used for infection assays. Silkworm infection models can contribute to establishing new preventive and therapeutic strategies by elucidating the infectious systems of emerging pathogenic fungi such as *C. auris*.

Silkworm larvae appear to have a lower chance of surviving if injected *C. auris* cells were pre-grown in a lactate-containing media, which was shown to trigger β-glucan masking. This may be explained by the reduction in the recognition of yeast cells by βGRP on the surface of hemocytes leading to immune evasion and enhanced survival of *C. auris.* This observation supports the phagocytosis assay result shown in Chapter 4, albeit using human and mouse macrophage cell cultures only. Therefore, lactate-induced β-glucan masking in *C. auris* could potentially lead to immune evasion leading to increased virulence of *C. auris* in a host organism.

Due to some limitations in institutional facilities, an *in vivo* work on mice was not performed to observe the pathogenesis of *C. auris* and recruitment of immune cells toward the infection site. As a recommendation for future studies, a more in-depth analysis of infection could be performed. Immunological markers of infection such as hemocyte activity based on ATP content quantification could be performed. In addition, antimicrobial peptide expression can be measured by a qRT-PCR analysis and activation of the proPO system can be monitored by measuring phenoloxidase (PO) enzyme activity.

CHAPTER 6: ELUCIDATION OF THE MOLECULAR MECHANISM BEHIND BETA-GLUCAN MASKING IN *CANDIDA AURIS*

6.1 INTRODUCTION

The emerging fungal pathogen, *C. auris*, is categorized as a global public health threat by the Centers for Disease Control and Prevention. In Chapter 2, it was shown that a clinical isolate of *C. auris* from Indonesia (UI001) exhibits masking of β-glucan when cultured in a lactate-containing media, as well as in a hypoxic environment and the presence of sublethal amounts of antifungal agents such as fluconazole and micafungin. This major PAMP masking leads to a reduction in the efficiency of phagocytosis, as shown in Chapter 4. The masking phenomenon is hypothesized to occur due to cell wall remodeling but so far, the specific mechanism for *C. auris* is still unknown as there are little to no studies performed in *C. auris*.

Several studies elucidated the molecular mechanism behind β-glucan masking in *C. albicans.* For lactate-induced β-glucan masking, Ballou et al (2017) figured that lactate is firstly sensed by the G-protein coupled receptor Gpr1, which then sends signals to the transcription factor, Crz1, in a calcineurin-independent manner to control the expression of cell wall-related genes. For the effect of low oxygen environment on β-glucan expression in *C.* a*lbicans*, Pradhan et al (2018) discovered that *GOA1, UPC2*, *SOD1*, *CYR1,* and *TPK1/TPK2* are indispensable for hypoxia-induced β-glucan masking. Hypoxia triggers the formation of oxygen free radicals in the mitochondria. Goa1 (Growth and Oxidant Adaptation 1) or transcription factor Upc2 is involved in reducing ROS production while Sod1 (Superoxide dismutase 1) in the mitochondrial inner membrane space converts superoxide into hydrogen peroxide, which in turn possibly results in the activation of adenylyl cyclase (Cyr1) and cAMP-PKA (Tpk1/2) signaling. For both lactate and hypoxia, Childers et al (2020) provided evidence that a secreted glucan 1,3-β-glucosidase (Xog1) is directly involved in "shaving" β-glucan off the cell surface.

Yang et al (2022) showed that yeast cell wall remodeling due to antifungal drugs, lactate, and N-acetylglucosamine are controlled by two highly expressed yeast proteins, the endo-1,3-β-glucanase Eng1 which is involved in β-glucan trimming and the Yeast Wall Protein Ywp1 which mediate β-glucan masking. Eng1 is also shown to trim exposed β-glucan in the dimorphic fungus, *Histoplasma capsulatum* (Garfoot et al, 2016). Moreover, Ywp1 is also shown to contribute to β-glucan masking in *C. albicans* (Granger, 2018) while protein expression is upregulated by 3.7-fold in *C. albicans* grown in lactate versus glucose (Childers et al, 2020). Moreover,

mannosyltransferases also play a role in cell wall remodeling as Graus et al (2018) showed that mannosyltransferases regulate the size and density of nanoscale glucan exposures in *C. albicans*.

In this chapter, the molecular mechanism behind the observed lactate-induced β-glucan masking in a clinical strain of *C. auris* is elucidated. To narrow down the search for the probable genes involved, genes shown to be involved in other species like *C. albicans* (Table 6-1) were chosen, and expression of these genes was measured in *C. auris* UI001 grown in lactate-containing media and compared to cells grown in glucose only.

Table 6-1. List of genes that may be involved in lactate-induced β-glucan masking in *C. auris* UI001. Information was collected from several papers as specified below*

Gene	Description
Genes related to β-glucan degradation:	
XOG1	Exo-1,3-β-glucanase; "shaves" β-glucan on the cell surface; Deletion of this gene does not completely block the β-glucan masking phenomenon observed in *C. albicans* wildtype (WT) cells; There is no difference in the mRNA transcript of *XOG1* in glucose- and lactate-grown cells so β-glucan masking-related function of XOG1 might be post-transcriptionally controlled
ENG1	Endo-1,3-beta-glucanase; Caspofungin and fluconazole repressed gene
Genes related to β-glucan synthesis:	
EXG2	GPI-anchored cell wall protein induced during cell wall regeneration; Upregulated by 3.6x in *C. albicans* WT cells grown in GluLac compared to cells grown in Glu only but *C. albicans exg2*Δ still exhibit β-glucan masking (fold change= 0.59; observed by flow cytometry analysis) when grown in GluLac
Genes related to mannan production:	
MNN2	α-1,2-mannosyltransferase; Has a role in maintaining cell wall integrity
MNN14	Predicted α-1,3-mannosyltransferase activity with a role in protein glycosylation; Upregulated by 5.6x in *C. albicans* WT cells grown in GluLac compared to cells grown in Glu only but *C. albicans mnn14*Δ still exhibit partial β-glucan masking (fold change= 0.74; observed by flow cytometry analysis) when grown in GluLac; Does not require transcription factor Crz1

Gene	Description
MNN15	Putative α-1,3-mannosyltransferase; Predicted role in protein O-linked glycosylation; Downregulated by 3.3x in *C. albicans* WT; requires Crz1
MNN22	α-1,2-mannosyltransferase; required for normal cell wall mannan; Execute cell wall or cell surface-related functions Downregulated by 3.9x in *C. albicans* WT; Does not require Crz1; *C. albicans mnn22*Δ exhibit β-glucan masking (fold change= 0.41; observed by flow cytometry) when grown in GluLac
MNN26	Putative α-1,2-mannosyltransferase; *Camnn2Δ/mnn26Δ* has 4x more exposed β-glucan
PMR1	Secretory pathway P-type Ca2+/Mn2+-ATPase; Required for protein glycosylation and cell wall maintenance; Pmr1 acts as a Golgi-resident ion pump that provides cofactors to mannosyltransferases, regulating the synthesis of mannans attached to glycoproteins
VAN1	Member of Mnn9 family of mannosyltransferases
Genes related to glucose sensing:	
GPR1	Plasma membrane G-protein-coupled receptor of the cAMP-PKA pathway; Detects lactate and triggers signaling pathway that regulates β-glucan masking and immune evasion; Deletion of this gene can block the β-glucan masking phenomenon observed in *C. albicans* wildtype cells
CDR1	Multidrug transporter belonging to ATP-binding cassette (ABC) superfamily; Upregulated by 5.9x in *C. albicans* WT (*CDR2*)
Transcription factor controlling cascade of reactions leading to cell wall remodeling:	
CRZ1	Calcineurin-regulated C2H2 transcription factor; Role in the maintenance of membrane integrity, azole tolerance; Repressed by low iron which is shown to trigger β-glucan masking in *C. albicans*; Regulates Ca++ influx during alkaline pH response; Deletion of this gene can block the β-glucan masking phenomenon observed in *C. albicans* wildtype cells

*Sources: Ballou et al (2017), Childers et al (2020), Graus et al (2018), Pradhan et al (2018), Suchodolski et al (2021), and http://www.candidagenome.org

6.2 MATERIALS AND METHODS

6.2.1 Use of enzyme inhibitors to determine signaling systems involved in β-glucan masking in *C. auris*

β-glucan staining in *Candida* cells was performed as in Chapter 2. Selected tubes were added with the following inhibitors, 100 µM H-89 (AdooQ Bioscience, cat # A11935) and 3.12 µg/mL FK506 (Fujifilm Wako Pure Chemical Corporation, cat # 063-06191). For the hypoxic set-up, 2 mL microcentrifuge tubes with screw caps were used.

6.2.2 Genomic DNA extraction

The basic protocol for the phenol-chloroform method of extraction of yeast gDNA was followed. Cells grown overnight were collected by centrifugation at 5,000 rpm for 2 min at 4°C and washed with dH_2O. The resulting cell pellet was mixed thoroughly with 200 µL of DNA isolation buffer [2% Triton X-100, 1% SDS, 100 mM NaCl, 10 mM Tris-HCl (pH 8.0), 1 mM EDTA (pH 8.0)]. The cell suspension was transferred to a 1.5 mL tube containing 300 mg of 0.45-0.5 mm acid-washed beads (Sigma, G8772). Then, 100 µL of Tris-saturated phenol (pH 8.0) and 100 µL chloroform were added to the tube that is then vortexed vigorously for 3-4 min. Next, 200 µL of TE buffer (pH 8.0) was added and the suspension was vortexed briefly and centrifuged at top speed for 5 min at 4°C. The supernatant was purified by repeating the following steps until cell debris disappeared. The supernatant was transferred to a new 1.5 mL tube with a pipette and an equal amount of 1:1 Tris-saturated phenol (pH 8.0)-chloroform was added, and the tube was vortexed and centrifuged at top speed. Using the purified supernatant, 250 µL of 99.5% ethanol was added and the sample was vortexed, incubated at -80°C for 20 min to 1 h, and centrifuged at top speed. The supernatant was discarded by decantation and 1 mL of 70% ethanol was added. The tube was centrifuged at top speed and the supernatant was discarded by decantation. DNA was dried using a centrifugal concentrator (Taitec Spin Dryer Mini VC-15SP) and resuspended in 400 µL TE buffer (pH 8.0) and 3 µL of RNase (10 mg/mL).

6.2.3 RNA extraction

C. auris clinical strain and ATCC strains were grown overnight in a Minimal medium with 2% glucose and subcultured (OD_{600} = 0.2) onto fresh Minimal medium with either Glu or GluLac. Cells were incubated for 5 h at 37°C at 200 rpm. Before extracting RNA, all materials and bench

space used were sprayed with RNase Quiet (Nacalai Tesque). RNA was generally isolated in two ways. One is by using QIAGEN RNeasy Mini Kit following the manufacturer's protocol. The other method is by hot phenol method. In this method, cells were centrifuged for 3 min at 1500 g and 4°C. The supernatant is discarded, and the pellet was washed twice with ice-cold water. The cell pellet was resuspended in 400 µL TES solution (10 mM Tris-Cl [pH 7.5], 10 mM EDTA, 0.5% SDS). Then, 400 µL acid phenol preheated to 65°C was added and the tube was vortexed vigorously for 10 s. Tubes were incubated for 60 min at 65°C with brief vortexing for 10 s every 15 min intervals. Tubes were then put on ice for 5 min and centrifuged at top speed (13,000 g) for 5 min at 4°C. The aqueous top phase was transferred to a clean 1.5 mL microcentrifuge tube, 400 µL acid phenol was added and the tube was vortexed vigorously, placed on ice for 5 min, and centrifuged at top speed (13,000 g) for 5 min at 4°C. Next, the aqueous phase was transferred to another clean 1.5 mL microcentrifuge tube, 400 µL chloroform was added and the tube was vortexed vigorously and centrifuged at top speed (13,000 g) for 5 min at 4°C. The aqueous phase was transferred to a clean 1.5 mL microcentrifuge tube, 40 µL of 3 M sodium acetate (pH 5.3), and 1 mL of ice-cold 100% ethanol were added consecutively. The tube was mixed by hand and kept at -80°C for at least 15 min to 1 h. Tube was centrifuged at top speed (13,000 g) for 5 min at 4°C and supernatant was removed. RNA pellet was washed with 1 mL ice-cold 70% ethanol. Tube was centrifuged to remove the supernatant and RNA was dried using a centrifugal concentrator (Taitec Spin Dryer Mini VC-15SP). RNA pellet was resuspended in 50 µL nuclease-free water and placed in a water bath set at 37°C for 5-10 min to ensure full resuspension of RNA. After extraction, RNA quality and concentration were spectrophotometrically determined using NanoDrop ND-1000.

To check for RNA quality through electrophoresis, a 1% denaturing agarose gel in 1x MOPS and 7% formaldehyde was prepared. Formamide (5 µL) was added to ~3.5 µg RNA and tubes were placed in a 65°C dry bath for 10 min. The tube was then kept in ice for 5 min after which 100 µg/mL ethidium bromide was added. For the electrophoresis, 1x MOPS was used as a running buffer and samples were run for 1 h at 50 V.

6.2.4 Real time-Quantitative Polymerase Chain Reaction (RT-qPCR)

Extracted RNA (Total RNA: 6.25 µg) was reverse transcribed using ReverTraAce qPCR RT Master Mix with gDNA Remover (Toyobo, Japan) following the manufacturer's protocol. Quantitative PCR was performed using Thunderbird SYBR qPCR mix (Toyobo, cat # QPS-201) in Roche LightCycler 96. The qPCR components consist of the following: 5.0 µL of 2x mix, 3.4 µL of nuclease-free water, 1.0 µL of 50 ng/ µL cDNA template, and 0.3 µL each of 10 µM primers

(Table 6-2). All primers were ordered from Integrated DNA Technologies (https://sg.idtdna.com/pages). There is a pre-incubation at 95°C for 60 s and 40-cycle amplification at 95°C for 10 s, 60°C for 30 s, and 72°C for 30 s. To show the melting curves, the tubes were subjected to 95°C for 10 s, 60°C for 60 s, and finally at 95°C for a continuous time. Samples were run in triplicate and data were analyzed using the 2-ΔΔCt method normalizing RNA expression against *ACT1* reference gene. Analysis was performed using LightCycler 96 SW1.1 software. Graphs and their corresponding statistical analyses were prepared using GraphPad Prism version 9.4.0 for Windows, GraphPad Software, San Diego, California USA, www.graphpad.com.

6.2.5 RNA sequencing for differential gene expression analysis

A different RNA extraction protocol was followed for RNA samples sent for sequencing. The yeast cell wall was first digested using the yeast processing buffer and enzyme solution from Takara (cat # 9089). Qiagen RNeasy Mini Kit was used to isolate RNA following the manufacturer's protocol. DNA digestion was performed using the following reagents from Takara: DNase I buffer, RNase-free DNase I, and RNase Inhibitor (Code #2313A). RNA clean-up was performed using the Qiagen RNeasy Mini Kit following the manufacturer's instructions. RNA quality and concentration were determined by NanoDrop ND-1000 and denaturing agarose gel electrophoresis.

Samples were sent to the Bioengineering Lab of 株式会社生物技研 (Kabushikigaisha Seibutsu Giken) in Kanagawa, Japan. Prior to library preparation, total RNA concentrations were measured using the Quantus Fluorometer and the QuantiFluor RNA system (Promega). Quality was then checked using the 5200 Fragment Analyzer System and the Agilent HS RNA Kit (Agilent Technologies). For the library preparation, MGIEasy RNA Directional Library Prep Set (MGI Tech Co., Ltd.) was used according to the manual.

Measurement of the concentration of the prepared library solutions was performed using the Synergy H1 (BioTek) and the QuantiFluor dsDNA System (Promega). The quality of the generated library was checked using Fragment Analyzer and dsDNA 915 Reagent Kit (Advanced Analytical Technologies). Next, the prepared library and MGIEasy Circularization Kit (MGI Tech Co., Ltd.), were used to prepare circularized DNA. DNBs were prepared according to the manual using the DNBSEQ-G400RS High-throughput Sequencing Kit (MGI Tech Co., Ltd.). For the sequencing analysis, DNBSEQ-G400 (MGI Tech Co., Ltd.) was used, and the generated DNB was sequenced under the condition of 2x100 bp.

Table 6-2. Primers used in the RT-qPCR analysis of expression of selected genes in *C. auris* grown in either glucose only or glucose-lactate.

Target Gene	Primer Name	Forward and Reverse Primers (5' → 3' sequence)	T_a (°C)*	Amplicon (bp)	Source
ACT1	F1-ACT1-Cau	GAGAGATTTAGAGCTGCTGAGG	52	90	This study
	R1-ACT1-Cau	GATAGAGTTGTAAGTCGTCTGGTC			
CDR1	F1-CDR1-Cau	GAGATGGGTGCTTACTCTGATG	52	155	This study
	R1-CDR1-Cau	GTCTGAGAGTCCAAACCAGAAG			
CRZ1	F1-CRZ1-Cau	CAGTGCAAGGGTTTGTTGAAAG	52	143	This study
	R1-CRZ1-Cau	CTCTCTCGCTCATCCTCTTCTA			
ENG1	F1-ENG1-Cau	GAGGCTCTCTACGATGGTAAATC	52	103	This study
	R1-ENG1-Cau	ATGCTAAACTCCATGTCCTACTC			
EXG2	F1-EXG2-Cau	TGGCAAGACAAGTCGGAATATG	52	97	This study
	R1-EXG2-Cau	CGTTGTACCTCTCACTGAACTC			
GPR1	F1-GPR1-Cau	GATCTCGCAGAGGGAGAATTTAG	52	99	This study
	R1-GPR1-Cau	GGTATCATGCTTTCCTCCTTGT			
MNN14	F1-MNN14-Cau	CCATCATTCCTCCGTTCGATAG	52	117	This study
	R1-MNN14-Cau	ATGAGTAGGCACACCAAAGATAG			
MNN15	F1-MNN15-Cau	GGACGCCTATCATACGGTAAAG	52	97	This study
	R1-MNN15-Cau	CCAGCCATTGATCTCGATTCTA			
MNN2	F1-MNN2-Cau	CCCTCCTTCTAGCACTCTACTAT	52	98	This study
	R1-MNN2-Cau	GAAAGTCTCTTTATCACCCTCTCC			
MNN22	F1-MNN22-Cau	CCAACTACCCTAAACTCAATCC	50	89	This study
	R1-MNN22-Cau	AAGACCGTATAGCCTGTATCTC			
MNN26	F1-MNN26-Cau	CAGTTGGACAGAGACTTTACTCA	52	113	This study
	R1-MNN26-Cau	TCCTTGAACTGATCCTTGTTCTC			
PMR1	F1-PMR1-Cau	GATATGGTGCTTACCGATGATG	50	107	This study
	R1-PMR1-Cau	GTGGACAACTGGAAGGTTATGA			
VAN1	F1-VAN1-Cau	GGTTTACTGGAGAGACGTTGAT	50	96	This study
	R1-VAN1-Cau	CAGATATTGGGAACCATGACATC			
XOG1	F1-XOG1-Cau	CACTGTCCCTGTGGATGAATAC	52	103	This study
	R1-XOG1-Cau	GTCGTCTTCAGTGTACCATGTATC			

*T_a for standard PCR

For the data analysis, adapter sequences and low-quality sequences were removed with "cutadapt" (ver. 4.0). Paired reads with a quality score of fewer than 20 bases and less than 40 bases were removed using sickle (ver. 1.33). Hisat2 (ver. 2.2.1) was used to perform mapping of high-quality reads to reference sequences with output data in sam format. The genomic sequence

data of *C. auris* (https://www.ncbi.nlm.nih.gov/assembly/GCF_002775015.1) was used as the reference. Then, the sam format was converted to bam format using Samtools (ver. 1.11), followed by sorting and indexing. For read counting and normalization, "featureCounts" (ver. 2.0.0) was used to count reads that mapped to the gene regions of the reference sequence. Reads Per Kilobase Million (RPKM) normalization and Transcripts Per Million (TPM) were then used to normalize each read count for total reads and gene length across samples. After normalization using the DEGES normalization method of TCC (ver. 1.18.0), genes with altered expression were identified using DESeq (ver. 1.30.0). Volcano plot was created using "bioinfokit" in Python.

The differential gene expression analysis result was validated by qPCR. The qPCR components and run protocol are the same in section 5.2.4. Primers that could detect the top ten most differentially expressed genes (Table 6-3) were designed and ordered from Integrated DNA Technologies (https://sg.idtdna.com/pages). Standard PCR using EmeraldAmp MAX PCR master mix (Takara Bio Inc.), following the manufacturer's recommended PCR conditions, was performed to confirm the amplification of the expected products. The annealing temperature for all primer pairs was set at 53°C. The qPCR validation of DEG8 expression was not performed since agarose gel electrophoresis of PCR products revealed that the primer pair for DEG8 amplified an unexpected ~500 bp product aside from the expected 105 bp. Graphs and their corresponding statistical analyses were prepared using GraphPad Prism version 9.4.0 for Windows, GraphPad Software, San Diego, California USA, www.graphpad.com.

6.2.6 Ploidy determination in *C. auris*

This protocol is adapted from Fan et al (2020) and Bravo Ruiz et al (2019). Overnight-grown yeast cells were inoculated onto fresh YPD broth and incubated at 37°C for 5 h at 200 rpm. The OD_{600} was adjusted to 1.0, which corresponds to approximately 3 x 10^7 cells/mL. Cells were harvested by centrifugation (5000 rpm, 3 min), washed once with ice-cold PBS, resuspended in ice-cold demineralized water, and fixed overnight at 4°C by adding 100% ethanol to a final concentration of 70% ethanol. Ethanol was added slowly with frequent vortexing of cells. Cells were then harvested by centrifugation, washed, and resuspended in 50 mM sodium citrate (pH 7.5). Cells were treated with RNase A (250 µg per 1 × 10^7 cells) for 2 h at 37°C and proteinase K (1000 µg per 1 × 10^7 cells) for 2 h at 50-55°C. Cells were resuspended in 50 mM sodium citrate containing 4 µg/mL propidium iodide (Dojindo, cat # 341-07881), sonicated for three pulses at 50/60 Hz for 1–2 s, and analyzed in a flow cytometer. Flow cytometry was performed on a Sony EC800 (Sony Biotechnology, Inc., Japan) using an excitation wavelength of 488 nm. Propidium iodide (PI) fluorescence was detected with a 640/30 bandpass filter. Signals from at least 60,000

events were recorded and an acquisition protocol was defined to measure the fluorescence intensity of PI on a linear scale. Data were analyzed using FlowJo 10.2 software (FlowJo LLC, USA).

Table 6-3. Primers used in the RT-qPCR-based validation of the differential gene expression analysis result.

Primer Name		Sequence (5' → 3')	Amplicon (bp)	Source
DEG1	DEG1_F	GGATTACTAGGCGATGCCAAAC	119	This study
	DEG1_R	CGTAGCCCACAATTCTTCTTCC		
DEG2	DEG2_F	GGTCGTATGGTTACTGGTCTTG	97	This study
	DEG2_R	CAAGAGTACCTCTCACCTGTTTG		
DEG3	DEG3_F	GGAACCAAAGGAGGAGTCTAAC	118	This study
	DEG3_R	TCAAAGAAGCAACAAAGCCATG		
DEG4	DEG4_F	GCCTTGTTCATGTCCACTTTGA	120	This study
	DEG4_R	TCTCAATTCACCCGTTGACTCG		
DEG5	DEG5_F	CTTTGACTTGCTGCCAAGTATG	118	This study
	DEG5_R	TCGCCTAGTAATCCACCGAATC		
DEG6	DEG6_F	CTAGCTCTCTTGAGCCTGTTTC	106	This study
	DEG6_R	GCCTCGGAGTAGTTTGAAGAAG		
DEG7	DEG7_F	GGAAGGAGAGTTCAGCATCAAAGAG	79	This study
	DEG7_R	GCTGTCAAACACACACGAGGAC		
DEG9	DEG9_F	CCGTGATGACTTGTACCCTAAC	120	This study
	DEG9_R	TCAATGTCGAGCGAGGAGTAAG		
DEG10	DEG10_F	CATTTATGCCAACACCATCGAAG	98	This study
	DEG10_R	TGAACACGTCTATCCACGAAAC		

6.2.7 Generation of gene disruption mutants of *C. auris*

Construction of gene deletion cassettes

Gene deletion mutants were generated through the SAT1-FLP method (Reuß et al, 2004). The DNA sequence of 1 kb upstream and downstream of *MNN14, MNN26, ENG1,* and *CDR1* ORFs were accessed from the Candida Genome Database (http://www.candidagenome.org) using the whole genome sequence of *C. auris* B8441, which is isolated in Pakistan last 2010 (Lockhart

et al, 2017) and was later on sequenced by the Centers for Disease Control and Prevention. The reference codes for these genes are *CDR1* (B9J08_000164), *ENG1* (B9J08_002109), *MNN14* (B9J08_001669), and *MNN26* (B9J08_004650).

Primers were designed using primer-BLAST. PCR amplification of the upstream and downstream sequences of the following genes: *MNN14, ENG1, MNN26*, and *CDR1* from *C. auris* UI001 gDNA, was performed using NEB Q5 High Fidelity DNA polymerase following the manufacturer's recommended protocol. All the primers used are in Table 6-4. The strategy for constructing the plasmid containing the gene deletion cassettes is shown in Figure 6-1.

Table 6-4. Primers used in generating gene deletion cassettes.

Primer Name	**Sequence (5' → 3')***	**Amplicon (bp)**
KpnI-CauMNN14-Up-F^	AAGGTACCATACTGAAAGGATTGGCCG	420
XhoI-CauMNN14-Up-R	ATATCTCGAGTCAGGCAAAGGTTGCGAG	
Not1-CauMNN14-Dw-F	AAGCGGCCGCAGGCATATAGCATTTTCCTC	700
SacI-CauMNN14-Dw-R^	ATATGAGCTCACTTCGTCATGCAACAACG	
KpnI-CauMNN26-Up-F^	AAGGTACCTTGGGCCAGCATCTACAG	406
XhoI-CauMNN26-Up-R	ATATCTCGAGTGAAAGGGCAGGGATCAAG	
Not1-CauMNN26-Dw-F	AAGCGGCCGCTCAAGAAAGACCGTGCATAG	618
SacI-CauMNN26-Dw-R^	ATATGAGCTCGGGTGCTCGAAGCTTTC	
KpnI-CauENG1-Up-F^	AAGGTACCAGATCGGAGTACGTGATTTC	414
XhoI-CauENG1-Up-R	ATATCTCGAGGCATGTCCCTTTTATGTCTC	
Not1-CauENG1-Dw-F	AAGCGGCCGCCGCTAGCTATGCTTTCTTTTGTG	444
SacI-CauENG1-Dw-R^	ATATGAGCTCGGCGGCCTAATTTCAACCAC	
KpnI-CauCDR1-Up-F^	AAGGTACCAAAGGCAAATTGTCCCGCTG	282
XhoI-CauCDR1-Up-R	ATATCTCGAGATAGGGAATTCTGGCGGCAA	
Not1-CauCDR1-Dw-F	AAGCGGCCGCGATTCAGATGAGTATCTGTTC	465
SacI-CauCDR1-Dw-R^	ATATGAGCTCTTTCCTCCTTATACTCTCTCACAA	

*The underlined part corresponds to the restriction enzyme cutting site

^ Primers that are also used in screening for gene deletion mutants after transformation

After PCR amplification, amplicons were loaded into agarose gels, and purified following the manufacturer's recommended protocol (Wizard SV Gel and PCR Clean-up System, Promega, USA). Restriction enzyme digestion of pSFS2 and the upstream and downstream fragments using enzymes from either Takara or New England Biolabs Inc. was performed overnight at 37°C. Digested products were loaded into agarose gels and target bands were excised and then purified. Ligation using T4 DNA Ligase (New England Biolabs) was performed overnight at 16°C. The online calculator (https://nebiocalculator.neb.com/#!/ligation) was used to calculate the mass of insert required at several molar insert:vector ratios in the range needed for typical ligation reactions. Transformation was performed using competent *Escherichia coli* DH5α cells which were heat-shocked at 42°C for 45 s to introduce the created plasmid. Cells were then plated on Luria Bertani (LB) agar (1% tryptone, 1% NaCl, 0.5% yeast extract, 1.5% agar, adjusted to pH 7) with 30 µg/mL chloramphenicol to screen for transformants. After approximately 18 h of incubation, colonies were picked up and streaked on LB agar plus 30 µg/mL chloramphenicol plate and used for colony PCR using EmeraldAmp MAX PCR Master Mix (Takara Bio Inc.) Colonies exhibiting the expected amplicon bands were grown in LB broth plus 30 µg/mL chloramphenicol, and the plasmid was extracted following the manufacturer's recommended protocol (Wizard Plus SV Minipreps DNA Purification System, Promega, USA). To further confirm if the insertion of the upstream and downstream fragments was successful, the extracted plasmid was double-digested, and the fragment sizes were compared with the vector (pSFS2). In addition, the upstream and downstream fragments of the constructed plasmids were sent for sequencing at the Open Facility Center of the Biomaterials Analysis Division at the Tokyo Institute of Technology. All DNA sequence analyses were performed using Applied Biosystems 3730xl DNA Analyzer, utilizing a 96 multi-capillary electrophoresis system analysis for approximately 850 bases in 150 min.

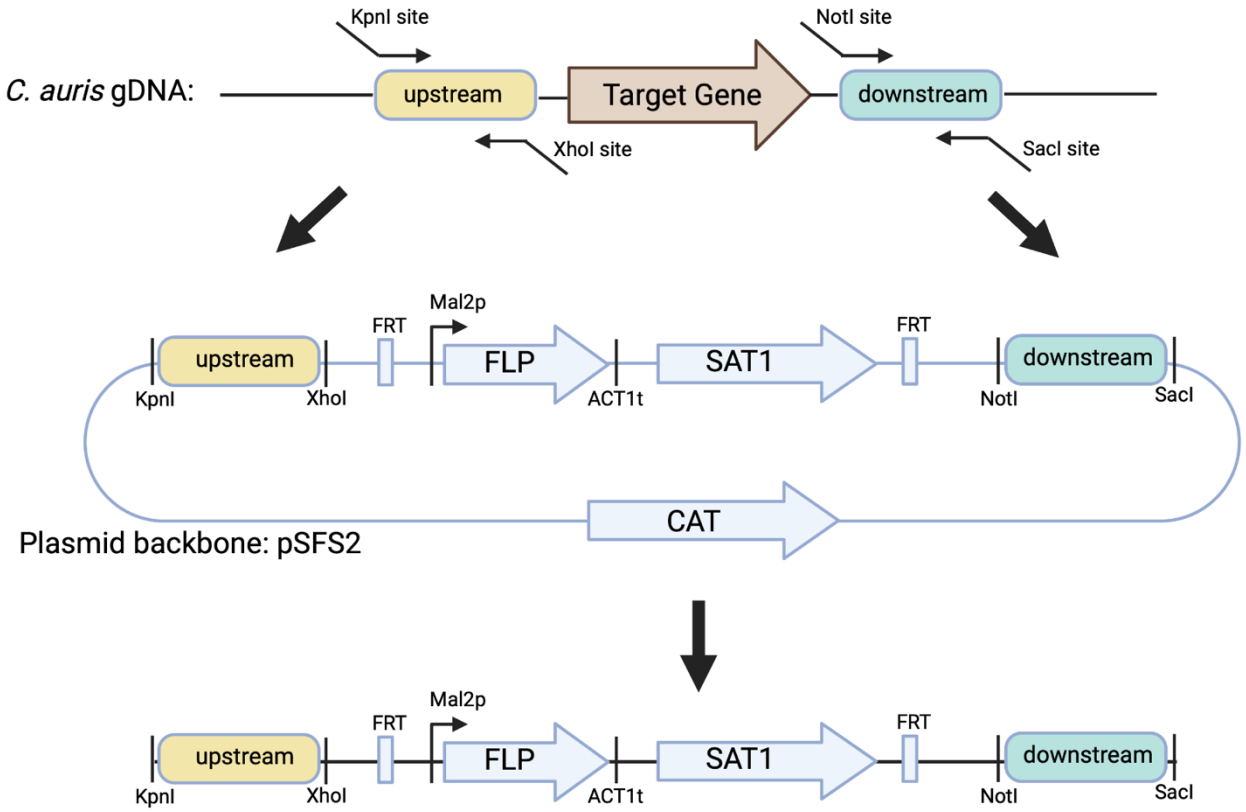

Figure 6-1. Strategy for constructing the gene deletion cassettes. Figure created in BioRender.com FRT: supports FLP-mediated excision but not integration; FLP: site-specific recombinase; SAT1: confers nourseothricin resistance; CAT: confers chloramphenicol resistance.

Determination of the minimum inhibitory concentration (MIC) of nourseothricin (NTC) in *C. auris* UI001

The MIC of NTC (Jena Bioscience GmbH, cat # AB-102L) was determined following the European Committee on Antimicrobial Susceptibility Testing protocol but with some modifications, YPD medium is used instead of RPMI medium and two-fold dilutions of the antifungal was not used. An overnight culture of *C. auris* in YPD broth was transferred (1:50) in fresh YPD and cultivated for 4 h at 37°C. Cells were collected and washed twice in saline solution. Cell number was counted in a hemocytometer and cell concentration was adjusted to $1x10^8$ cells/mL of stock. Ten-fold dilutions of the stock were prepared and 5 µL of the cell suspension was spotted on YPD plates. Plates were incubated at 37°C and observed every day for 2 weeks.

Transformation of *C. auris*

This protocol is adapted from Horton et al (2021). An overnight culture of *C. auris* was transferred on a 1:100 ratio to fresh YPD broth and incubated with shaking at 37°C until cells reach the mid-exponential phase (OD_{600} of 0.5 to 0.8, ~ 3-4 h). Cells were pelleted by centrifugation and resuspended in 19.8 mL of transformation buffer (10 mM Tris-HCl, 1 mM EDTA, and 100 mM LiAc in ddH_2O). Cells were then incubated on a shaker incubator for 1 h at 37°C, then 200 µL of 10 mM dithiothreitol was added and cells were incubated further for 30 min. Cells were washed twice in ice-cold ddH_2O, once in ice-cold 1 M sorbitol, and resuspended in ice-cold 1 M sorbitol. Cell suspension (40 µL) was combined with ~5 µL (1 µg) of gene deletion cassette and the tube was kept for 5 min on ice. Electroporation (GenePulser Xcell, Bio-Rad Laboratories, Inc.) set at a capacitance of 25 µF and resistance of 200 Ω with a manual 1.8 kV pulse was performed using a pre-chilled 0.2 cm cuvette (Bio-Rad Laboratories, cat #165-2086). Cells were immediately resuspended in ice-cold 1 M sorbitol, centrifuged at 1,000 g for 3 min, and resuspended in 1 mL YPD broth. Following 2 h of incubation at 37°C with shaking, cells were collected and plated on YPD plates containing 200 µg/mL nourseothricin and incubated at 37°C for 2 days. The strategy used to disrupt genes in *C. auris* is shown in Figure 6-2.

Screening for gene deletion mutants

Colonies that grew on YPD + NTC plates were picked and streaked onto fresh YPD + NTC plates. Plates were incubated at 37°C for 2 days. Isolated colonies were used for a colony PCR using EmeraldAmp MAX PCR Master Mix (Takara Bio Inc.) following the manufacturer's recommended protocol. The expected amplicon lengths of all possible PCR products are shown in Figure 6-3 and Figure 6-4. The primers used in screening are the same as the ones used in creating the gene deletion cassettes shown in Table 6-4. To further screen for insertion of *SAT1* in the transformed colonies, the following primers that produce a 579-bp amplicon were used:

SAT1_insert_for	5'- TGCTTTAGTTATCGATAACGGTTCTCAT-3'
SAT1_insert_rev	5'-ATCTCCCCCTTCACACTTCAC-3'

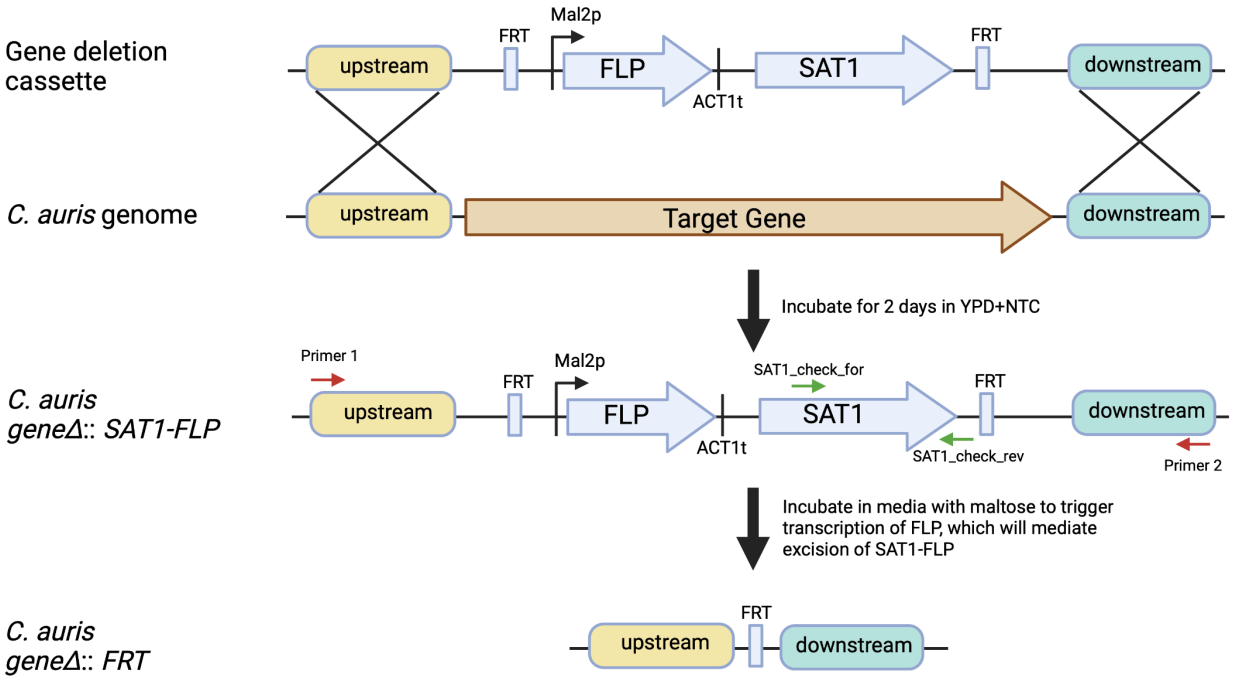

Figure 6-2. Strategy for disrupting genes in *C. auris*. Figure created in BioRender.com. Primer 1 and Primer 2 refer to primers used in creating the gene deletion cassettes, as shown in Table 6-4.

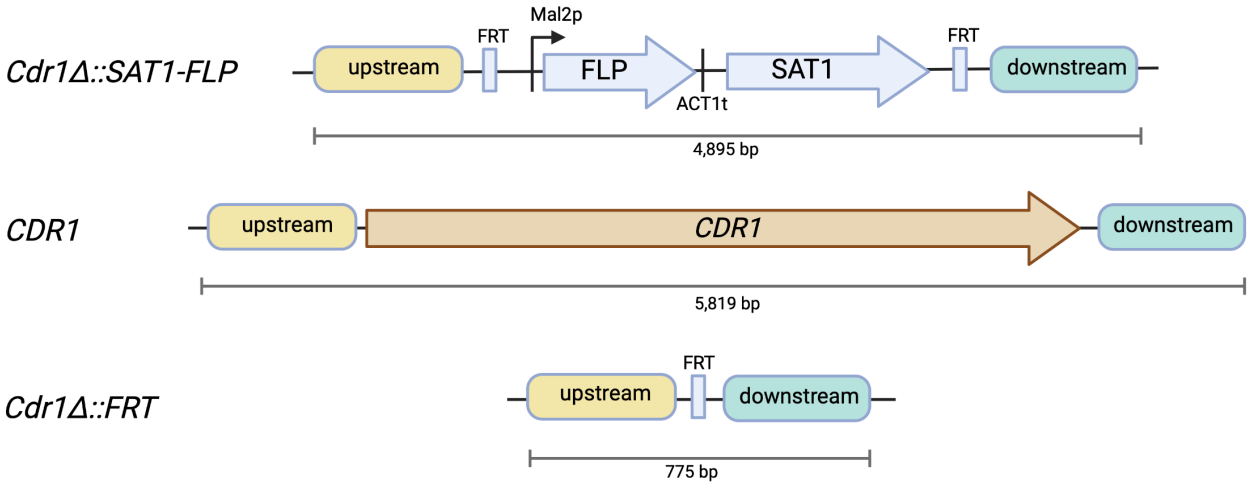

Figure 6-3. Probable colony PCR amplicons, with their corresponding size, for cells previously transformed with the *CDR1* deletion cassette. Figure created in BioRender.com.

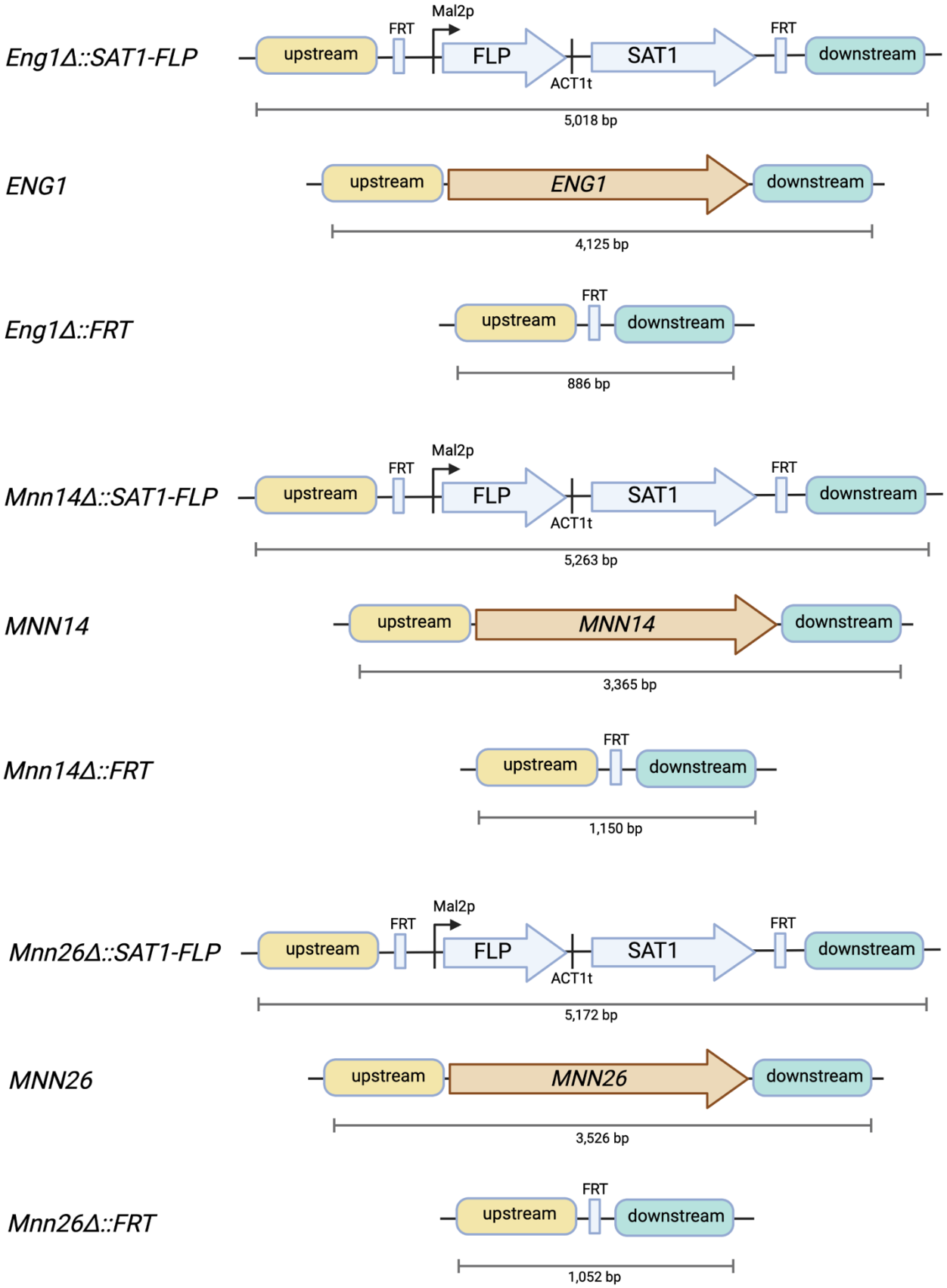

Figure 6-4. Probable colony PCR amplicons, with their corresponding size, for cells previously transformed with the *ENG1, MNN14,* and *MNN26* deletion cassettes. Figure created in BioRender.com

6.3 RESULTS AND DISCUSSION

6.3.1 Use of enzyme inhibitors to determine signaling systems involved in β-glucan masking in *C. auris*

The β-glucan masking profile of *C. auris* UI001 and *C. albicans* SC5314 is highly similar, as shown in Chapter 2. As a preliminary investigation, this experiment aimed to determine if both strains will exhibit similar changes in β-glucan exposure levels in the presence of key enzyme inhibitors. It was shown that cAMP-PKA signaling is necessary for hypoxia-induced β-glucan masking in *C. albicans* (Pradhan et al, 2018). Moreover, Ballou et al (2017) showed that lactate-induced β-glucan masking involves the transcription factor Crz1, which is activated via a calcineurin-independent pathway. So, H-89 which is a potent inhibitor of cyclic AMP-dependent protein kinase A (PKA) for fungal and mammalian cells, and tacrolimus (FK506) which is a calcineurin inhibitor, were used in this study. According to a review by Murray (2008), H-89 works through competitive inhibition of the adenosine triphosphate site on the PKA catalytic subunit, and is 30 times more potent than H-8 at inhibiting PKA and 10 times less potent at inhibiting protein kinase G. Powell and Zheng (2006) stated that FK506 blocks the activation of calcineurin, a serine/threonine protein phosphatase 2B, through the formation of complexes with an immunophilin called FK506 binding protein 12 (FKBP12).

Results are shown in Figure 6-5. *C. auris* grew well in the presence of 100 μM H-89 and 3.12 μg/mL FK506 which are both diluted in DMSO ("vehicle"). Both inhibitors were not able to abrogate β-glucan masking in the presence of lactate and a hypoxic environment. This means that like *C. albicans,* cAMP-PKA and calcineurin are not involved in lactate-induced β-glucan masking. On the contrary, cAMP-PKA signaling may not be involved in hypoxia-induced β-glucan masking in *C. auris*. This is a preliminary study so in-depth studies must be performed to confirm this observation.

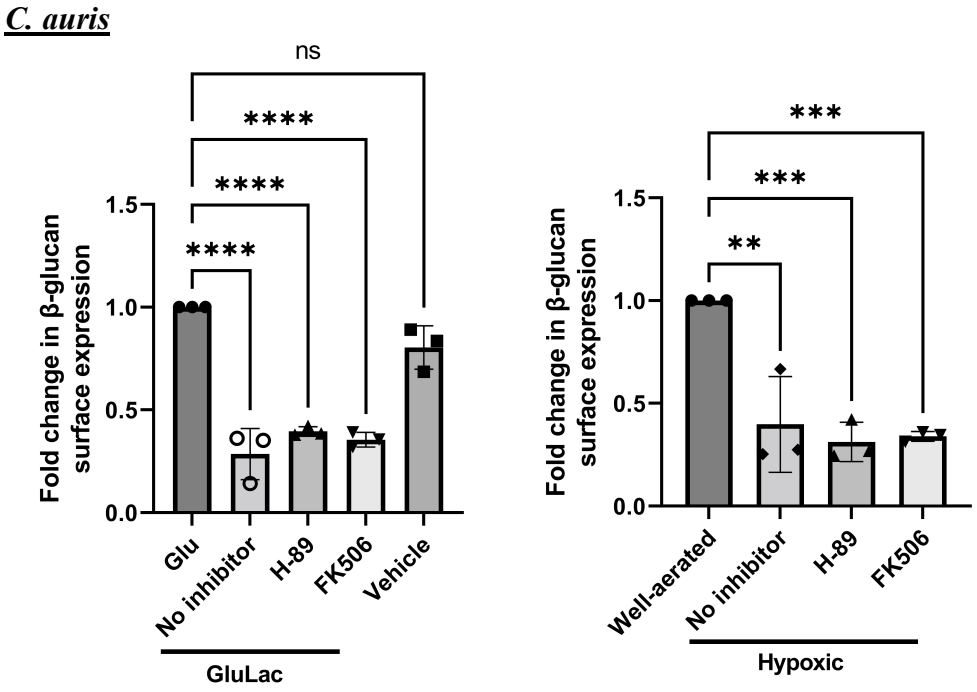

Figure 6-5. Effect of PKA inhibitor H-89 and calcineurin inhibitor FK506 on β-glucan masking in *C. auris* UI001 triggered by lactate (left) and hypoxia (right).

6.3.2 RT-qPCR analysis of expression of selected genes in *C. auris* grown in glucose only or glucose-lactate

To quickly search for possible genes involved in β-glucan masking in *C. auris*, the expression of selected genes (refer to Table 6-1) in *C. auris* grown in either glucose only or glucose-lactate were compared. Prior to qPCR, standard PCR was performed to compare the band intensities of amplicons. Through visual inspection, there is not much difference in the band thickness of the samples. ImageJ software (https://imagej.nih.gov/ij/) was then used to analyze all bands. Results show that there is no difference in the integrated density values of bands corresponding to all genes tested in *C. auris* UI001 grown with or without lactate.

For the qPCR analysis, the expression level of selected genes from the extracted RNA of UI001 and ATCC MYA-5002 strain of *C. auris* grown with or without lactate were normalized to the reference gene *ACT1*. MYA-5002 does not exhibit β-glucan masking in the presence of lactate so gene expression was compared to UI001. The experiment was independently performed thrice with 2-3 technical replicates per run. In all runs, the "no template control" did not show any significant amplification. Melting curves were also checked to make sure that there is only one amplification product per well. *ACT1* expression seems stable regardless of the strain used and the

culture condition to which the yeast cells were grown before RNA extraction. Results are shown in Figure 6-6 and Figure 6-7. The equations used in the calculation are shown below:

$$\Delta Ct = \text{Ave } Ct_{(\text{target gene})} - \text{Ave } Ct_{(ACT1)}$$

$$\Delta\Delta Ct = \Delta Ct_{(\text{lactate})} - \Delta Ct_{(\text{glucose})}$$

Based on the result, the following genes were hypothesized to be potentially involved in lactate-induced masking of β-glucan: *CDR1*, *ENG1, MNN14,* and *MNN15.* To confirm this hypothesis, an attempt to create deletion mutants was performed.

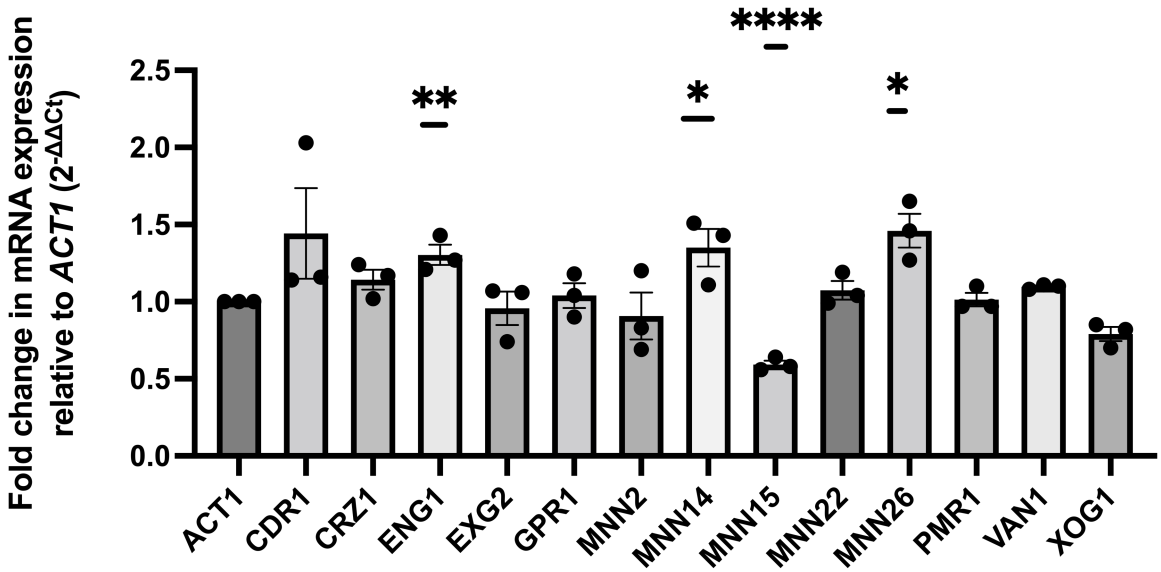

Figure 6-6. Fold change in the expression of selected genes in the clinical strain of *C. auris* grown with or without lactate. Bar graph shows the mean and SEM from three independent experiments analyzed through multiple unpaired t-test against *ACT1*.

CDR1 is a multidrug transporter that is shown to be upregulated 5.9-fold in *C. albicans* cells grown in lactate versus glucose (Ballou et al, 2017). Upregulation in UI001 was also observed. *MNN14* is a predicted α-1,3-mannosyltransferase activity with a role in protein glycosylation and is upregulated 5.6-fold in *C. albicans* grown in lactate (Ballou et al, 2017). Upregulation of this gene was also observed in UI001. *MNN15* is a putative α-1,3-mannosyltransferase and is downregulated 3.3-fold in *C. albicans* grown in lactate (Ballou et al, 2017). Downregulation was also observed in both UI001 and MYA-5002. *ENG1* and *MNN26* are already described in Table 6-1.

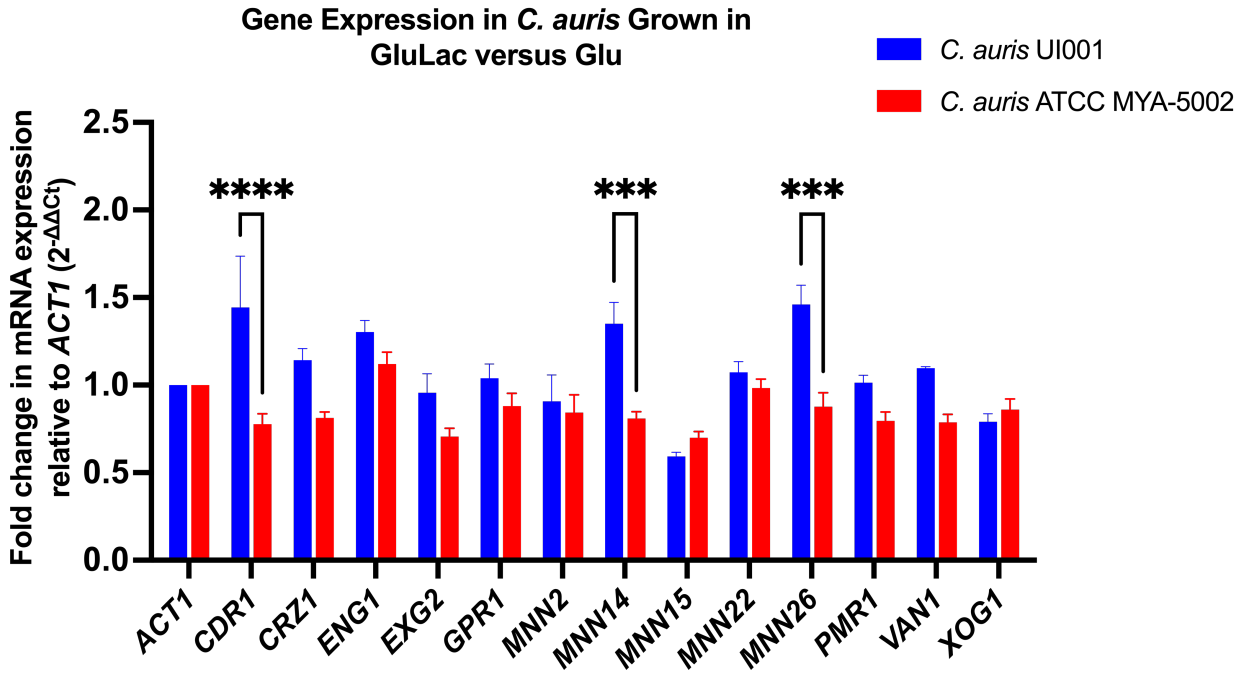

Figure 6-7. Relative gene expression of selected genes in *C. auris* strains grown in glucose only or glucose-lactate. Bar graph shows the mean and SEM from three independent experiments analyzed through two-way ANOVA with Holm Sidak's multiple comparison test. **** $P < 0.0001$, *** $P < 0.001$

6.3.3 Generation of gene disruption mutants of *C. auris*

Ploidy determination in *C. auris*

Although *C. auris* is known to be haploid, a recent study by Fan et al (2020) discovered a diploid form of this species, especially in clinical isolates. To ensure that the appropriate gene deletion protocol is followed, the ploidy level of *C. auris* UI001 is determined by flow cytometric analysis of the DNA content of PI-stained cells. The haploid reference strain of *C. auris* and diploid wild type strain of *C. albicans* were used as controls. Figure 6-8 shows that *C. auris* UI001 is haploid, the same as the *C. auris* reference strain (ATCC MYA-5001).

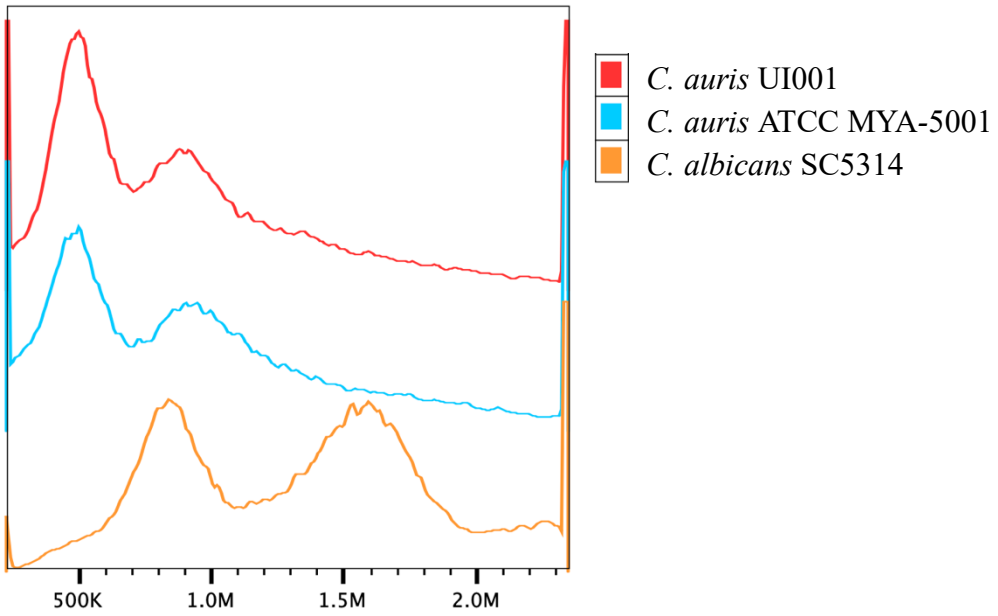

Figure 6-8. Cell cycle profiles of *Candida* sp. obtained by flow cytometric analysis of cells stained with propidium iodide. Histogram shown is a representative of three independent trials showing consistent results.

Determination of MIC of nourseothricin in *C. auris* UI001

To determine the appropriate concentration of nourseothricin (NTC) to be used in screening for transformants, the MIC of NTC in *C. auris* UI001 was determined. Tenfold dilutions of yeast cells were each spotted onto YPD supplemented with varying amounts of NTC (0-600 µg/mL).

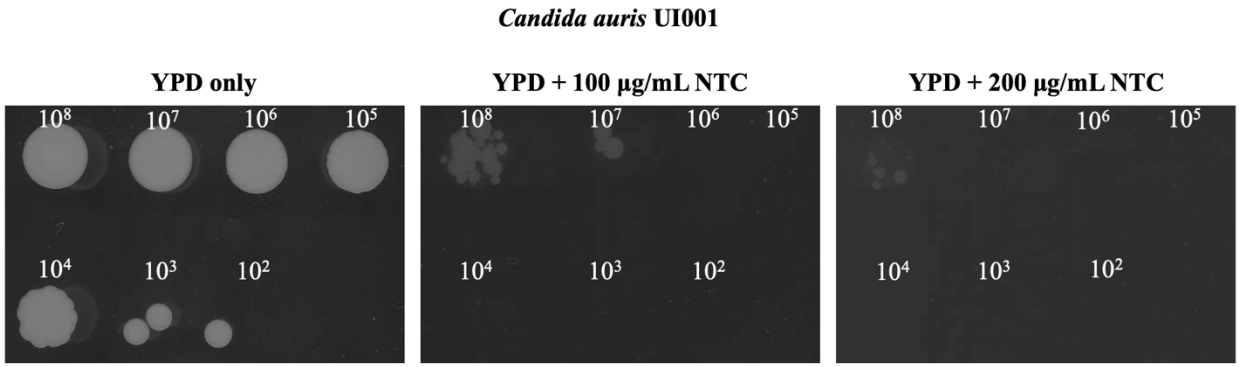

Figure 6-9. Growth of *C. auris* in YPD supplemented with 100-200 µg/mL nourseothricin after 3 days of incubation at 37°C.

Small colonies start to form after 2 days of incubation. After 3 days, distinct colonies formed in plates with 100 μg/mL and 200 μg/mL NTC, where 10^7-10^8 cells were spotted (Figure 6-9). NTC inhibits protein synthesis by interfering with the mRNA translocation step thereby causing misreads of the RNA molecule. Furthermore, it blocks mRNA translocation, hindering peptide chain synthesis of the peptide. NTC is a mixture of streptothricin D and F (>85%) and streptothricin C and E (<15%) and selection of recombinant strains is based on the inactivation of NTC by mono-acetylation of the β-amino group of the β-lysine residue by nourseothricin N-acetyltransferase, the product of the SAT1 or NAT1 genes (Jena Bioscience Data Sheet, 2023). Assuming that *C. auris* does not have the *SAT1* gene, this could mean that there is a high rate of spontaneous mutation leading to NTC resistance. Another probability is that there are other NTC resistance genes in *C. auris* UI001 or the strain developed special mechanisms to grow in the presence of NTC. *SAT1* codes for streptothricin acetyltransferase, an enzyme that can break down NTC. The presence of *SAT1* was checked using the BLASTN feature of NCBI and CGD (*Candida* Genome Database) and search results show that the reference strain of *C. auris* does not have *SAT1*.

Construction of gene deletion cassettes and transformation of *C. auris*

Gene deletion cassettes for the four target genes (*CDR1, ENG1, MNN14, MNN26*) were successfully created. For the sequencing result, the *MNN14* upstream fragment sequence is similar to the sequence found in the Candida Genome Database except for four extra Ts. The sequencing result using both forward and reverse primers show this and is most probably the correct sequences for *C. auris* UI001 used in this research. In addition, the *ENG1* downstream fragment sequence is similar to the sequence found in the Candida Genome Database except for one less A. All the rest are 100% similar to the sequence of the reference strain, considering results from using both forward and reverse primers.

Transformation of *C. auris* was performed but surprisingly, a lot of colonies grew in YPD + 200 μg/mL NTC after 2 days of incubation (Figure 6-10). Screening for all selected isolated colonies, as shown in Figure 6-11 and Figure 6-12, indicates that the target gene is still intact. For the next transformation trial, YPD + 600 μg/mL NTC was used. Three colonies formed in the plate with samples added with *CDR1* deletion cassette and one colony each for *ENG1* and *MNN14.* There are zero colonies for *MNN26.* However, colony PCR revealed that the target genes were still intact in all five colonies. *SAT1* was also detected in selected colonies in YPD+NTC plates and was in fact, present in some colonies as shown in Figure 6-13. Therefore, it seems like the gene deletion cassette successfully entered *C. auris* but was not able to integrate into its intended locus. Rybak et al (2019) and Wang et al (2022) also used the SAT1-FLP cassette to disrupt genes in *C.*

auris but the former employed Cas9-RNP-mediated transformations to disrupt *CDR1* while the latter used pSFS2A to create *PHO84* deletion cassette. Day et al (2018) used NAT1-Clox disruption cassette to disrupt *HOG1*. These three studies successfully created the mutants. However, Bravo-Ruiz et al (2020) mentioned that homology-directed repair does not seem to work well in *C. auris* as it tends to integrate DNA randomly into the genome. The same phenomenon was observed in this study.

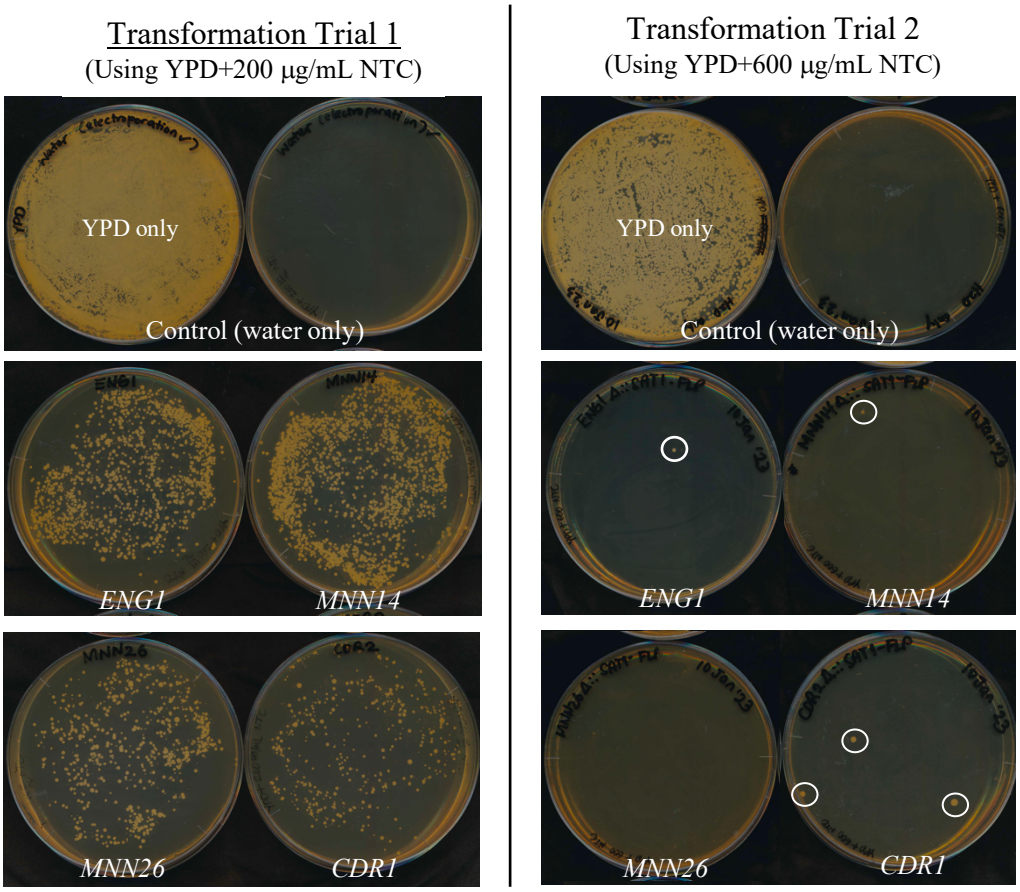

Figure 6-10. Plates generated after two independent attempts to transform *C. auris* UI001 to produce deletion mutants. Isolated colonies produced in the 2nd trial are in white circles. Plates were incubated at 37°C for two days.

As a general observation, small colonies can appear after prolonged incubation in YPD+NTC, possibly from untransformed background colonies tolerant or spontaneously resistant to NTC. It is clear from the MIC experiment (Figure 6-9) that some colonies of *C. auris* UI001 developed resistance to NTC. Although integrated into the genome, the gene deletion cassettes do not seem to efficiently recombine to the target locus because no colonies are having the expected band for a *GeneΔ::SAT1-FLP* genotype. With all the experiments performed, the attempt to create gene deletion mutants of *C. auris* UI001 failed.

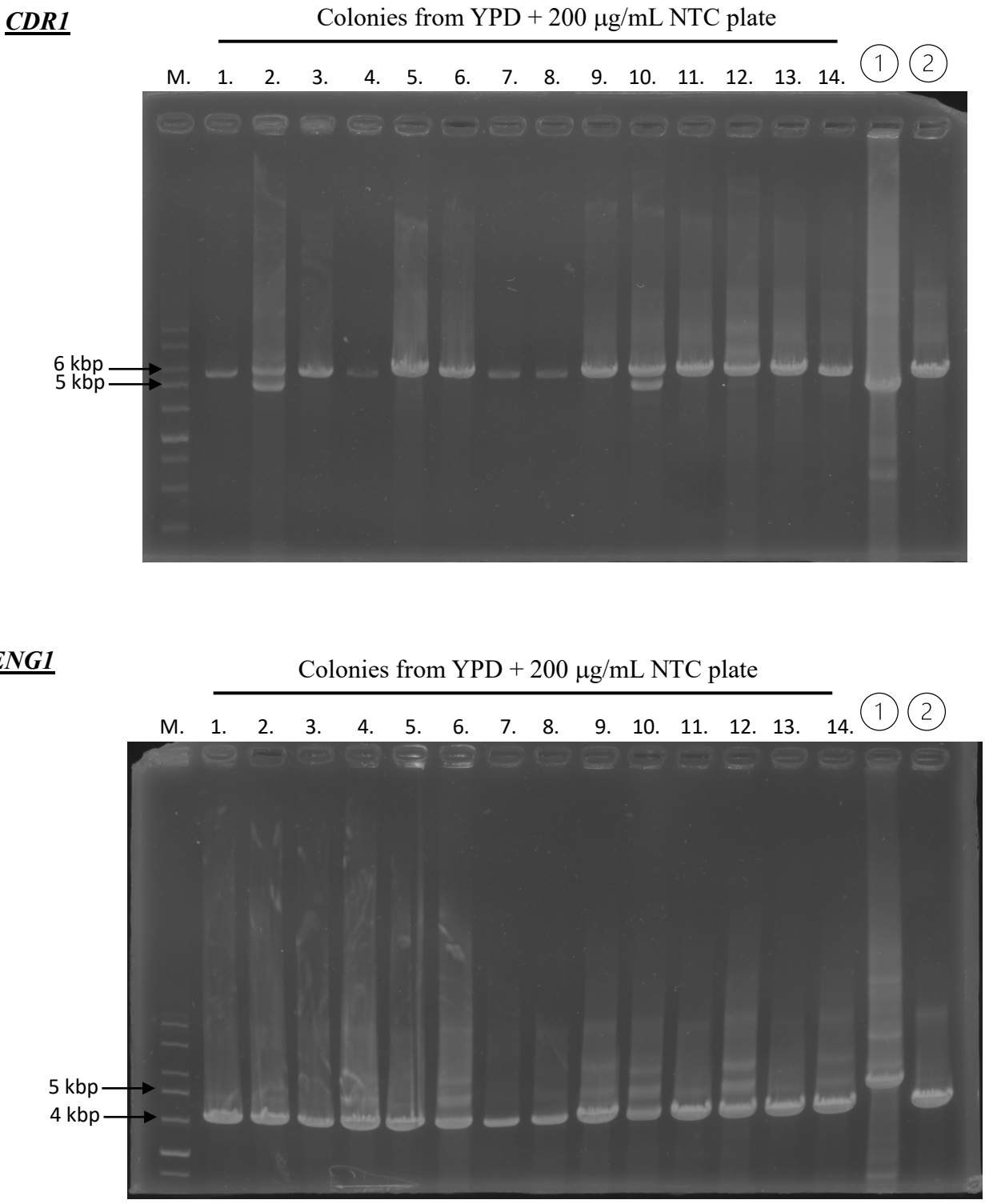

Figure 6-11. Gel electropherogram showing amplicons from probable *CDR1* and *ENG1* deletion mutants screened through colony PCR. "M" corresponds to the DNA size marker while "1" is from the plasmid containing the gene deletion cassette showing *GeneΔ::SAT1-FLP* size and "2" is from a random colony in the control YPD only plate showing undisrupted gene size.

MNN14

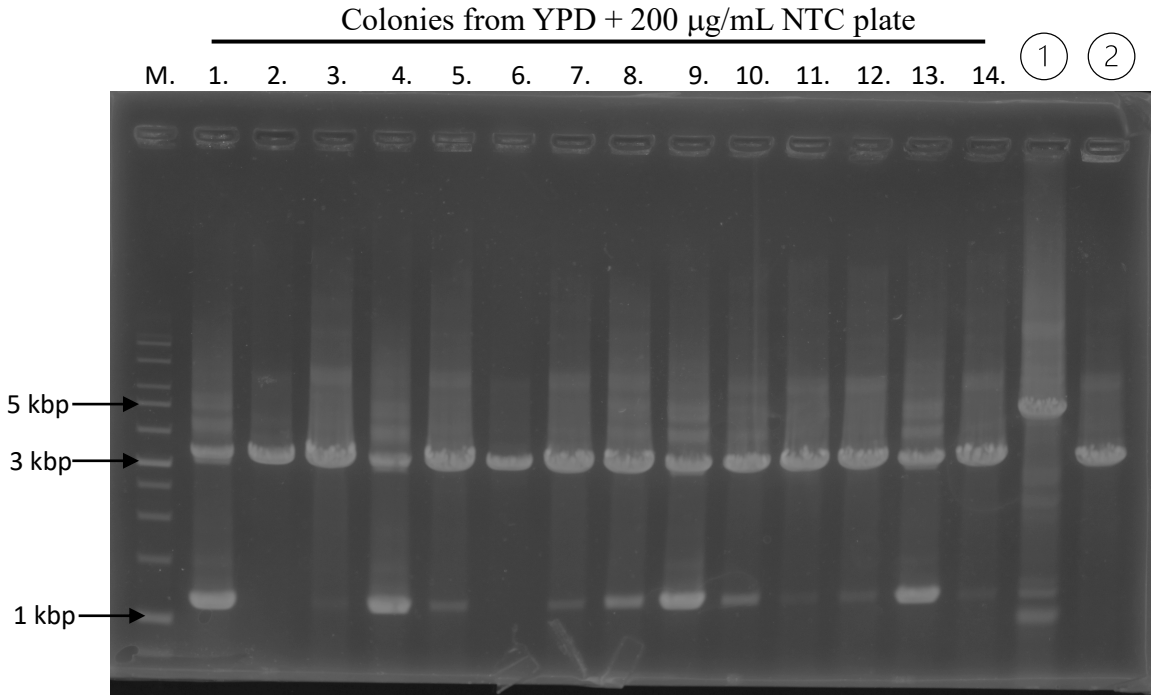

MNN26

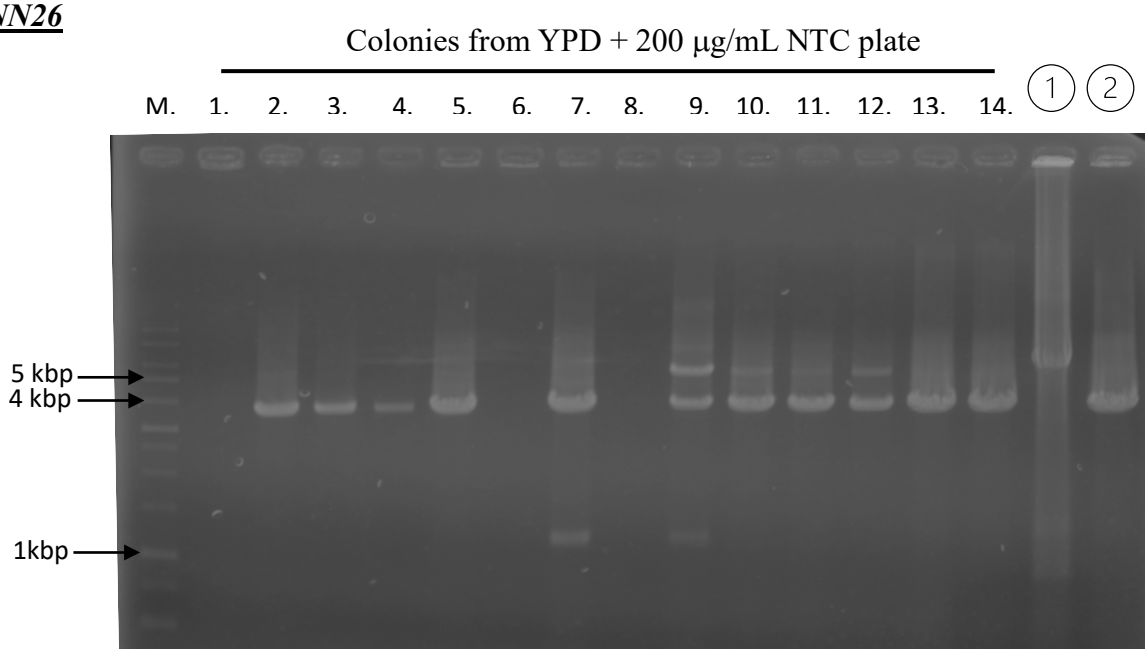

Figure 6-12. Gel electropherogram showing amplicons from probable *MNN14* and *MNN26* deletion mutants screened through colony PCR. "M" corresponds to the DNA size marker while "1" is from the plasmid containing the gene deletion cassette showing *GeneΔ::SAT1-FLP* size and "2" is from a random colony in the control YPD only plate showing undisrupted gene size.

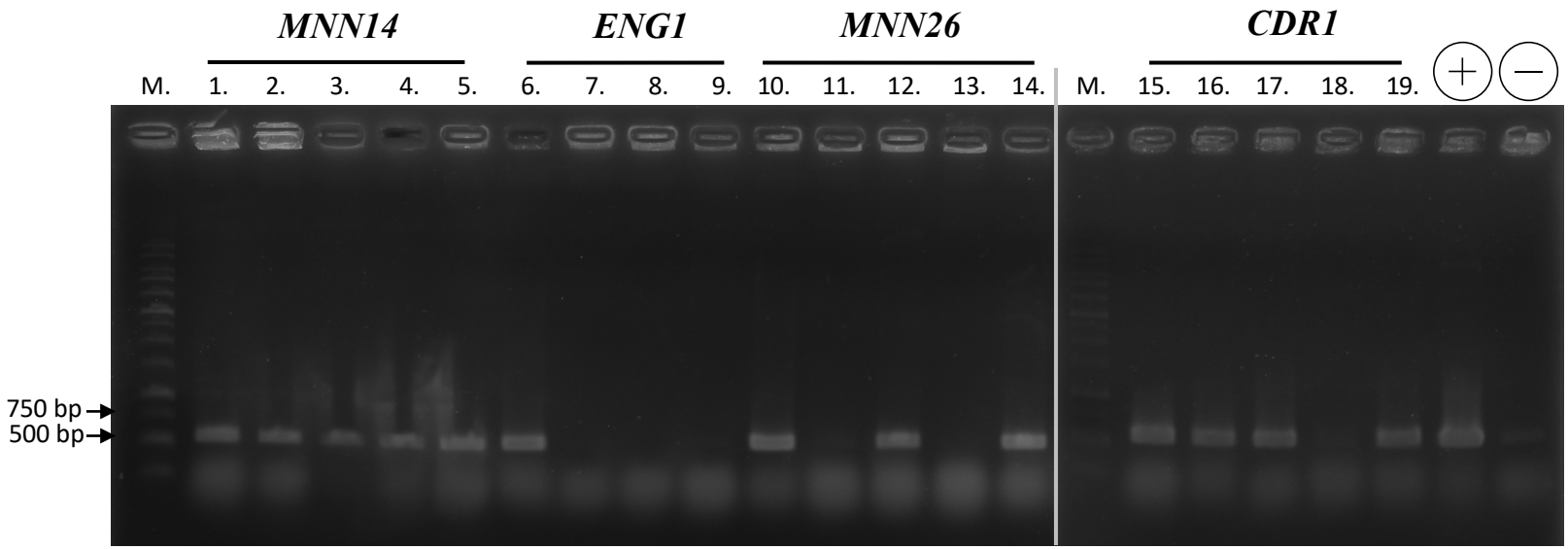

Figure 6-13. Detection of *SAT1* by colony PCR using selected colonies grown in YPD supplemented with 200 µg/mL NTC. "M" corresponds to the DNA size marker while "+" serves as a positive control which is a random transformed *E. coli* colony containing the gene deletion cassette and "-" serves as a negative control which is a random colony in the control YPD only plate.

6.3.4 RNA-seq analysis as a method to elucidate potential novel mechanisms of β-glucan masking in *C. auris* UI001

RNA sequencing

RNA samples were sent to the Bioengineering Lab of *Kabushikigaisha Seibutsu Giken* in Kanagawa, Japan. Before library preparation, the quality and integrity of RNA is assessed and reported as RQN (RNA quality number). Only RNA samples with RQN > 7.0 was accepted for RNA sequencing analysis. The RQN, number of paired reads, and mapping results for each total RNA sample are shown in Table 6-5.

Table 6-5. RNA sequencing of *C. auris* UI001 grown in either glucose only (Glu) or glucose-lactate (GluLac).

Sample	RNA Quality Number (RQN)	Sequencing Result		Summary of Mapping Results		
		Total no. of paired reads	No. of High Quality reads	No. of reads not mapped to reference	No. of reads mapped to reference (one locus)	No. of reads mapped to reference (multi-locus)
C. auris UI001 (Glu)	7.4	12,930,604	12,871,552	677,243 (5.26%)	9,016,821 (70.05%)	3,177,488 (24.69%)
C. auris UI001 (GluLac)	7.6	12,088,954	12,034,058	480,462 (3.99%)	9,770,264 (81.19%)	1,783,332 (14.82%)

To compare the RNA-seq data with the qPCR analysis result shown in Figure 6-6. All four genes (*CDR1, ENG1, MNN14,* and *MNN15*) were not differentially expressed in cells grown with or without lactate since *P* values are ≥ 0.05. The exact *P* values are 0.50 (*CDR1* and *ENG1*) 0.89 (*MNN14*), and 0.94 (*MNN26*). This could mean that these genes were not truly differentially expressed.

Differential Gene Expression analysis

After RNA sequencing, the differentially expressed genes were determined and a volcano plot is created, as shown in Figure 6-14.

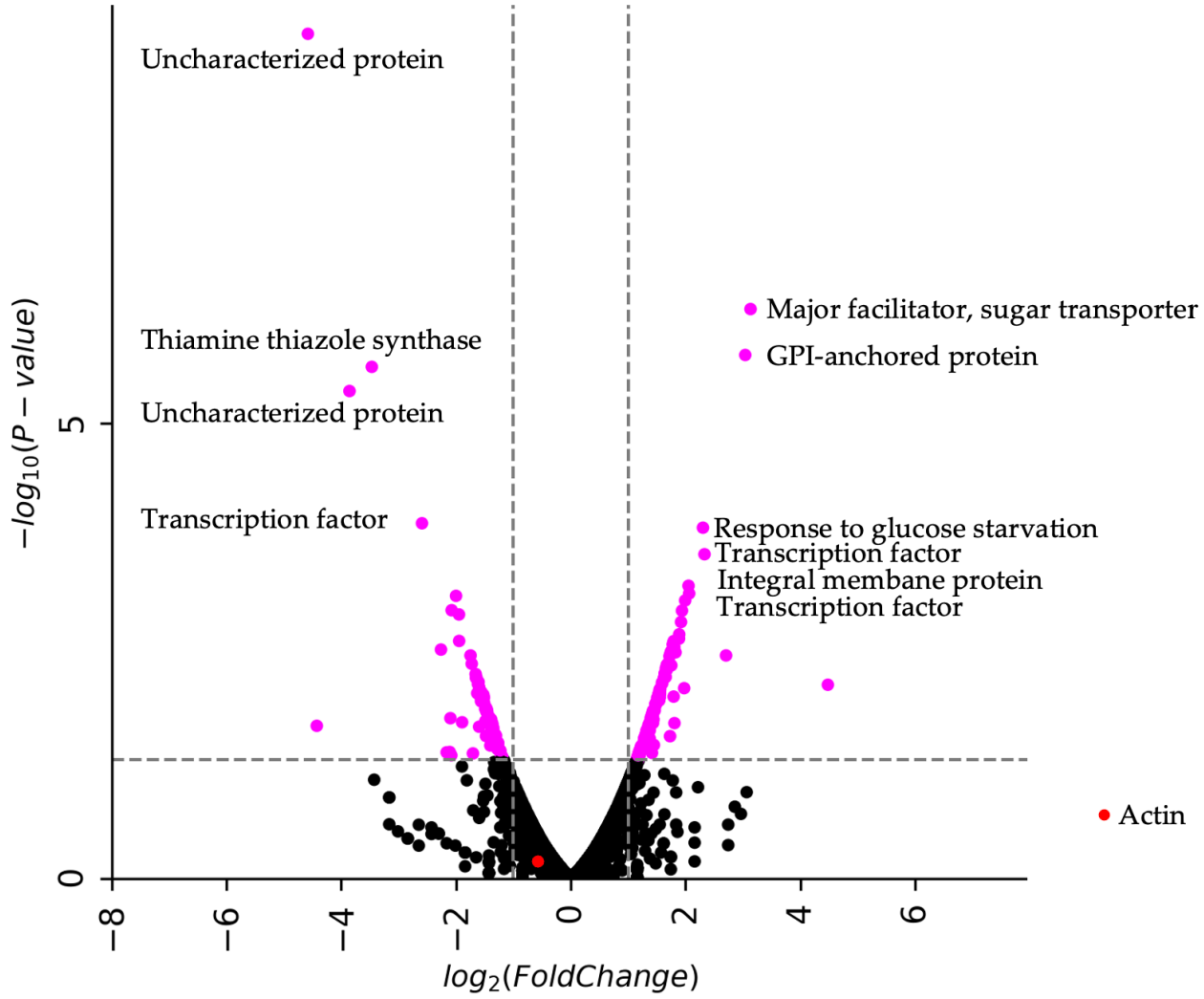

Figure 6-14. Volcano plot generated after analysis of differential gene expression.

Considering a *P* value cut-off of 0.05, there are 213 differentially expressed genes (DEGs). However, only five genes are significantly differentially expressed with FDR < 0.05. The probable identity of the top 10 most differentially expressed genes, based on the calculated *P* value, was determined by the following method: mRNA sequence was searched in NCBI using the indicated Genbank ID from the sequencing analysis, the FASTA sequence was copied, and BLASTN was performed in the Candida Genome Database (http://www.candidagenome.org). From the BLASTN result, possible orthologs of those DEGs were determined. To gain more information on the protein coded for by those DEGs, protein sequence derived from the mRNA sequence was used in UniProt (https://www.uniprot.org) and InterPro (https://www.ebi.ac.uk/ interpro/) analysis (Paysan-Lafosse et al, 2023).

DEG2, the most upregulated mRNA (NCBI Reference Sequence: XM_029034054.1), is similar to the verified *C. albicans* SC5314 *HGT7* ORF (Accession code: C2_01000W_A) wherein

BLASTN search identity is equal to 68.6% (977/1424) while gaps are only 1% (26/1424). *HGT7* encodes a putative glucose transporter of the major facilitator superfamily. It is expressed in a YPD medium with 2% glucose and is induced by growth on a non-fermentable carbon source (Fan et al, 2002). InterPro analysis of the encoded protein revealed that the Gene Ontology biological process of this protein is transmembrane transport. *C. albicans* glucose transporter family comprises 20 members, from *HGT1* to *HGT20*. According to Ballou et al (2017), *C. albicans HGT10* is upregulated by 3.90-fold in cells grown in GluLac versus Glu.

For DEG3, the second most upregulated mRNA (NCBI Reference Sequence: XM_029033823.1), BLASTN result revealed that it potentially codes for a GPI-anchored protein which is generally involved in membrane protein transportation, cell adhesion, cell wall synthesis, and cell surface protection. In yeast, GPI-anchored proteins are components of the cell wall and are necessary for cellular integrity. According to Ballou et al (2017), GPI-anchored proteins coded by the following mRNAs are upregulated in lactate-grown versus glucose-only grown *C. albicans*: *RHD3* (5x upregulated; coded protein requires Crz1), *EXG2* (4x upregulated; coded protein does not require Crz1), *PLB3* (2x upregulated; coded protein requires Crz1), and *CHT2* (2x upregulated; coded protein does not require Crz1). Crz1 is a transcription factor that is involved in lactate-induced β-glucan masking in *C. albicans*. Based on the qPCR result shown in Figure 6-6, there is no difference in the expression of *EXG2* in *C. auris* grown in either GluLac or Glu. To expound on the proteins coded for by these upregulated genes, RHD3 is a GPI-anchored yeast-associated cell wall protein that is covalently linked to the β-1,3-glucan framework of the cell wall via β-1,6-glucan. RHD3 is not essential for cell wall integrity but *rhd3* mutants display a significant reduction of cell wall mannan (de Boer et al, 2010). Rhd3 is much more abundant in the cell wall at pH 4 suggesting regulation by pH (Sosinska et al, 2011). *EXG2* is already described in Table 6-1. Plb3 is a fungal-specific and possibly secreted GPI-anchored cell surface phospholipase B (De Groot et al, 2003) whereas Cht2 is a pH-regulated GPI-linked chitinase which is important for remodeling of chitin in the fungal cell wall (McCreath et al, 1995).

For DEG7, the third most upregulated mRNA (NCBI Reference Sequence: XM_029032981.1), BLASTN result revealed that DEG7 is similar to the uncharacterized *C. albicans* SC5314 *REG1* ORF (Accession code: C2_01200C_A). Reg1 is a putative protein phosphatase regulatory subunit (Candida Genome Database)

For DEG8, the fourth most upregulated mRNA (NCBI Reference Sequence: XM_029035970.1), BLASTN result revealed that DEG8 is similar to the verified *C. albicans* SC5314 *WOR1* ORF (Accession: C1_10150W_A). Wor1 is a transcriptional regulator of white-opaque phenotypic switching (Huang et al, 2006).

For DEG9, the fifth most upregulated mRNA (NCBI Reference Sequence: XM_029032901.1), the BLASTN search did not yield any orthologous verified ORFs. No relevant information is acquired by using the Gene Ontology search in InterPro.

For DEG10, the sixth most upregulated mRNA (NCBI Reference Sequence: XM_029033597.1), BLASTP result revealed that DEG10-encoded protein is similar to the verified *C. albicans* SC5314 CTA7 (orf19.11764). CTA7 is a $Zn(II)_2Cys_6$ transcription factor that has similarities to *S. cerevisiae* Stb4 (Maicas et al, 2005).

Validation of the differential gene expression analysis result

The qPCR was performed thrice using cDNAs from three sets of independently collected RNAs. There are three technical replicates per DEG per condition per trial and all trials include "no template controls" for all DEG primer pairs. Melting curves were checked to make sure that there is only one amplification product in each well. Results are shown in Figure 6-15 and a summary of the comparison between the RNA-seq and qPCR analysis results are shown in Table 6-6.

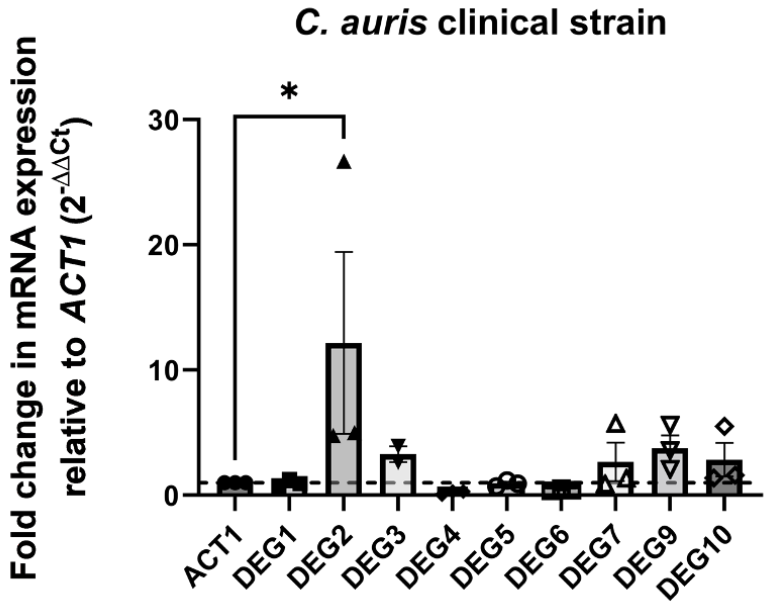

Figure 6-15. Quantitative PCR-based validation of the differential gene expression analysis result. Bar graph shows the mean and SEM from three independent experiments in triplicates analyzed through one-way ANOVA with Dunnett's multiple comparisons test, * $P < 0.05$

Table 6-6. RNA-seq DGE analysis and qPCR-based analysis of expression of selected genes in *C. auris* grown in glucose only (Glu) or glucose-lactate (GluLac).

	Up-/Down-regulated	RNA-seq DGE Analysis				qPCR-based Analysis
		RPKM/TPM* normalized expression		p value	q value^	Ave. 2^-ΔΔCt
		Glu	GluLac			
DEG1	down	695	26	5.E-10	3.E-06	0.99
DEG2	up	1214	9541	6.E-07	0.0016	12.17
DEG3	up	255	1880	2.E-06	0.0034	3.28
DEG4	down	358	29	2.E-06	0.0034	0.23
DEG5	down	194	12	4.E-06	0.0050	0.95
DEG6	down	458	68	1.E-04	0.1144	0.44
DEG7	up	2025	8957	1.E-04	0.1144	2.67
DEG9	up	3118	11588	6.E-04	0.3868	3.76
DEG10	up	457	1711	7.E-04	0.4085	2.84

*RPKM: Reads Per Kilobase of exon per Million mapped reads

TPM: Transcripts Per Million

^q-value: adjusted p-value considering false discovery rate

Generally, the qPCR result supports the RNA-seq data, except for DEG1 and DEG5. The number of DEGs was relatively low considering the q values. This could be explained by a study by Childers et al (2020) where genome-wide transcriptomic comparisons of lactate-exposed versus control *C. albicans* cells did not highlight differentially expressed cell wall genes that might contribute to β-glucan masking. The authors explained that proteins involved in β-glucan masking might be subjected to posttranscriptional and/or posttranslational regulation and thus, not detected in transcriptomics.

6.4 CONCLUSION AND RECOMMENDATION

As a preliminary study, enzyme inhibitors such as H89 and FK506 were used to determine if cAMP-PKA or calcineurin signaling, respectively, are involved in the masking of β-glucan due to lactate or hypoxia. Flow cytometric analysis of stained *C. auris* reveals that both signaling systems may not be involved since the presence of these inhibitors was not able to abrogate the masking of β-glucan.

To determine the probable genes involved in the masking of β-glucan, the level of expression of selected genes was evaluated by RT-qPCR using extracted RNA from *C. auris* grown with or without lactate. Although the expression levels were just less than 1.5-fold, the following genes were statistically upregulated when cells are grown in the presence of lactate: *CDR1, ENG1, MNN14,* and *MNN26.* To design an appropriate genetic manipulation protocol, the ploidy level of *C. auris* UI001 was determined. Flow cytometric analysis of PI-stained cells reveals that *C. auris* is haploid. There was an attempt to create deletion mutants of these genes, but transformation trials were all unsuccessful. The gene deletion cassettes were able to enter *C. auris* cells but failed to integrate into its intended locus.

RNA sequencing was also performed to check which genes in *C. auris* UI001 are significantly upregulated or downregulated in the presence of lactate. With a cut-off *P* value of 0.05, there are 213 differentially expressed genes. Among these, only five have FDR values less than 0.05. Among these five genes, two are upregulated. A gene that is upregulated by 12-fold codes for a putative glucose transporter while a gene upregulated by 3-fold codes for a GPI-anchored protein, which are common components of the cell wall and are necessary for cellular integrity.

As a recommendation especially for the gene disruption experiment, other strategies such as the following could be employed: use CRISPR-Cas9 to disrupt the target gene, use plasmids other than pSFS2 like the NAT1-Clox disruption cassette, or follow the same strategy used in this study but the size of the flanking regions should be increased to 1-2 kbp.

CHAPTER 7: CONCLUSION AND FUTURE PERSPECTIVES

This study showed that the emerging and often multidrug-resistant fungal pathogen, *Candida auris,* undergoes a strain-specific cell wall remodeling when exposed to certain environmental stimuli. Among all conditions tested, lactate (0.25-2.0%), low oxygen (<0.1%), and sublethal concentrations of antifungals such as fluconazole (16 μg/mL) and micafungin (0.63 - 40 μg/mL) trigger a significant reduction in exposure levels of β-glucan in *C. auris* UI001. On the contrary, low pH triggers a six-fold increase in β-glucan levels. There is no inverse relationship between cell wall β-glucan and mannan exposure levels.

The effect of the observed masking of β-glucan on the innate immune response was experimented using human THP-1-derived macrophages and murine RAW 264.7 macrophages. A series of phagocytosis assays reveal that for both types of macrophages, the efficiency of phagocytosis is reduced by more than 50% when yeast cells are pre-cultivated in a lactate-containing medium. The amount of cytokines (CCL3/MIP-1α, TNF-α, IL-10, and IL-6) released after a 24-hr co-incubation was quantified and results show that macrophages incubated with cells exhibiting lactate-induced β-glucan masking release 84% less of CCL3/MIP-1α. The levels of other cytokines were unaffected. ROS production of macrophages in the first two hours of interaction is not influenced by β-glucan masking. Mechanisms other than macrophage ROS production may be involved in the observed increased rate of killing of glucose-only grown *C. auris*.

There was an attempt to elucidate the molecular mechanism behind the observed masking of β-glucan. The use of enzyme inhibitors reveals that cAMP-PKA and calcineurin signaling systems may not be involved in β-glucan masking in *C. auris*. The expression of selected genes was evaluated in glucose-only (Glu) and glucose-lactate (GluLac) grown cells. Although gene expression is increased by only less than 1.5-fold, the following genes were significantly upregulated in lactate-grown cells, *CDR1, ENG1, MNN14*, and *MNN26.* RNA sequencing was also performed wherein 213 differentially expressed genes were discovered. However, only five genes have an FDR value of less than 0.5. Of

these five genes, two were upregulated. One gene codes for a glucose transporter and the other one codes for a GPI-anchored protein, which is common in fungal cell walls.

To determine the effect of the observed lactate-induced β-glucan masking *in vivo*, yeast cells were injected into silkworm larvae (*Bombyx mori*). Survival analysis shows that cells undergoing β-glucan masking are more virulent to the host, probably due to evasion of immune recognition and proliferation inside the host.

Indeed, cell wall modifications like masking of β-glucan play key roles in the virulence of *C. auris* as it triggers a reduction in the visibility of the fungus to the immune system thereby decreasing the inflammatory response.

To date, no vaccines for human use have been approved to block the spread of fungal diseases, therefore the ability to study fungal diseases and create novel antifungal therapies is critical. Environmental condition-induced exposure of β-glucan may increase the chances that fungal cells will be recognized by recently developed anti-β-glucan antibodies.

Going forward, systems biology techniques that open new avenues for uncovering key pathways in the pathophysiology of fungal infections are important. To get a better knowledge of the host immune response to *C. auris* infections and to build novel antifungal therapies, future research must integrate cutting-edge molecular and cell biological techniques with translational approaches.

REFERENCES

Abrams, W. R., Diamond, L. W., & Kane, A. B. (1983). A flow cytometric assay of neutrophil degranulation. *Journal of Histochemistry & Cytochemistry*, *31*(6), 737–744. https://doi.org/10.1177/31.6.6404983

Antachopoulos, C., & Roilides, E. (2005). Cytokines and fungal infections. *British Journal of Haematology*, *129*(5), 583–596. https://doi.org/10.1111/j.1365-2141.2005.05498.x

Antifungal Susceptibility Testing and Interpretation | Candida auris | Fungal Diseases | CDC. (2023, April 5). https://www.cdc.gov/fungal/candida-auris/c-auris-antifungal.html

Ashida M. (2004). *Tanpakushitsu Kakusan Koso. Protein, Nucleic acid, Enzyme*, *49*(8), 1168–1173. [Article in Japanese].

Ballou, E. R., Avelar, G. M., Childers, D. S., Mackie, J., Bain, J. M., Wagener, J., Kastora, S. L., Panea, M. D., Hardison, S. E., Walker, L. A., Erwig, L. P., Munro, C. A., Gow, N. A. R., Brown, G. D., MacCallum, D. M., & Brown, A. J. P. (2017). Lactate signalling regulates fungal β-glucan masking and immune evasion. *Nature Microbiology*, *2*(2), 16238. https://doi.org/10.1038/nmicrobiol.2016.238

Benjamini, Y., and Hochberg, Y. (1995). Controlling the false discovery rate: a practical and powerful approach to multiple testing. *Journal of the Royal Statistical Society Series B*, 57, 289–300. doi:10.1111/j.2517-6161.1995.tb02031.x.

Bhavsar, I., Miller, C. S., & Al-Sabbagh, M. (2015). Macrophage Inflammatory Protein-1 Alpha (MIP-1 alpha)/CCL3: As a Biomarker. *General Methods in Biomarker Research and Their Applications*, 223–249. https://doi.org/10.1007/978-94-007-7696-8_27.

Binggeli, O., Neyen, C., Poidevin, M., & Lemaitre, B. (2014). Prophenoloxidase Activation Is Required for Survival to Microbial Infections in *Drosophila*. *PLOS Pathogens*, *10*(5), e1004067. https://doi.org/10.1371/journal.ppat.1004067

Brandt, M. E., & Lockhart, S. R. (2012). Recent Taxonomic Developments with *Candida* and Other Opportunistic Yeasts. *Current Fungal Infection Reports*, *6*(3), 170–177. https://doi.org/10.1007/s12281-012-0094-x

Bravo Ruiz, G., Ross, Z. K., Holmes, E., Schelenz, S., Gow, N. A. R., & Lorenz, A. (2019). Rapid and extensive karyotype diversification in haploid clinical *Candida auris* isolates. *Current Genetics*, *65*(5), 1217–1228. https://doi.org/10.1007/s00294-019-00976-w

Brown, G. D., Denning, D., & Levitz, S. (2012). Tackling Human Fungal Infections. *Science*, *336*(6082), 647. https://doi.org/10.1126/science.1222236

Bruno, M., Kersten, S., Bain, J. M., Jaeger, M., Rosati, D., Kruppa, M. D., Lowman, D. W., Rice, P. J., Graves, B., Ma, Z., Jiao, Y. N., Chowdhary, A., Renieris, G., van de Veerdonk, F. L., Kullberg, B.-J., Giamarellos-Bourboulis, E. J., Hoischen, A., Gow, N. A. R., Brown, A. J. P., … Netea, M. G. (2020). Transcriptional and functional insights into the host immune response against the emerging fungal pathogen *Candida auris*. *Nature Microbiology*, *5*(12), 1516–1531. https://doi.org/10.1038/s41564-020-0780-3

Brzicova, T., Javorkova, E., Vrbova, K., Zajicova, A., Holan, V., Pinkas, D., Philimonenko, V., Sikorova, J., Klema, J., Topinka, J., Rossner, P., Jr, & Jr. (2019). Molecular Responses in THP-1 Macrophage-Like Cells Exposed to Diverse Nanoparticles. *Nanomaterials (Basel, Switzerland)*, *9*(5), 687. https://doi.org/10.3390/nano9050687

Byvaltsev, V. A., Bardonova, L. A., Onaka, N. R., Polkin, R. A., Ochkal, S. V., Shepelev, V. V., Aliyev, M. A., & Potapov, A. A. (2019). Acridine Orange: A Review of Novel Applications for Surgical Cancer Imaging and Therapy. *Frontiers in Oncology*, *9*, 925. https://doi.org/10.3389/fonc.2019.00925

Calderone RA and Fonzi WA. (2001). Virulence factors of *Candida albicans*. *Trends in Microbiology*. 9 (7): 327-35. https://doi.org/10.1016/S0966-842X(01)02094-7

Cannom, R. R., French, S. W., Johnston, D., Edwards, J. E., Jr, & Filler, S. G. (2002). *Candida albicans* stimulates local expression of leukocyte adhesion molecules and cytokines in vivo. *The Journal of Infectious Diseases*, *186*(3), 389–396. https://doi.org/10.1086/341660

Centers for Disease Control and Prevention. (2020). Tracking *Candida auris*. Accessed January 11, 2021. https://www.cdc.gov/fungal/candida-auris/tracking-c-auris.html#world

Chamilos, G., Lewis, R. E., Albert, N., & Kontoyiannis, D. P. (2007). Paradoxical effect of Echinocandins across *Candida* species in vitro: evidence for echinocandin-specific and *Candida* species-related differences. *Antimicrobial Agents and Chemotherapy*, *51*(6), 2257–2259. https://doi.org/10.1128/AAC.00095-07

Chamilos, G., Lionakis, M. S., Lewis, R. E., & Kontoyiannis, D. P. (2007). Role of mini-host models in the study of medically important fungi. *The Lancet Infectious Diseases*, *7*(1), 42–55. https://doi.org/10.1016/S1473-3099(06)70686-7

Chatterjee, S., Alampalli, S. V., Nageshan, R. K., Chettiar, S. T., Joshi, S., & Tatu, U. S. (2015). Draft genome of a commonly misdiagnosed multidrug resistant pathogen *Candida auris*. *BMC Genomics*, *16*(1), 686. https://doi.org/10.1186/s12864-015-1863-z

Chazotte B. (2011). Labeling membrane glycoproteins or glycolipids with fluorescent wheat germ agglutinin. *Cold Spring Harbor Protocols*, *2011*(5), pdb.prot5623. https://doi.org/10.1101/pdb.prot5623

Childers, D. S., Avelar, G. M., Bain, J. M., Pradhan, A., Larcombe, D. E., Netea, M. G., Erwig, L. P., Gow, N. A. R., & Brown, A. J. P. (2020). Epitope Shaving Promotes Fungal Immune Evasion. *mBio*, *11*(4), e00984-20, /mbio/11/4/mBio.00984-20.atom. https://doi.org/10.1128/mBio.00984-20

CM-H2DCFDA (General Oxidative Stress Indicator). (n.d.). Retrieved June 26, 2023, from https://www.thermofisher.com/order/catalog/product/C6827

Cottier, F., Sherrington, S., Cockerill, S., del Olmo Toledo, V., Kissane, S., Tournu, H., Orsini, L., Palmer, G. E., Pérez, J. C., & Hall, R. A. (2019). Remasking of *Candida albicans* β-Glucan in Response to Environmental pH Is Regulated by Quorum Sensing. *mBio*, *10*(5), e02347-19, /mbio/10/5/mBio.02347-19.atom. https://doi.org/10.1128/mBio.02347-19

Cui, S., Hassan, R., Heintz-Buschart, A., & Bilitewski, U. (2016). Regulation of *Candida albicans* Interaction with Macrophages through the Activation of HOG Pathway by Genistein. *Molecules*, *21*(2), 162. https://doi.org/10.3390/molecules21020162

Cummings JH. (1981). Short chain fatty acids in the human colon. *Gut* 22, 763–779. http://dx.doi.org/10.1136/gut.22.9.763

Daigneault, M., Preston, J. A., Marriott, H. M., Whyte, M. K. B., & Dockrell, D. H. (2010). The Identification of Markers of Macrophage Differentiation in PMA-Stimulated THP-1 Cells and Monocyte-Derived Macrophages. *PLoS ONE*, *5*(1), e8668. https://doi.org/10.1371/journal.pone.0008668

Day, A. M., McNiff, M. M., Da Silva Dantas, A., Gow, N. A. R., & Quinn, J. (2018). Hog1 Regulates Stress Tolerance and Virulence in the Emerging Fungal Pathogen *Candida auris*. *mSphere*, *3*(5), e00506-18. https://doi.org/10.1128/mSphere.00506-18

de Boer, A. D., de Groot, P. W., Weindl, G., Schaller, M., Riedel, D., Diez-Orejas, R., Klis, F. M., de Koster, C. G., Dekker, H. L., Gross, U., Bader, O., & Weig, M. (2010). The *Candida albicans* cell wall protein Rhd3/Pga29 is abundant in the yeast form and contributes to virulence. *Yeast (Chichester, England)*, *27*(8), 611–624. https://doi.org/10.1002/yea.1790

Debruyne D. (1997). Clinical pharmacokinetics of fluconazole in superficial and systemic mycoses. *Clinical Pharmacokinetics*, *33*(1), 52–77. https://doi.org/10.2165/00003088-199733010-00005

de Groot, P. W., Hellingwerf, K. J., & Klis, F. M. (2003). Genome-wide identification of fungal GPI proteins. *Yeast 20*(9), 781–796. https://doi.org/10.1002/yea.1007

de Groot, T., Puts, Y., Berrio, I., Chowdhary, A., & Meis, J. F. (2020). Development of *Candida auris* Short Tandem Repeat Typing and Its Application to a Global Collection of Isolates. *mBio*, *11*(1), e02971-19, /mbio/11/1/mBio.02971-19.atom. https://doi.org/10.1128/mBio.02971-19.

Ene, I. V., Adya, A. K., Wehmeier, S., Brand, A. C., MacCallum, D. M., Gow, N. A. R., & Brown, A. J. P. (2012). Host carbon sources modulate cell wall architecture, drug resistance and virulence in a fungal pathogen. *Cellular Microbiology*, *14*(9), 1319–1335. https://doi.org/10.1111/j.1462-5822.2012.01813.x

Fan, J., Chaturvedi, V., & Shen, S. H. (2002). Identification and phylogenetic analysis of a glucose transporter gene family from the human pathogenic yeast *Candida albicans*. *Journal of Molecular Evolution*, *55*(3), 336–346. https://doi.org/10.1007/s00239-002-2330-4

Fan, S., Li, C., Bing, J., Huang, G., & Du, H. (2020). Discovery of the Diploid Form of the Emerging Fungal Pathogen *Candida auris*. *ACS Infectious Diseases*, *6*(10), 2641–2646. https://doi.org/10.1021/acsinfecdis.0c00282

Flint H.J, Scott KP, Louis P, Duncan SH. (2012). The role of the gut microbiota in nutrition and health. *Nature Reviews Gastroenterology and Hepatology*. 9:577–589. https://doi.org/10.1038/nrgastro. 2012.156

FlowJo™ Software for Mac. Version 10. Ashland, OR: Becton, Dickinson and Company; 2023.

Galán-Díez, M., Arana, D. M., Serrano-Gómez, D., Kremer, L., Casasnovas, J. M., Ortega, M., Cuesta-Domínguez, Á., Corbí, A. L., Pla, J., & Fernández-Ruiz, E. (2010). *Candida albicans* β-Glucan Exposure Is Controlled by the Fungal CEK1-Mediated Mitogen-Activated Protein Kinase Pathway That Modulates Immune Responses Triggered through Dectin-1. *Infection and Immunity*, *78*(4), 1426–1436. https://doi.org/10.1128/IAI.00989-09

Galocha, M., Pais, P., Cavalheiro, M., Pereira, D., Viana, R., & Teixeira, M. C. (2019). Divergent Approaches to Virulence in *C. albicans* and *C. glabrata*: Two Sides of the Same Coin. *International Journal of Molecular Sciences*, *20*(9), 2345. https://doi.org/10.3390/ ijms20092345

Garcia-Bustos, V., Pemán, J., Ruiz-Gaitán, A., Cabañero-Navalon, M. D., Cabanilles-Boronat, A., Fernández-Calduch, M., Marcilla-Barreda, L., Sigona-Giangreco, I. A., Salavert, M., Tormo-Mas, M. Á., & Ruiz-Saurí, A. (2022). Host-pathogen interactions upon *Candida auris* infection: fungal behaviour and immune response in *Galleria mellonella*. *Emerging Microbes & Infections*, *11*(1), 136–146. https://doi.org/10.1080/ n22221751.2021.2017756

Garcia-Rubio, R., de Oliveira, H. C., Rivera, J., & Trevijano-Contador, N. (2020). The Fungal Cell Wall: *Candida, Cryptococcus,* and *Aspergillus* Species. *Frontiers in Microbiology*, *10*. https://www.frontiersin.org/articles/10.3389/fmicb.2019.02993

Garfoot AL, Shen Q, Wüthrich M, Klein BS, Rappleye CA. (2016). The Eng1 β-glucanase enhances *Histoplasma* virulence by reducing β-glucan exposure. *mBio 7*(2):e01388-15. doi:10.1128/mBio.01388-15.

Granger, B. L. (2018). Accessibility and contribution to glucan masking of natural and genetically tagged versions of yeast wall protein 1 of *Candida albicans*. *PLoS ONE*, *13*(1), e0191194. https://doi.org/10.1371/journal.pone.0191194

Goldman, G. H., & Osmani, S. A. (Eds.). (2007). The Aspergilli: Genomics, medical aspects, biotechnology, and research methods (illustrated ed.). CRC Press. https://doi.org/10.1201/ 9781420008517

Goodridge, H. S., Reyes, C. N., Becker, C. A., Katsumoto, T. R., Ma, J., Wolf, A. J., Bose, N., Chan, A. S., Magee, A. S., Danielson, M. E., Weiss, A., Vasilakos, J. P., & Underhill, D. M. (2011). Activation of the innate immune receptor Dectin-1 upon formation of a 'phagocytic synapse'. *Nature*, *472*(7344), 471–475. https://doi.org/10.1038/nature10071

Graus, M. S., Wester, M. J., Lowman, D. W., Williams, D. L., Kruppa, M. D., Martinez, C. M., Young, J. M., Pappas, H. C., Lidke, K. A., & Neumann, A. K. (2018). Mannan Molecular Substructures Control Nanoscale Glucan Exposure in *Candida*. *Cell Reports*, *24*(9), 2432-2442.e5. https://doi.org/10.1016/j.celrep.2018.07.088

Guembe, M., Guinea, J., Marcos-Zambrano, L. J., Fernández-Cruz, A., Peláez, T., Muñoz, P., & Bouza, E. (2014). Micafungin at physiological serum concentrations shows antifungal activity against *Candida albicans* and *Candida parapsilosis* biofilms. *Antimicrobial Agents and Chemotherapy*, *58*(9), 5581–5584. https://doi.org/10.1128/AAC.02738-14

Hall RA. (2015). Dressed to impress: impact of environmental adaptation on the *Candida albicans* cell wall. *Molecular Microbiology,* 97:7–17. https://doi.org/10.1111/mmi.13020

Hall, R. A., & Gow, N. A. (2013). Mannosylation in *Candida albicans*: role in cell wall function and immune recognition. *Molecular Microbiology*, *90*(6), 1147–1161. https://doi.org/ 10.1111/mmi.12426

Hamamoto, H., Kurokawa, K., Kaito, C., Kamura, K., Manitra Razanajatovo, I., Kusuhara, H., Santa, T., & Sekimizu, K. (2004). Quantitative evaluation of the therapeutic effects of antibiotics using silkworms infected with human pathogenic microorganisms. *Antimicrobial Agents and Chemotherapy*, *48*(3), 774–779. https://doi.org/10.1128/AAC.48.3.774-779.2004

Hanaoka, N., Takano, Y., Shibuya, K., Fugo, H., Uehara, Y., & Niimi, M. (2008). Identification of the Putative Protein Phosphatase Gene *PTC1* as a Virulence-Related Gene Using a Silkworm Model of *Candida albicans* Infection. *Eukaryotic Cell*, *7*(10), 1640–1648. https://doi.org/10.1128/EC.00129-08

Hanaoka, N., Umeyama, T., Ueno, K., Ueda, K., Beppu, T., Fugo, H., Uehara, Y., & Niimi, M. (2005). A putative dual-specific protein phosphatase encoded by *YVH1* controls growth, filamentation and virulence in *Candida albicans*. In *Microbiology* (Vol. 151, Issue 7, pp. 2223–2232). Microbiology Society. https://doi.org/10.1099/mic.0.27999-0

Hernandez-Chavez, M. J., Perez-Garcia, L. A., Nino-Vega, G. A., and Mora-Montes, H. M. (2017). Fungal strategies to evade the host immune recognition. *Journal of Fungi* 3:51. doi: 10.3390/jof3040051

Hof, H. (2006), A new, broad-spectrum azole antifungal: posaconazole – mechanisms of action and resistance, spectrum of activity. *Mycoses*, *49*(1): 2-6. https://doi.org/10.1111/j.1439-0507.2006.01295.x

Horton M.V., Eix, E.F., Johnson, C.J., Dean, M.E.B, Andes, B.D., Wartman, K.M., & Nett, J.E. (2024) Impact of Micafungin on *Candida auris* β-glucan Masking and Neutrophil Interactions. *The Journal of Infectious Diseases* jiae043. https://doi.org/10.1093/infdis/jiae043

Horton, M. V., Johnson, C. J., Zarnowski, R., Andes, B. D., Schoen, T. J., Kernien, J. F., Lowman, D., Kruppa, M. D., Ma, Z., Williams, D. L., Huttenlocher, A., & Nett, J. E. (2021). *Candida auris* Cell Wall Mannosylation Contributes to Neutrophil Evasion through Pathways Divergent from *Candida albicans* and *Candida glabrata*. *mSphere*, *6*(3). https://doi.org/10.1128/mSphere.00406-21

Huang, G., Wang, H., Chou, S., Nie, X., Chen, J., & Liu, H. (2006). Bistable expression of WOR1, a master regulator of white-opaque switching in *Candida albicans*. *Proceedings of the National Academy of Sciences of the United States of America*, *103*(34), 12813–12818. https://doi.org/10.1073/pnas.0605270103

Ikeda F. (2003). Antifungal activity and clinical efficacy of micafungin sodium (Funguard). *Nihon yakurigaku zasshi. Folia Pharmacologica Japonica*, *122*(4), 339–344. https://doi.org/10.1254/fpj.122.339

InvivoGen Review. (2013). β-Glucans: bittersweet ligands of Dectin-1. Retrieved from https://www.invivogen.com/sites/default/files/invivogen/resources/documents/reviews/review-BGlucans-invivogen.pdf

Ishii, M., Matsumoto, Y., & Sekimizu, K. (2016). Usefulness of silkworm as a host animal for understanding pathogenicity of *Cryptococcus neoformans*. *Drug Discoveries & Therapeutics*, *10*(1), 9–13. https://doi.org/10.5582/ddt.2016.01015

Ivanovic Z. (2009). Hypoxia or in situ normoxia: The stem cell paradigm. *Journal of Cellular Physiology*, *219*(2), 271–275. https://doi.org/10.1002/jcp.21690

Jeffery-Smith A, Taori SK, Schelenz S, Jeffery K, Johnson EM, Borman A, *Candida auris* Incident Management Team, Manuel R, Brown CS. (2017). *Candida auris*: a Review of the Literature. *Clinical Microbiology Reviews,* 31 (1) e00029-17. https://doi.org/10.1128/cmr.00029-17

Jena Bioscience Data Sheet. (2023). *Nourseothricin—Solution, Selection Antibiotics for LEXSY*. Jena Bioscience, Version: 0006. https://www.jenabioscience.com/images/PDF/AB-101.0005.pdf

Johnson, C. J., Davis, J. M., Huttenlocher, A., Kernien, J. F., & Nett, J. E. (2018). Emerging Fungal Pathogen *Candida auris* Evades Neutrophil Attack. *mBio*, *9*(4), e01403-18, /mbio/9/4/mBio.01403-18.atom. https://doi.org/10.1128/mBio.01403-18

Kaneko, Y., Ohno, H., Kohno, S., & Miyazaki, Y. (2010). Micafungin alters the expression of genes related to cell wall integrity in *Candida albicans* biofilms. *Japanese Journal of Infectious Diseases*, *63*(5), 355–357. PMID: 20859005

Kaplan, E.L. and Meier, P. (1958). Nonparametric Estimation from Incomplete Observations. *Journal of the American Statistical Association, 53*, 457-481. http://dx.doi.org/10.1080/01621459.1958.10501452

Kasper, L., Seider, K., & Hube, B. (2015). Intracellular survival of *Candida glabrata* in macrophages: Immune evasion and persistence. *FEMS Yeast Research*, *15*(5), fov042. https://doi.org/10.1093/femsyr/fov042

Kassambara, A., Kosinski, M., Biecek, P., (2019). survminer: Drawing Survival Curves using "ggplot2"[WWW Document]. URL https://CRAN.R-project.org/package=survminer.

Kavanagh, K., & Sheehan, G. (2018). The Use of *Galleria mellonella* Larvae to Identify Novel Antimicrobial Agents against Fungal Species of Medical Interest. *Journal of Fungi (Basel, Switzerland)*, *4*(3), 113. https://doi.org/10.3390/jof4030113

Kean, R., Brown, J., Gulmez, D., Ware, A., & Ramage, G. (2020). *Candida auris*: A Decade of Understanding of an Enigmatic Pathogenic Yeast. *Journal of Fungi*, *6*(1), 30. https://doi.org/10.3390/jof6010030

Kogan, G., Pavliak, V., Sandula, J., & Masler, L. (1988). Novel structure of the cellular mannan of the pathogenic yeast *Candida krusei*. *Carbohydrate Research*, *184*, 171–182. https://doi.org/10.1016/0008-6215(88)80015-6

Kullberg, B. J., & Arendrup, M. C. (2015). Invasive candidiasis. *New England Journal of Medicine 373*:1445-1456. DOI: 10.1056/NEJMra1315399

Kurakado, S., Matsumoto, Y., & Sugita, T. (2021). Efficacy of Posaconazole against *Rhizopus oryzae* Infection in Silkworm. *Medical Mycology Journal*, *62*(3), 53–57. https://doi.org/10.3314/mmj.21-00004

Lamoth F, Kontoyiannis DP. (2018). The *Candida auris* alert: facts and perspectives. *The Journal of Infectious Diseases,* 217:516 –520. https://doi.org/10.1093/infdis/jix597

Lima, S. L., Rossato, L., & Salles de Azevedo Melo, A. (2020). Evaluation of the potential virulence of *Candida haemulonii* species complex and *Candida auris* isolates in *Caenorhabditis elegans* as an in vivo model and correlation to their biofilm production capacity. *Microbial Pathogenesis*, *148*, 104461. https://doi.org/10.1016/j.micpath.2020.104461

Li, M., Liu, Z. H., Chen, Q., Zhou, W. Q., Yu, M. W., Lü, G. X., Lü, X. L., Shen, Y. N., Liu, W. D., & Wu, S. X. (2009). Insoluble beta-glucan from the cell wall of *Candida albicans* induces immune responses of human THP-1 monocytes through Dectin-1. *Chinese Medical Journal*, *122*(5), 496–501.

Lockhart SR, Etienne KA, Vallabhaneni S, Farooqi J, Chowdhary A, Govender NP, Colombo AL, Calvo B, Cuomo CA, Desjardins CA, Berkow EL, Castanheira M, Magobo RE, Jabeen K, Asghar RJ, Meis JF, Jackson B, Chiller T, Litvintseva AP. (2017). Simultaneous emergence of multidrug-resistant *Candida auris* on 3 continents confirmed by whole-genome sequencing and epidemiological analyses. *Clinical Infectious Diseases* 64:134 –140.

Lohse, M. B., & Johnson, A. D. (2008). Differential Phagocytosis of White versus Opaque *Candida albicans* by *Drosophila* and Mouse Phagocytes. *PLoS ONE*, *3*(1), e1473. https://doi.org/10.1371/journal.pone.0001473

Lopes JP, Stylianou M, Backman E, Holmberg S, Jass J, Claesson R, Urban CF. (2018). Evasion of immune surveillance in low oxygen environments enhances *Candida albicans* virulence. *mBio* 9:e02120-18. https://doi.org/10.1128/mBio.02120-18

Maicas, S., Moreno, I., Nieto, A., Gómez, M., Sentandreu, R., & Valentín, E. (2005). In silico analysis for transcription factors with Zn(II)(2)C(6) binuclear cluster DNA-binding domains in *Candida albicans*. *Comparative and Functional Genomics*, *6*(7-8), 345–356. https://doi.org/10.1002/cfg.492

Marcil, A., Gadoury, C., Ash, J., Zhang, J., Nantel, A., & Whiteway, M. (2008). Analysis of *PRA1* and Its Relationship to *Candida albicans*—Macrophage Interactions. *Infection and Immunity*, *76*(9), 4345–4358. https://doi.org/10.1128/IAI.00588-07

Mathur, P., Hasan, F., Singh, P. K., Malhotra, R., Walia, K., & Chowdhary, A. (2018). Five-year profile of candidaemia at an Indian trauma center: High rates of *Candida auris* bloodstream infections. *Mycoses*, *61*(9), 674–680. https://doi.org/10.1111/myc.12790

Matsumoto, Y., & Sekimizu, K. (2019). Silkworm as an experimental animal for research on fungal infections. *Microbiology and Immunology*, *63*(2), 41–50. https://doi.org/10.1111/1348-0421.12668

Matsumoto, Y., Yoshikawa, A., Nagamachi, T., Sugiyama, Y., Yamada, T., & Sugita, T. (2022). A critical role of calcineurin in stress responses, hyphal formation, and virulence of the pathogenic fungus *Trichosporon asahii*. *Scientific Reports*, *12*(1), Article 1. https://doi.org/10.1038/s41598-022-20507-x

McMillin JM. Blood Glucose. In: Walker HK, Hall WD, Hurst JW, editors. Clinical Methods: The History, Physical, and Laboratory Examinations. 3rd edition. Boston: Butterworths; 1990. Chapter 141. Available from: https://www.ncbi.nlm.nih.gov/books/NBK248/

Miceli, M.H., Diaz, J.A., & Lee, S.A. (2011). Emerging opportunistic yeast infections. *Lancet Infectious Diseases, 11*:142–51. https://doi.org/10.1016/S1473-3099(10)70218-8

Mortimer, R. K., & Johnston, J. R. (1986). Genealogy of principal strains of the yeast genetic stock center. *Genetics*, *113*(1), 35–43. https://doi.org/10.1093/genetics/113.1.35

Muñoz, J. F., Gade, L., Chow, N. A., Loparev, V. N., Juieng, P., Berkow, E. L., Farrer, R. A., Litvintseva, A. P., & Cuomo, C. A. (2018). Genomic insights into multidrug-resistance, mating and virulence in *Candida auris* and related emerging species. *Nature Communications*, *9*(1), Article 1. https://doi.org/10.1038/s41467-018-07779-6

Murray, A. J. (2008). Pharmacological PKA inhibition: all may not be what it seems. *Science Signaling.* 1:re4. doi: 10.1126/scisignal.122re4

Navarro-Arias, M. J., Hernández-Chávez, M. J., Garcia-Carnero, L. C., Amezcua-Hernández, D. G., Lozoya-Pérez, N. E., Estrada-Mata, E., Martínez-Duncker, I., Franco, B., & Mora-Montes, H. M. (2019). Differential recognition of *Candida tropicalis, Candida guilliermondii, Candida krusei,* and *Candida auris* by human innate immune cells. *Infection and Drug Resistance*, *12*, 783–794. https://doi.org/10.2147/IDR.S197531

Netea, M. G., Joosten, L. A. B., van der Meer, J. W. M., Kullberg, B.-J., & van de Veerdonk, F. L. (2015). Immune defence against *Candida* fungal infections. *Nature Reviews Immunology*, *15*(10), 630–642. https://doi.org/10.1038/nri3897

Ochiai, M., & Ashida, M. (2000). A pattern-recognition protein for beta-1,3-glucan. The binding domain and the cDNA cloning of beta-1,3-glucan recognition protein from the silkworm, *Bombyx mori*. *The Journal of Biological Chemistry*, *275*(7), 4995–5002. https://doi.org/10.1074/jbc.275.7.4995

Ohta, M., Watanabe, A., Mikami, T., Nakajima, Y., Kitami, M., Tabunoki, H., Ueda, K., & Sato, R. (2006). Mechanism by which *Bombyx mori* hemocytes recognize microorganisms: Direct and indirect recognition systems for PAMPs. *Developmental & Comparative Immunology*, *30*(10), 867–877. https://doi.org/10.1016/j.dci.2005.12.005

Orekhov AN, Orekhova VA, Nikiforov NG, Myasoedova VA, Grechko AV, Romanenko EB, Zhang D, Chistiakov DA. (2019). Monocyte differentiation and macrophage polarization. *Vessel Plus* ; 3:10. http://dx.doi.org/10.20517/2574-1209.2019.04

Panchision, D.M. (2009). The role of oxygen in regulating neural stem cells in development and disease. *Journal of Cellular Physiology*, *220*(3), 562–8. https://doi.org/10.1002/jcp.21812

Park, E. K., Jung, H. S., Yang, H. I., Yoo, M. C., Kim, C., & Kim, K. S. (2007). Optimized THP-1 differentiation is required for the detection of responses to weak stimuli. *Inflammation Research*, *56*(1), 45–50. https://doi.org/10.1007/s00011-007-6115-5

Paudel, Atmika, Suresh Panthee, Hiroshi Hamamoto, and Kazuhisa Sekimizu. (2020). A Simple Artificial Diet Available for Research of Silkworm Disease Models. *Drug Discoveries & Therapeutics, 14*(4): 177–80. https://doi.org/10.5582/ddt.2020.03061.

Paysan-Lafosse, T., Blum, M., Chuguransky, S., Grego, T., Pinto, B. L., Salazar, G. A., Bileschi, M. L., Bork, P., Bridge, A., Colwell, L., Gough, J., Haft, D. H., Letunić, I., Marchler-Bauer, A., Mi, H., Natale, D. A., Orengo, C. A., Pandurangan, A. P., Rivoire, C., … Bateman, A. (2023). InterPro in 2022. *Nucleic Acids Research*, *51*(D1), D418–D427. https://doi.org/10.1093/nar/gkac993

Pereira, T. C., de Barros, P. P., Fugisaki, L. R. O., Rossoni, R. D., Ribeiro, F. C., de Menezes, R. T., Junqueira, J. C., & Scorzoni, L. (2018). Recent Advances in the Use of *Galleria mellonella* Model to Study Immune Responses against Human Pathogens. *Journal of Fungi (Basel, Switzerland)*, *4*(4), 128. https://doi.org/10.3390/jof4040128

Perez-Garcia, L. A. Diaz-Jimenez,D., Lopez-Esparza, A. & Mora-Montes, H. (2011). Role of Cell Wall Polysaccharides during Recognition of *Candida albicans* by the Innate Immune System. *Journal of Glycobiology*, *01*(01). https://doi.org/10.4172/2168-958X.1000102

Pfaller, M. A., & Diekema, D. J. (2007). Epidemiology of Invasive Candidiasis: A Persistent Public Health Problem. *Clinical Microbiology Reviews*, *20*(1), 133–163. https://doi.org/10.1128/CMR.00029-06

Pittrow, L., & Penk, A. (1997). Plasma and tissue concentrations of fluconazole and their correlation to breakpoints. *Mycoses*, *40* (1-2), 25–32. https://doi.org/10.1111/j.1439-0507.1997.tb00167.x

Powell, J. D., & Zheng, Y. (2006). Dissecting the mechanism of T-cell anergy with immunophilin ligands. *Current Opinion in Investigational Drugs, 7*(11), 1002-1007. doi:10.1016/j.coi.2006.09.001

Pradhan A, Avelar GM, Bain JM, Childers DS, Larcombe DE, Netea MG, Shekhova E, Munro CA, Brown GD, Erwig LP, Gow NAR, Brown AJP. (2018). Hypoxia promotes immune evasion by triggering β-glucan masking on the *Candida albicans* cell surface via mitochondrial and cAMP-protein kinase A signaling. *mBio* 9:e01318-18. https://doi.org/10.1128/mbio.01318-18

Pradhan A, Avelar GM, Bain JM, Childers D, Pelletier C, Larcombe DE, Shekhova E, Netea MG, Brown GD, Erwig L, Gow NAR, Brown AJP. (2019). Non-canonical signalling mediates changes in fungal cell wall PAMPs that drive immune evasion. *Nature Communications* 10: 5315. https://doi.org/10.1038/s41467-019-13298-9

Rane, H. S., Hayek, S. R., Frye, J. E., Abeyta, E. L., Bernardo, S. M., Parra, K. J., & Lee, S. A. (2019). *Candida albicans* Pma1p Contributes to Growth, pH Homeostasis, and Hyphal Formation. *Frontiers in Microbiology*, *10*, 1012. https://doi.org/10.3389/fmicb.2019.01012

RAW 264.7—TIB-71 | ATCC. (n.d.). Retrieved July 3, 2023, from https://www.atcc.org/products/tib-71

R Core Team (2020). R: The R Project for Statistical Computing. R Foundation for Statistical Computing, Vienna, Austria.

Reuß, O., Vik, Å., Kolter, R., & Morschhäuser, J. (2004). The SAT1 flipper, an optimized tool for gene disruption in *Candida albicans*. *Gene*, *341*, 119–127. https://doi.org/10.1016/j.gene.2004.06.021

Riendeau, C. J., & Kornfeld, H. (2003). THP-1 Cell Apoptosis in Response to Mycobacterial Infection. *Infection and Immunity*, *71*(1), 254–259. https://doi.org/10.1128/IAI.71.1.254-259.2003

Robles, A. I., Bemmels, N. A., Foraker, A. B., & Harris, C. C. (2001). APAF-1 is a transcriptional target of p53 in DNA damage-induced apoptosis. *Cancer Research*, *61*(18), 6660–6664.

Romanowski, K., Zaborin, A., Valuckaite, V., Rolfes, R. J., Babrowski, T., Bethel, C., Olivas, A., Zaborina, O., & Alverdy, J. C. (2012). *Candida albicans* Isolates from the Gut of Critically Ill Patients Respond to Phosphate Limitation by Expressing Filaments and a Lethal Phenotype. *PLoS ONE*, *7*(1), e30119. https://doi.org/10.1371/journal.pone.0030119

Rosenbach A, Dignard D, Pierce JV, Whiteway M, Kumamoto CA. (2010). Adaptations of *Candida albicans* for growth in the mammalian intestinal tract. *Eukaryotic Cell* 9:1075–1086. https://doi.org/10.1128/EC.00034-10.

Rost, F. W. D. (2006). Fluorescence microscopy. Cambridge University Press. ISBN 978-0-521-42277-2.

Rybak, J. M., Doorley, L. A., Nishimoto, A. T., Barker, K. S., Palmer, G. E., & Rogers, P. D. (2019). Abrogation of Triazole Resistance upon Deletion of *CDR1* in a Clinical Isolate of *Candida auris*. *Antimicrobial Agents and Chemotherapy*, *63*(4), e00057-19. https://doi.org/10.1128/AAC.00057-19

Santos, E. O. L., Azzolini, A. E. C. S., & Lucisano-Valim, Y. M. (2015). Optimization of a flow cytometric assay to evaluate the human neutrophil ability to phagocytose immune complexes via Fcγ and complement receptors. *Journal of Pharmacological and Toxicological Methods*, *72*, 67–71. https://doi.org/10.1016/j.vascn.2014.10.005

Satoh K, Makimura K, Hasumi Y, Nishiyama Y, Uchida K, Yamaguchi H. (2009). *Candida auris* sp. nov., a novel ascomycetous yeast isolated from the external ear canal of an inpatient in a Japanese hospital. *Microbiology and Immunology* 53:41–44. http://doi.wiley.com/10.1111/j.1348-0421.2008.00083.x

Sharma, C., Kumar, N., Pandey, R., Meis, J. F., & Chowdhary, A. (2016). Whole genome sequencing of emerging multidrug resistant *Candida auris* isolates in India demonstrates low genetic variation. *New Microbes and New Infections*, *13*, 77–82. https://doi.org/10.1016/j.nmni.2016.07.003

Sherrington, S. L., Sorsby, E., Mahtey, N., Kumwenda, P., Lenardon, M. D., Brown, I., Ballou, E. R., MacCallum, D. M., & Hall, R. A. (2017). Adaptation of *Candida albicans* to environmental pH induces cell wall remodelling and enhances innate immune recognition. *PLoS Pathogens*, *13*(5), e1006403. https://doi.org/10.1371/journal.ppat.1006403

Shibata, N., Suzuki, A., Kobayashi, H., and Okawa, Y. (2007). Chemical structure of the cell-wall mannan of *Candida albicans* serotype A and its difference in yeast and hyphal forms. *Biochemical Journal, 404*, 365–372. doi: 10.1042/bj20070081

Smith, A. J., Graves, B., Child, R., Rice, P. J., Ma, Z., Lowman, D. W., Ensley, H. E., Ryter, K. T., Evans, J. T., & Williams, D. L. (2018). Immunoregulatory Activity of the Natural Product Laminarin Varies Widely as a Result of Its Physical Properties. *The Journal of Immunology*, *200*(2), 788–799. https://doi.org/10.4049/jimmunol.1701258

Smith, D. F. Q., Mudrak, N. J., Zamith-Miranda, D., Honorato, L., Nimrichter, L., Chrissian, C., Smith, B., Gerfen, G.; Stark, R.E.; Nosanchuk, J.D.; Casadevall, A. (2022). Melanization of *Candida auris* Is Associated with Alteration of Extracellular pH. *Journal of Fungi*, *8*(10), 1068. http://dx.doi.org/10.3390/jof8101068

Sosinska, G. J., de Koning, L. J., de Groot, P. W. J., Manders, E. M. M., Dekker, H. L., Hellingwerf, K. J., de Koster, C. G., & Klis, F. M. (2011). Mass spectrometric quantification of the adaptations in the wall proteome of *Candida albicans* in response to ambient pH. *Microbiology (Reading, England)*, *157*(Pt 1), 136–146. https://doi.org/10.1099/mic.0.044206-0

Strijbis, K., Tafesse, F. G., Fairn, G. D., Witte, M. D., Dougan, S. K., Watson, N., Spooner, E., Esteban, A., Vyas, V. K., Fink, G. R., Grinstein, S., & Ploegh, H. L. (2013). Bruton's Tyrosine Kinase (BTK) and Vav1 Contribute to Dectin1-Dependent Phagocytosis of *Candida albicans* in Macrophages. *PLoS Pathogens*, *9*(6), e1003446. https://doi.org/10.1371/journal.ppat.1003446

Spruijtenburg, B., Badali, H., Abastabar, M., Mirhendi, H., Khodavaisy, S., Sharifisooraki, J., Taghizadeh Armaki, M., de Groot, T., & Meis, J. F. (2022). Confirmation of fifth *Candida auris* clade by whole genome sequencing. *Emerging Microbes & Infections*, *11*(1), 2405–2411. https://doi.org/10.1080/22221751.2022.2125349

Suchodolski, J., Muraszko, J., Bernat, P., & Krasowska, A. (2021). Lactate Like Fluconazole Reduces Ergosterol Content in the Plasma Membrane and Synergistically Kills *Candida albicans. International Journal of Molecular Sciences*, *22*(10), 5219. https://doi.org/10.3390/ijms22105219

Suphavilai, C. *et al.* Discovery of the sixth *Candida auris* clade in Singapore. *medRxiv* 2023.08.01.23293435 (2023) doi:10.1101/2023.08.01.23293435.

Surat, P. (2018, June 13). *pH in the Human Body*. News-Medical.Net. https://www.news-medical.net/health/pH-in-the-Human-Body.aspx

The UniProt Consortium. UniProt: the Universal Protein Knowledgebase in 2023 Nucleic Acids Res. 51:D523–D531 (2023)

Thomé, M. P., Filippi-Chiela, E. C., Villodre, E. S., Migliavaca, C. B., Onzi, G. R., Felipe, K. B., & Lenz, G. (2016). Ratiometric analysis of acridine orange staining in the study of acidic organelles and autophagy. *Journal of Cell Science*, jcs.195057. https://doi.org/10.1242/jcs.195057

Tortorano, A. M., Kibbler, C., Peman, J., Bernhardt, H., Klingspor, L., & Grillot, R. (2006). Candidaemia in Europe: epidemiology and resistance. *International Journal of Antimicrobial Agents*, *27*(5), 359–366. https://doi.org/10.1016/j.ijantimicag.2006.01.002

Tripathi, A., Liverani, E., Tsygankov, A. Y., & Puri, S. (2020). Iron alters the cell wall composition and intracellular lactate to affect *Candida albicans* susceptibility to antifungals and host immune response. *Journal of Biological Chemistry*, *295*(29), 10032–10044. https://doi.org/10.1074/jbc.RA120.013413

Tucey, T. M., Verma, J., Harrison, P. F., Snelgrove, S. L., Lo, T. L., Scherer, A. K., Barugahare, A. A., Powell, D. R., Wheeler, R. T., Hickey, M. J., Beilharz, T. H., Naderer, T., & Traven, A. (2018). Glucose Homeostasis Is Important for Immune Cell Viability during *Candida* Challenge and Host Survival of Systemic Fungal Infection. *Cell Metabolism*, *27*(5), 988-1006.e7. https://doi.org/10.1016/j.cmet.2018.03.019

Uwamahoro, N., Verma-Gaur, J., Shen, H.-H., Qu, Y., Lewis, R., Lu, J., Bambery, K., Masters, S. L., Vince, J. E., Naderer, T., & Traven, A. (2014). The Pathogen *Candida albicans* Hijacks Pyroptosis for Escape from Macrophages. *mBio*, *5*(2). https://doi.org/10.1128/mBio.00003-14

Van der Graaf, C. A. A., Netea, M. G., Verschueren, I., Van der Meer, J. W. M., & Kullberg, B. J. (2005). Differential Cytokine Production and Toll-Like Receptor Signaling Pathways by *Candida albicans* Blastoconidia and Hyphae. *Infection and Immunity*, *73*(11), 7458–7464. https://doi.org/10.1128/IAI.73.11.7458-7464.2005

Vendele, I., Willment, J. A., Silva, L. M., Palma, A. S., Chai, W., Liu, Y., Feizi, T., Spyrou, M., Stappers, M. H. T., Brown, G. D., & Gow, N. A. R. (2020). Mannan detecting C-type lectin receptor probes recognise immune epitopes with diverse chemical, spatial and phylogenetic heterogeneity in fungal cell walls. *PLoS pathogens*, *16*(1), e1007927. https://doi.org/10.1371/journal.ppat.1007927

Wagener, J., Malireddi, R. K. S., Lenardon, M. D., Köberle, M., Vautier, S., MacCallum, D. M., Biedermann, T., Schaller, M., Netea, M. G., Kanneganti, T.-D., Brown, G. D., Brown, A. J. P., & Gow, N. A. R. (2014). Fungal Chitin Dampens Inflammation through IL-10 Induction Mediated by NOD2 and TLR9 Activation. *PLoS Pathogens*, *10*(4), e1004050. https://doi.org/10.1371/journal.ppat.1004050

Walker, L. A., & Munro, C. A. (2020). Caspofungin Induced Cell Wall Changes of *Candida* Species Influences Macrophage Interactions. *Frontiers in Cellular and Infection Microbiology*, *10*, 164. https://doi.org/10.3389/fcimb.2020.00164

Wang, Y., Zhou, J., Zou, Y., Chen, X., Liu, L., Qi, W., Huang, X., Chen, C., & Liu, N.-N. (2022). Fungal commensalism modulated by a dual-action phosphate transceptor. *Cell Reports*, *38*(4), 110293. https://doi.org/10.1016/j.celrep.2021.110293

Wasko, B. M., Carr, D. T., Tung, H., Doan, H., Schurman, N., Neault, J. R., Feng, J., Lee, J., Zipkin, B., Mouser, J., Oudanonh, E., Nguyen, T., Stetina, T., Shemorry, A., Lemma, M., & Kaeberlein, M. (2013). Buffering the pH of the culture medium does not extend yeast replicative lifespan. *F1000 Research*, *2*, 216. https://doi.org/10.12688/f1000research.2-216.v1

Watanabe, A., Miyazawa, S., Kitami, M., Tabunoki, H., Ueda, K., & Sato, R. (2006). Characterization of a novel C-type lectin, *Bombyx mori* multibinding protein, from the *B. mori* hemolymph: mechanism of wide-range microorganism recognition and role in immunity. *Journal of Immunology (Baltimore, Md. : 1950)*, *177*(7), 4594–4604. https://doi.org/10.4049/jimmunol.177.7.4594

Wellington, Melanie, Kristy Dolan, and Damian J. Krysan. 2009. Live *Candida albicans* Suppresses Production of Reactive Oxygen Species in Phagocytes. *Infection and Immunity* 77 (1): 405–13. https://doi.org/10.1128/IAI.00860-08.

Yadav, A., Singh, A., Wang, Y., Haren, M. H. van, Singh, A., de Groot, T., Meis, J. F., Xu, J., & Chowdhary, A. (2021). Colonisation and Transmission Dynamics of *Candida auris* among Chronic Respiratory Diseases Patients Hospitalised in a Chest Hospital, Delhi, India: A Comparative Analysis of Whole Genome Sequencing and Microsatellite Typing. *Journal of Fungi*, *7*(2), Article 2. https://doi.org/10.3390/jof7020081

Yang, M., Solis, N. V., Marshall, M., Garleb, R., Zhou, T., Wang, D., Swidergall, M., Pearlman, E., Filler, S. G., & Liu, H. (2022). Control of β-glucan exposure by the endo-1,3-glucanase Eng1 in *Candida albicans* modulates virulence. *PLoS Pathogens*, *18*(1), e1010192. https://doi.org/10.1371/journal.ppat.1010192